Cortical Reorganization and Sensorimotor Recovery in a Mouse Model of Intracerebral Hemorrhagic Stroke

Ségolène Chevallier Rufigny, MSc. Candidate in Neurosciences

A thesis submitted to the university of Ottawa in partial fulfillment of the requirements for the Master's degree in Neurosciences

Department of Cellular and Molecular Medicine

Faculty of Medicine

University of Ottawa

© Ségolène Chevallier Rufigny, Ottawa, Canada, 2025

Abstract

Intracerebral haemorrhage (ICH) is a subtype of stroke that accounts for approximately 10-15% of stroke cases in Canada. Neurological deficits following ICH are common and most patients will suffer long-term impairments. Spontaneous recovery facilitated by the remodeling of functional areas through neuronal reorganization has been observed in both stroke patients and animal models. However, the precise relationship between cortical remodeling and functional recovery is not completely understood. This thesis aims to characterize the reorganization of the sensorimotor cortex as well as quantify sensorimotor function longitudinally during the recovery period. Young Thy1-Chr2-YFP mice with an implanted chronic window over the intact skull allowed visualization of sensorimotor cortex functional assessments through light-based motor mapping and intrinsic signal optical imaging over a 6-week period. Additionally, a battery of behavioral tests was conducted in parallel to evaluate motor deficits. Following a striatal ICH, behavioral impairments were observed with both acute and chronic recovery. The deficits shown in ICH mice were linked with a disruption of motor maps. When stimulating the injured hemisphere, evoked movement of both forelimbs showed smaller amplitude compared to sham animals, which was accompanied with a reduction in the motor map size. On the other side, the contralesional hemisphere did not show any differences compared to the sham animals, demonstrating a potential compensatory mechanism. A trend toward recovery in the motor maps occurred on the 6th week, matching the late recovery of impaired forelimb use deficit. Conversely, the sensory responses evoked from mechanical forelimb stimulation did not show any changes following ICH induction. This is the first study to investigate the longitudinal impact of striatal ICH on bilateral sensorimotor maps in relation to behavioral deficits. Our findings revealed that injury in the striatum leads to long-term functional impact in the motor cortex accompanied by behavioral motor deficits, with a recovery of motor functions matching the recovery initiation in motor representations.

Index

List of Figures ..... **v**

List of Supplemental Figures ..... **v**

List of Abbreviations ..... **vi**

Acknowledgements ..... **vii**

1. Introduction **1**

1.1 Intracerebral Haemorrhage 1

1.2 The striatum and its sensorimotor functions 1

1.3 Motor cortex as a sensorimotor hub 4

1.4 ICH, behavioral deficits and spontaneous recovery 6

1.5 Remapping in the sensorimotor cortex 8

1.5.1 Intracortical microstimulation 8

1.5.2 Light-based motor mapping 10

1.5.3 Intrinsic Signaling Optical Imaging 11

1.6 Correlation between striatal-restricted injury and changes in motor cortex 13

1.7 ICH rodent models 14

1.8 What parts are missing in the puzzle? 15

2.Methodology **17**

2.1 Animals and Timeline 17

2.2 Surgical Procedures 18

2.3 Behavioral Tests 20

2.3.1 Cylinder Test 21

2.3.2 Grid Walking 21

2.3.3 Neurological Deficit Score 22

2.3.4 Corner Turn Test 22

2.4 Mapping Experiments 23

2.4.1 Intrinsic Signaling Optical Imaging 23

2.4.2 Light-Based Motor Mapping 26

2.5 MRI 28

2.6 Histology 29

2.7 Statistical Analysis 30

3. Results 30

3.1 ICH was delivered in the right striatum and led atrophy of the injured hemisphere 30

3.2 Acute sensorimotor deficits were identified following ICH induction 33

3.3 Cylinder test and NDS found long-lasting forelimb impairments in ICH animals 37

3.4 Striatal ICH did not alter cortical responses from sensory stimulation 39

3.5 Motor maps showed bilateral decrease in size and amplitude after striatal injury 42

3.6 Larger movement latencies were observed in ICH mice 46

4. Discussion 49

4.1 Collagenase injection induced ICH leading to an atrophy of the lesioned hemisphere 49

4.2 Behavioral impairments followed striatal ICH with long-lasting forelimb sensorimotor functions deficits 51

4.3 Stimulus-evoked sensory responses are not impaired by striatal ICH 55

4.4 LBMM showed motor map alterations 56

4.5 Bilateral sensorimotor representations with no recovery over time 58

5. Conclusion 61

5.1 Significance 61

5.2 Limitations and future direction 62

5.2.1 Isoflurane neuroprotection 62

5.2.2 Anesthesia-induced LBMM and ISOI 62

5.2.3 Baseline measurements 63

5.2.4 Spontaneous behavioral task for a motor skilled-related brain region 63

5.2.5 Neurovascular coupling disruption and ISOI 63

5.2.6 Individual correlation between sensorimotor mapping, behavior and ICH lesion size 64

5.2.7 Age group in ICH 64

6. Supplemental Figures 65

7. Bibliography 70

List of Figures

Figure 1. Experimental Timeline 18

Figure 2. Intracerebral Haemorrhagic Stroke Surgery and Transcranial Window Implantation 20

Figure 3. Intrinsic Signaling Optical Imaging Characterization 25

Figure 4. Motor Maps Characterization 28

Figure 5. Lesion Volume Measurements Performed Through MRI and Histology 32

Figure 6. Grid Walking 35

Figure 7. Neurological Deficit Score and Corner Turn Test 36

Figure 8. Cylinder Test 39

Figure 9. Evoked Area in Impaired Forelimb 41

Figure 10. ISOI: Evoked Peak Amplitude in Impaired Forelimb 42

Figure 11. Motor Maps Amplitude and Map Size for Impaired Forelimb 45

Figure 12. Motor Maps Sagittal Coordinates Distribution of Mean Amplitude 45

Figure 13. Latency of Peak Amplitude Maps 48

List of Supplemental Figures

Figure S1.ISOI: Evoked Response from Sensory Stimulation in Both Hemispheres 65

Figure S2. ISOI: Evoked Area in Non-Impaired Forelimb 66

Figure S3. ISOI: Evoked Peak Amplitude in Non-Impaired Forelimb 67

Figure S4. Motor Maps Amplitude and Map Size for Unimpaired Forelimb 69

Table 1. Neurological Deficit Score 69

List of Abbreviations

CFA – Caudal Forelimb Area

ChR2 – Channelrhodopsin 2

FL – Forelimb

HL - Hindlimb

ICH – Intracerebral Haemorrhage

ICMS – Intracranial Magnetic Stimulation

ISOI – Intrinsic Signaling Optical Imaging

LBMM – Light-based Motor Mapping

MCA – Middle Cerebral Artery

MRI – Magnetic Resonance Imaging

M1 – Primary Motor Cortex

M2 – Secondary Motor Cortex

SNc – Substancia Nigra Pars Compacta

S1 – Primary somatosensory cortex

TMS – Transcranial Magnetic Stimulation

RFA – Rostral Forelimb Area

ROIs – Regions of Interest

VTA – Ventral Tegmental Area

Acknowledgements

It is with a weird feeling that I am finishing one of the shortest yet most important part of my education, and my life. The completion of this project could have not occurred without the support and the help of many people around me.

First of all, I would like to thank my supervisor, Greg Silasi, who supported me during my master's, helped me grow as a person, and gave me the chance to work on such an amazing project. I would also like to thank the members of the Silasi Lab that have come and go but left me all with good memories of this period of my life. A special thanks to Zachary Eckert, who established an important part of my project, and shared with me his precious knowledge. A very big thank you to Sierra Darryl Hedges, who worked beautifully on the histological section of this thesis. I would also like to thank Shafik Algharbi, for his work on my scripts and his unlimited support, Rana Abdelhalim, for making me feel at home on my first day at the lab, Irina Morozov, the best lab tech someone can ask for, Patrick Charry, for the wonderful conversation about sciences and many other things, Fiona Haugen, for the laughs and all the picture of your cat, and finally the last but not least, Beatriz Romero Quineche, for the support through the hard times and the good times, and for the many DQDs that kept me sane.

I would also like to thank Bruno Souza and Maxime Abran, from LabeoTech, for their software and hardware engineering support, allowing me to complete an efficient data analysis through their rapid work.

Thank you to my thesis advisory committee, Dr. Richard Aviv and Dr. Armen Saghatelyan, for their knowledgeable advice and feedback providing me the tools to complete this project.

Thank you to my family and friends who listened to me and helped me when I needed advice, and forced me to allow myself some breaks. A special thank to my partner, Amine, who was there when I needed it the most and pushed me until the end.

Thank you to the F1 Ferrari team, who taught me to go through failure and always land back on my feet.

And finally, a small yet very important thanks to my mice, without whom this project would have not been possible.

1. Introduction

1.1 Intracerebral Haemorrhage

Intracerebral haemorrhage (ICH) is a subtype of stroke that accounts for approximately 10-15% of stroke cases in Canada (1). With recent biomedical advancements, many stroke treatments have been developed, increasing survival rates following stroke incidents. However, the majority of survivors end up with long-lasting disabilities (2,3). This increase in ICH burden highlights the importance of having a better understanding of stroke impairments and recovery.

ICH is caused by the spontaneous disruption of the blood vessels in the brain, leading to a hematoma and subsequent oedema provoking an increase of intracranial pressure. ICH is characterized by two phases of injury: the primary injury occurs in the first hours after stroke onset, while a phase of secondary injury takes place later and can last for multiple days (4). An initial rapid expansion of the hematoma exerts a mass effect in the brain, disrupting the parenchyma, which may lead to brain herniation (5–7). Following this first phase, an inflammation cascade paired with oxidative stress, thrombin accumulation and iron toxicity takes place, contributing to brain tissue death and functional damage (8,9). Over time, a reduction of the edema with clot absorption is observed, leaving a lesion that is typically smaller than the initial hematoma, but also significant atrophy of surrounding brain tissue (10).

Haemorrhage in the brain commonly occurs in deeper brain regions by smaller vessels branching from larger arteries. The drastic increase in blood pressure within these smaller vessels can result in microvessels bursting (7). One brain region where this commonly occurs is the striatum, where the leticulostriate arteries branch off from the main middle cerebral artery (11).

1.2 The striatum and its sensorimotor functions

The striatum is known as the primary motor input of the basal ganglia. Being the initial recipient of the cortico-basal ganglia-thalamic pathway, the striatum plays a role in the cortical information relay and processing to downstream premotor target. Receiving descending projections from the cortex, the striatum computes the motor information and sends it to the substantia nigra for further

assimilation of the input (12). Three main subregions are widely accepted in the striatum: the dorsolateral striatum involved in sensorimotor functions, the dorsomedial striatum playing a role in goal-driven behavior and the ventral striatum, known as the limbic domain (13–15).

The use of rodent models to study the basal ganglia has been increasing in the last decades. Despite the larger complexity of the human brain structure compared to rodents, functional and topographical similarities exist between them. The three main subregions of the striatum, the associative, limbic and sensorimotor field, have been found in both species with a similar spatial localization (16). Moreover, in a recent comparison between humans and mice cortico-striatal pathways, it was found that sensorimotor regions shared similar functional connections (17). Although it is important to note that this was true for the posterior and medial part only. This similitude was also functionally comparable with a convergence in the pattern activation of dorsolateral striatum following motor behavior testing in patients and mice (18). These studies demonstrate that rodents are an acceptable model for translational research of the striatum.

Projections from many brain regions innervate the different striatal subregions. A major portion comes from the motor cortex, but the thalamus, the pre-frontal cortex and other nuclei, such as the midbrain and globus pallidus, also send inputs (19). One important input of the striatum is dopaminergic neurons from the ventral tegmental area (VTA) and the substantia nigra pars compacta (SNc). The VTA innervates in the ventral part of the striatum whereas the SNc directs dopaminergic output in the dorsal striatum (20,21). Motivation and sensorimotor functions were correlated with dopamine release in the ventral and dorsal subregions respectively. Inputs from dopaminergic neurons in the ventral striatum have been found to modulate reward-seeking behavior (22–24). Indeed, development of addiction behaviors and certain neuropathological diseases have been linked with dysregulation in the ventral striatum (25,26). Alternatively, changes in dopamine neurotransmission within the dorsal striatum has been correlated with locomotor and movement vigor alterations (27,28).

In addition to dopaminergic implication in striatal behavioral regulation, other inputs play a major role in sensorimotor functions. In the past few years, with refined labelling techniques, cortico-striatal connections have been investigated in depth due to their important implication in the

integration and processing of information related to sensorimotor and cognitive functions. Most of the cortical input descending to the striatum are from layer V neurons and connects to the dorsal domain of the striatum (29). It was previously reported that these projections are segregated in functional parallel pathways to the distinct striatal subregions (16,30). However, recent research has found that they connect to striatal neurons in heterogeneous and granular patterns (31). To elucidate the functional subdivisions of the striatum in greater detail, Hunnicutt et al. (32) completed an anatomical map of the excitatory striatal inputs. By injecting anterograde fluorescent tracers in the different regions of the cortex, this group captured dense sensorimotor innervation in the lateral striatum. More specifically, they showed compact and overlapping projections to the dorsolateral domain coming from the primary motor and sensory cortex as well as the frontal association cortex. On the other hand, in another study aiming to create a cortico-striatal projectome, researchers have found that sensorimotor domains innervate parallel to functionally related dorsolateral striatum subregions but also send convergent inputs to the rostral and caudal part of the dorsal striatum demonstrating a topographically intermingled pattern (33). These studies highlight the complexity of a heterogenous cortico-striatal network composed of convergent connections as well as segregation.

The neuronal associations between the cortex and the striatum participates in the role of basal ganglia regulating behavior. The striatum is acknowledged for its involvement in reward-directed behavior and skilled motor learning (18,34), but it also serves functions in movement kinematics control and decision-making behavior (29,35,36). In a study of Forstmann et al. (37), patients in an MRI were required to indicate the direction of movement of a collection of dots on a screen by clicking a button on either the left or the right. Vocal cues were employed to determine either a speed or accuracy conditions for the following stimulation and informing participants of their performance at the end of the trial. MRI results showed that cortico-striatal tract activity was predicting the response efficiency of the patients, suggesting that these connections are correlated with the speed-accuracy trade-off imposed during the trials. Work in rodents have also demonstrated the implication of the striatum in decision-making regarding which motor sequences to execute during spontaneous exploration. Neuronal activity in the dorsolateral striatum was recorded (using fiber photometry) while mice explored an open-field to measure the neuronal mechanisms behind naturalistic behavior sequencing (38). Simultaneous recording of spontaneous

behavior through motion sequencing allowed the investigators to partition the activity of mice in multiple sub-second behavioral syllables. An increase in neuronal activity was observed during syllable transitions accompanied by comparable photometry waveforms in morphologically related behavior syllables. These behavioral sequence transitions were altered when the dorsolateral striatum was lesioned, demonstrating the importance of this brain region in modulating and organizing the specific behavioral structure at a sub-second temporal scale. Execution of precise motions and action-based sequences requires the capacity to prevent movement completion as well. A number of papers have reported that the probability of making a stop motor response in humans, when completing STOP and GO assessments, has been correlated with activity within the striatum (39–41). In addition, activation of cortico-striatal pathways using light-sensitive neurons led to behavioral inhibition in mice (42), reaffirming the influence of the striatum in inhibition of motor program.

Although less studied and known, the dorsal striatum is also involved in sensory modulation. Recordings of striatal neurons using whole-cell patch clamp was completed in mice and their activity assessed using whisker and visual stimulation (43). Bilateral whisker stimulation led to an increase in both dorsolateral and dorsomedial region activity whereas the visual cues only exhibited responses in the dorsomedial striatum. Another study found that the temporal component of a set behavioral habit was dependent of the dorsolateral striatum somatosensory representations (44).

Overall, making a series of various kinematics-composed movement when spontaneously behaving implicates major striatal functions that plays a part in overall sensorimotor regulation. Its motor regulation through dopamine together with its important connections with sensorimotor regions make the striatum a key region for sensorimotor behavior.

1.3 Motor cortex as a sensorimotor hub

In sensorimotor functions, the motor cortex is a crucial part of transmitting descending commands to the body. Accessing both the spinal cord and the regions in the brain controlling body parts, the motor cortex participates in the integration and control of sensorimotor information. The primary motor cortex (M1) and secondary motor cortex (M2, or supplementary motor cortex in humans), are

the basic sensorimotor cortical regions. While both M1 and M2 have projections to the spinal cord, most of the motor cortical projections are found in M1 (45,46). These cortico-spinal neurons are innervating directly on spinal motor neurons in human M1 whereas the connections between M1 and the spinal cord are not direct in mice (47). Although there are differences between the human motor cortex and that of the rodents, the cortical functional organization has been shown to be well preserved in the mouse brain (48).

M1 and M2 are located in the agranular cortex of the mouse, with M1 residing in the frontal agranular region and expanding in the medial area and M2 within the medial agranular field (49). With specific distinctions in their connectivity, M1 and M2 have been found to possess functional differences. M2, receiving a large amount of sensory inputs, is thought to participate in the primary motor planning and action control, whereas M1 regulates the overall movement execution (46). While these two cortical regions define the broader borders of the motor cortex, the forelimb motor regions in mice have been extensively studied. The rostral forelimb area (RFA) located within M2 was originally reported as the second cortical region able to evoke forelimb movement, the first one being the caudal forelimb area (CFA) in M1 (50). The two motor representations were since then validated using intracranial microstimulation, with the CFA occupying a large area and expressing distal forelimb movements, and a smaller RFA region anterior to the CFA evoking more proximal movements (51). As both the CFA and RFA are necessary for proper control of forelimb movements, the RFA seems to be correlated with fine skilled motor movements (52). Brown and Teskey (53) reported a specific segregation of movement representations between the rat CFA and RFA using ICMS, where the RFA expressed grasping movements and the CFA led to reaching movements. Moreover, the forelimb motor regions have also been linked with sensory-input transmission. In a study from Kunori and Takashima (54), they were able to measure excitatory response *in vivo* with voltage-sensitive dye in both the CFA and RFA following forelimb stimulation. This activation was shown to be relayed from the CFA to the RFA via cortico-cortical pathways after observing responses in the CFA following deactivation of the RFA but no response in any forelimb regions after CFA inactivation. Many other studies have reported the different connections between the two motor regions, important for the control of forelimb movements (55–57).

Bilateral connections also exist for the CFA and the RFA, allowing the forelimb motor regions to modulate both the ipsilateral and contralateral forelimb (57,58). Indeed, neuronal activation was observed in the ipsilateral hemisphere as rodents were utilizing their forelimb for different behavioral tasks (59,60). Both forelimb motor representations share connections with their homologs in the other hemisphere with some functional and topographic differences. The RFA has been found to induce more facilitatory response to its homolog contrarily to the CFA which modulates more inhibitory effects (61). There is also divergence in the density of their interhemispheric connections where the RFA sends less inputs to the opposite hemisphere compared to the CFA (57).

The motor cortex has a definite and important role in relaying and processing motor information to control movements. With M1 and M2, present in both humans and rodents, sensorimotor modulation occurs bilaterally to define broader but also fine motor behavior. Its functions make it an important brain region to study in relation to motor impairment following brain injury.

1.4 ICH, behavioral deficits and spontaneous recovery

As described earlier, the striatum is commonly affected by ICH, resulting in motor and sensory dysfunction following ICH. As a result of the haemorrhage, structural modifications of the brain happen, such as changes in axonal organization and projections, leading to behavioral deficits. White matter injury is a frequent occurrence seen in patients following ICH, leading to poor motor outcomes (62,63). In rodent models, the destruction of axonal fibers was observed six hours after ICH onset with significant suppression in axonal transport in the contralateral hemisphere (64). In rats, peri-hematoma axonal injury was also assessed one to three days after ICH induction including myelin fragmentation and axonal damage (65).

As a consequence of ICH injury, asymmetric limb impairments, walking difficulties and dysregulated balance have been observed (66,67). Early-onset deficits are observed in human patients during their hospital stay and are commonly lasting for a long-period of time without full recovery (67,68). A similar injury progression has been replicated and evaluated in rodents. In a rat model, it was discovered that ICH causes a reduction in activity level, turning bias (the animal is more likely to turn

in one direction), and limb dysfunctions (11). These impairments can be seen in the first week following stroke onset and can last for multiple weeks. In stroke-induced rats, Clarke and colleagues (69) noticed impaired forelimb reaching in a skilled reaching motor task. The impaired paw showed a reduction in both the reaching attempts and successful attempted reaching that lasted four weeks post-stroke with little behavioral improvement. In another study, ICH mice exhibited forelimb dysfunction up to five weeks after stroke induction with a high number of hand misplacement in a grid walking test compared to sham animals. This dysfunction was correlated with axonal disruptions in the brain (70). However, despite long-term functional deficits, recovery of behavioral function and brain structure during the weeks following ICH has been studied in both humans and animal models.

If full recoveries are unusual, patients see their functional impairments partially restored after their incident. This process is time-dependent, lasting for weeks after the stroke onset. These recovery events have been considered by Cassidy and Cramer (71) in three different epochs in humans who have experienced a stroke episode. The first epoch occurs in the few hours post-stroke. Brain repair starts in the second epoch with the most robust phase of spontaneous recovery, which is lasting in the first month after onset. During this period, neuroplasticity has been observed with increase in dendritic spines and dendritic branches in addition to axonal sprouting leading to the creation of new connections (72–75). The last epoch is seen as the chronic phase of brain repair with stable endogenous repair-related events but also possibility of further structural adjustments. This chronic phase is thought to last generally until the third month post-stroke but can be longer (76). Due to the repair processes and stability of brain activity, this period is thought to be critical to promote recovery and deliver therapy, although there are contradictory views on the subject (77,78). This time-dependant injury progression highlights the importance of time in recovery. The presence of heterogeneity and variability across patients lesion size and severity has brought challenges to pinpoint a precise effective recovery period, stressing the importance of additional studies on the subject.

Along these different recovery time periods, spontaneous sensorimotor behavioral recovery has been observed. A clinical study from *Lee et al.* (79) demonstrated an improvement in upper and lower limb sensorimotor functions up to 3 months following ICH incident. Using MRI, they found that

the recovery of the upper limb seemed to be related to the striatum, internal capsule and thalamus. In a similar manner, hand and arm dexterity were shown to improve in stroke subjects starting at four weeks and increasing until the third month after stroke onset (80). Many animals studies were able to assess improvement of functions acutely and chronically following ICH induction as well (81–83).

This spontaneous mechanism of brain repair after injury leading to improvement of motor functions demonstrates the possibility of better outcomes for ICH patients. Understanding the underlying functional processes could allow greater restorative therapies to ameliorate the long-term deficits observed after ICH.

1.5 Remapping in the sensorimotor cortex

1.5.1 Intracortical microstimulation

The behavioral recovery process occurring after stroke injury could be explained by a reorganization of sensorimotor representations in the brain. The functional recovery following brain injury has been thought to emerge from three mechanisms: an increase of activity within the peripheral zone of the lesion, an increase of activity in the opposite hemisphere and a rearrangement of the regions surrounding the affected area (76). Sprouting of new axons and regrowth of dendritic spines have been observed in the partially-lesioned area surrounding and adjacent to the injury, suggesting a repair process in which peri-lesion area and intact regions of the ipsilesional hemisphere participates (84–88).

Additionally, an increase of contralateral projections innervating to the connected motor regions of the lesion area and greater dendritic arborization in the non-lesioned hemisphere were exhibited following stroke (89–91). Bi-hemispheric influence on motor recovery is a phenomenon that was largely studied. Observations of plasticity within the contralesional hemisphere linked with functional activation suggested that the opposite hemisphere might play a role in recovery (92–94). Other studies, on the other hand, have found that contralateral activity might lead to maladaptive plasticity. The augmentation of the non-lesioned hemisphere motor cortex pathways could participate in abnormal motor functions where the paretic limb will be used less and recover poorly

(95,96). The implication of both hemispheres in the stroke injury progression exposes the importance of considering the whole brain when studying the disease.

The third mechanism suggest that adjacent regions to the lesion reorganize following stroke. Somatotopic reorganization is observed by the displacement of functional regions around the injured area, or at more distant sites for larger injury, to compensate for the loss of function within the stroke site. One great approach to evaluate this mechanism is the mapping of sensorimotor representations. Mapping experiments have first started with Fritsch and Hitzig in 1870 (97), who discovered that electrically stimulating the brain led to evoked movements. Since then, brain mapping techniques have developed and become more precise. In humans, transcranial magnetic stimulation (TMS) is used to stimulate neurons in the motor cortex allowing evaluation of functional motor pathways (98,99). However, stimulation can only be done at the surface of the brain and lacks spatial precision. Using animal models, intracortical microstimulation (ICMS) allows evaluation of evoked motor responses from direct synaptic stimulation by applying electrical stimulation directly within the brain parenchyma (100). By exciting the motor cortex with short-train pulses ICMS, simple movements outputs were observed (101,102). On the other hand, complex multi-joint movements such as reaching and grasping in addition to multiple simultaneously evoked body-part movements were observed when using long-train pulses (103–105). These different types of evoked movements demonstrate the capacity to characterize cortical representations using ICMS. As such, the reorganization of somatotopic regions following stroke injury was well studied using ICMS.

When inducing a stroke in the motor cortex, studies have shown that the lesioned functional regions are displaced and represented in other brain area (106,107). In a study by Frost et al., (108), the disruption of the hand representation by ischemic stroke in squirrel monkeys led to an enlargement of that representation in the premotor cortex. The remapping observed in the primates was correlated with an improvement of hand motor skills. The resulting modification of sensorimotor maps after stroke has been shown to be influenced by the size of the lesion. Smaller lesions in the CFA caused an increase of plasticity in the peri-lesion area whereas larger lesions have been found to impact more distal regions (109–111). The demonstration of an increase of cortico-spinal connectivity and an expansion of the contralesional representation was seen after large injury

following motor cortex stroke. (112,113). Overall, ICMS experiments were able to exhibit a compensation of stroke injury in the brain represented by reorganization of partially or non-damaged regions. However, the use of ICMS limits the research possibility in stroke recovery.

ICMS is an invasive procedure in which numerous electrodes are implanted into the brain multiple times. Additionally, in order to use the electrodes, a craniotomy is required, adding to the invasiveness of the experiment. The stimulation repetition with electrodes in various brain regions ultimately results in disruption of the cortical tissue, preventing the subsequent utilization of the animal. Consequently, multiple animal cohorts are needed when evaluating different timepoints thereby preventing statistical correlation on a longitudinal temporal scale. Furthermore, ICMS experiments are not able to study specific type of neurons, as the electrodes stimulate electrically all the cells in a distinct range. To overcomes these limitations, a new mapping tool has been developed: light-based motor mapping (LBMM).

1.5.2 Light-based motor mapping

LBMM utilizes light to stimulate specific cells through activation of light-sensitive ions channels. These channels, also called ospins, originally came from algae and were expressed in animal cells to facilitate their activation (114). Following this novel technique, transgenic mice were developed incorporating channelrhodospsin (ChR2) within the pyramidal neurons of the layer V, driven by the Thy1 promoter (115). In these transgenic mice, movements can be evoked through the application of light, within a spectrum of 350nm to 550nm, on the cortex (116). Layer V pyramidal neurons possess elongated dendrites that span across the cortex to the superficial layers permitting their excitation without penetrating the brain tissue. Motor maps and evaluation of cortical sensorimotor functions has been accomplished with the use of this mice expressing opsins in various cell populations, providing researchers a more comprehensive understanding of the motor cortex and its activity related to movement control (117).

An additional advantage of LBMM is the activation of cortical neurons through an intact skull. The development of a cranial chronic window surgically implanted on top of the mouse skull opened the door to longitudinal assessment of motor cortex functions (118). With an intact brain and skull, the

rodents can be mapped multiple times on a long temporal scale enabling measurements of the cortical state at different phases of injury in the same animal. Evoked movements from the light-sensitive stimulation of neuronal cells can be used to evaluate the remapping of the sensorimotor representations following stroke. Harrison et al. (119) used LBMM paired with sensory mapping to assess spontaneous cortical reorganization up to 8 weeks after inducing a cortical stroke in either the forelimb sensory area or motor area. Thy1-ChR2 mice with a unilateral transcranial window were utilized to stimulate and image the sensorimotor regions. A displacement of the forelimb sensory representation within the motor forelimb representation was observed after sensory cortex injury without impacting the motor map itself. Even if sensory responses were evoked in the motor representations at baseline, the sensory responses were reduced only when injuring the sensory forelimb region. This study shows that longitudinal analysis of cortical remapping subsequent to stroke injury can be accomplished using LBMM. Moreover, sensory mapping demonstrated the implication of sensory representations within the motor regions.

LBMM, as a non-invasive tool, has been utilized to advance the study of unilateral motor cortex changes following a stroke injury within the cortex. This sensorimotor mapping methodology represents a progressive advancement toward a more comprehensive knowledge of the mechanisms underlying stroke rehabilitation.

1.5.3 Intrinsic Signaling Optical Imaging

Sensory integration plays a major role in the planning and execution of movements. The primary somatosensory cortex (S1) is situated in the anterior parietal cortex in humans with four connected regions. One of this region, the main area for cutaneous sensory information integration, is the homolog of the rodent's S1 and sends projections to similar regions in both species (120). Connections between S1 and M1 are well known and have been shown to play a role in relaying and processing sensory information but also in the modulation of sensorimotor functions (121–123). Additionally, an overlap between the limb sensory and motor representations in rodents was revealed, emphasizing the functional proximity between sensory and motor activity (124–126). This sensorimotor information integration is needed for precise motor control and participates in the

kinematics and prediction of motor movements (127–129). With the importance of sensory information processing within motor behavior, its evaluation in relation to motor function injury is essential.

The assessment of sensory responses in the motor cortex can be accomplished by providing a sensory stimulus to the animal and recording the evoked activity in the brain. One such tool for sensory mapping is intrinsic signaling optical imaging (ISOI). ISOI can evaluate non-invasively the functional sensory representations evoked from afferent stimulation in real time (130,131). ISOI is performed by capturing the intensity of reflected light from the cortex. The reflective properties of the brain are modulated by local blood flow; therefore, this method allows for quantification of activity dependent changes in blood flow. The activity-dependent changes observed are referred to as intrinsic signal and represent the dynamic response of oxygen consumption by neuronal cells and blood volume changes following brain activity increase (132). Different light wavelengths are absorbed by the blood in varying degrees; however, the wavelengths predominantly used for ISOI are the red light, which indicates the alterations in deoxyhaemoglobin level and the green light, which reflects the total haemoglobin concentration (133,134). In ISOI, blood flow is used as a proxy for neuronal activity. Following firing changes in the brain, a hemodynamic response can be observed (135,136). First, an initial increase of deoxyhaemoglobin blood signal occurs as a result of the neuronal activity metabolic demands. Compensating this change, oxyhaemoglobin blood flow augments, followed by a final delayed increase of oxygen-filled blood flow to answer the high-energy demand of blood flowing through the tissue (137). This process, also called neurovascular coupling, can be employed to measure functional sensory impairments following cortical injury, thereby offering critical understanding of the underlying recovery mechanism.

Various studies have assessed the reorganization of sensory representations after a stroke in the sensorimotor cortex (119,136,138). In a study from Clarkson *et al.* (139), forelimb and hindlimb sensory cortical maps were greatly reduced after the cortical injury. However, from 28-56 days after the injury, a substantial recovery in their sensory maps was observed, without returning to pre-injury level. This alteration in sensory representations was associated with impairments in sensorimotor functions. The animals exhibited a heightened incidence of foot faults when walking on a grid, which

persisted for 8 weeks, alongside an increase difficulty to retrieve food pellets, which recovered by day 14 following stroke onset. In an additional study, the reorganization of forelimb sensory maps together with neuronal activity and connectivity changes were shown (140). ISOI demonstrated a shift in the forelimb sensory representations in adjacent regions subsequent to stroke induction. Stimulation of the forelimb 8 weeks post-stroke evoked a response within the primary motor cortex and hindlimb cortex, suggesting that the functional forelimb representations took over the surrounding brain area. This remapping was paired with an increase of neuronal activation in the peri-infarct region. Moreover, the stroke resulted in a reduction of connections between the forelimb representation and the somatosensory cortex while eliciting an increase in cortico-striatal pathways, implying a functional compensation from the striatum. These studies demonstrate that ISOI is a sensitive tool to investigate brain changes following stroke in relation to sensory function, and when paired with other techniques, it can provide a comprehensive assessment of stroke recovery.

1.6 Correlation between striatal-restricted injury and changes in motor cortex

Functional effects arising following stroke can result from associated brain areas outside of the peri-infarct region. Structurally undamaged regions of the brain can show reduction of functional maps, suggesting efferent projections are implicated in the neurophysiological dysfunction. Work from Gharbawie and colleagues (141) presented behavioral defects in middle cerebral artery (MCA) stroke rats which damaged the lateral neocortex but spared the M1 brain region. The forelimb movement representation in M1 was reduced after stroke induction. In addition, they observed skilled reaching impairments in the animals. This demonstrates that the MCA rats had impaired primary motor cortex function although the structure was not directly lesioned.

A following study of Gharbawie and others (142) examined a similar influence of MCA stroke lesions in M1 motor maps and related behavior. Striatal and sub-cortical lesions were produced in rats without impacting the M1 region. Consistently, performance of skilled reaching behavior in the animals was shown to be diminished after the stroke, demonstrating motor impairments. Furthermore, forelimb motor maps were diminished in MCA rats, with representations being

completely absent in some animals. Damage in the striatum and sub-cortex led to neurophysiological dysfunction in the spared M1, showing that stroke impacts can act beyond the peri-infarct region.

The numerous connections between the striatum and the motor cortex have been shown to influence sensorimotor functions in a healthy state. Conversely, striatal injury was shown to elicit functional damage in motor representations. The impact of cortico-striatal connections within striatal lesion appears to add a new dimension to the injury progression. In order to understand the complete mechanisms around striatal stroke, additional investigation on this process is needed.

1.7 ICH rodent models

Rodent models are widely used to characterize the deficit progression following ICH as they replicate the injury in a controlled environment with a smaller amount of time and lower cost compared to clinical studies. The ability to control for comorbidities and individual variability allows powerful statistical results and generates replicable data. As mentioned earlier, the rodent striatum has structural and functional similarities with humans, making them reliable in translational studies. Consequently, different rodent models have been established for ICH studies.

The injection of autologous whole blood model and the collagenase model are two predominantly used models (70). In the whole blood model, stroke is induced by injecting autologous blood in the brain mimicking a single intracerebral bleed. In the collagenase model, collagenase, a bacterial enzyme, generates an intracerebral hemorrhage by rupturing the collagen of the blood vessel walls in the brain (143). Both models have differences in lesion size and structural and functional impacts. The blood model shows a reduced hematoma compared to the collagenase model with less associated structural injury. Barrat and colleagues (70) saw a great decrease of cortical projections, especially in the uninjured hemisphere, in the collagenase model compared to autologous blood injection. This relates to ICH patients that had lower measure of connectivity in the contralesional motor cortex. Additionally, functional recovery from the collagenase model persisted longer and did not return to baseline after 28 days in rats, mimicking the long-lasting motor impairments in ICH patients (144). For longitudinal studies examining long-term recovery, the collagenase model is thought to be more relevant.

1.8 What parts are missing in the puzzle?

The precise relationship between cortical remodeling and functional recovery is not completely understood, especially in the relatively less studied ICH models (71,80). Gharbawie and colleagues have discussed the effect of striatal injury on M1 forelimbs motor maps and associated behavioral dysfunction (142), but evaluation of the cortical impact following striatal stroke is lacking in the literature.

Additionally, we know that sensory and motor functions are closely related. Their tight relationship has underlined the importance of studying their implication in relation to brain sensorimotor functions injury. However, only the impact of M1 representation was assessed after striatal injury. Moreover, the RFA has been shown to send a lot of projections to the striatum (57). Expanding the evaluation of cortical impact to both the CFA and RFA would allow a better comprehension of striatal stroke's impact on motor representations.

Sensorimotor mapping tools can lead to a better understanding of this brain reorganization post-stroke and its behavioral correlation (145). Compared to electrode-based mapping tools commonly used in previous studies, we see several advantages of light-based motor mapping. Optogenetics is less invasive and eliminates brain damage caused by the insertion of electrodes allowing longitudinal studies to be completed in the same animals. In contrast to prior studies, our methodology employs quantitative movement metrics (measure the size of evoked movements) instead of just annotating brain regions based on types of movements that is produced when stimulated.

Lastly, most studies looking at the association between rearrangement of brain areas and behavioral deficits in rodents did unilateral analysis. The evaluation of a single limb with its corresponding hemisphere gives a precise measurement but fails to consider the important contribution of the opposite hemisphere in sensorimotor functions. To improve our comprehension of the recovery mechanisms, investigation of the responses of both hemispheres is needed as they both act in the process.

In light of the identified gaps in the literature, this thesis aims to assess the injury and recovery progression of the sensorimotor cortex following a striatal ICH in conjunction to the related behavioral impairments' changes over time. By using LBMM and ISOI, a bilateral and non-invasive measurements of sensorimotor cortex functions will be done longitudinally. Various spontaneous behavior tests will be performed on a similar temporal scale to evaluate the functional deficits from the striatal injury at different timepoints.

2.Methodology

2.1 Animals and Timeline

The experiments in this thesis include 19 Thy1-Chr2-YFP mice (12 females and 7 males) that were 3-4 months old at the start of the experiment. The ICH group includes 5 males and 6 females, and the sham group is composed of 2 males and 6 females. Animals were housed in same-sex groups of 3-5 mice in standard cages with food and water access *ad libitum* on a 12-hour light/dark cycle. Two mice passed away during experiments, one sham and one ICH, due to complication from anesthesia injections. No mice died from ICH injury.

The animals were tested on a battery of behavioral tests twice before ICH induction for a baseline period starting one week before surgery. On the day of surgery, the mice were subjected to either sham or ICH procedures followed by implantation of a chronic transcranial window on top of the intact skull. Three days after surgery, mice repeated the behavioral tests battery and ICH animals (as well as one sham) were imaged with MRI. Motor maps were acquired on post-ICH day 4 and sensory maps on day 6. The behavior tests were performed on day 7. Mapping experiments and behavioral tests were then repeated weekly for 5 additional weeks (Fig 1B). MRI images were acquired for ICH mice on post-ICH day 14 (Fig 1A). After the 6^{th} week post-ICH, animals were perfused and their brains collected for histological analysis.

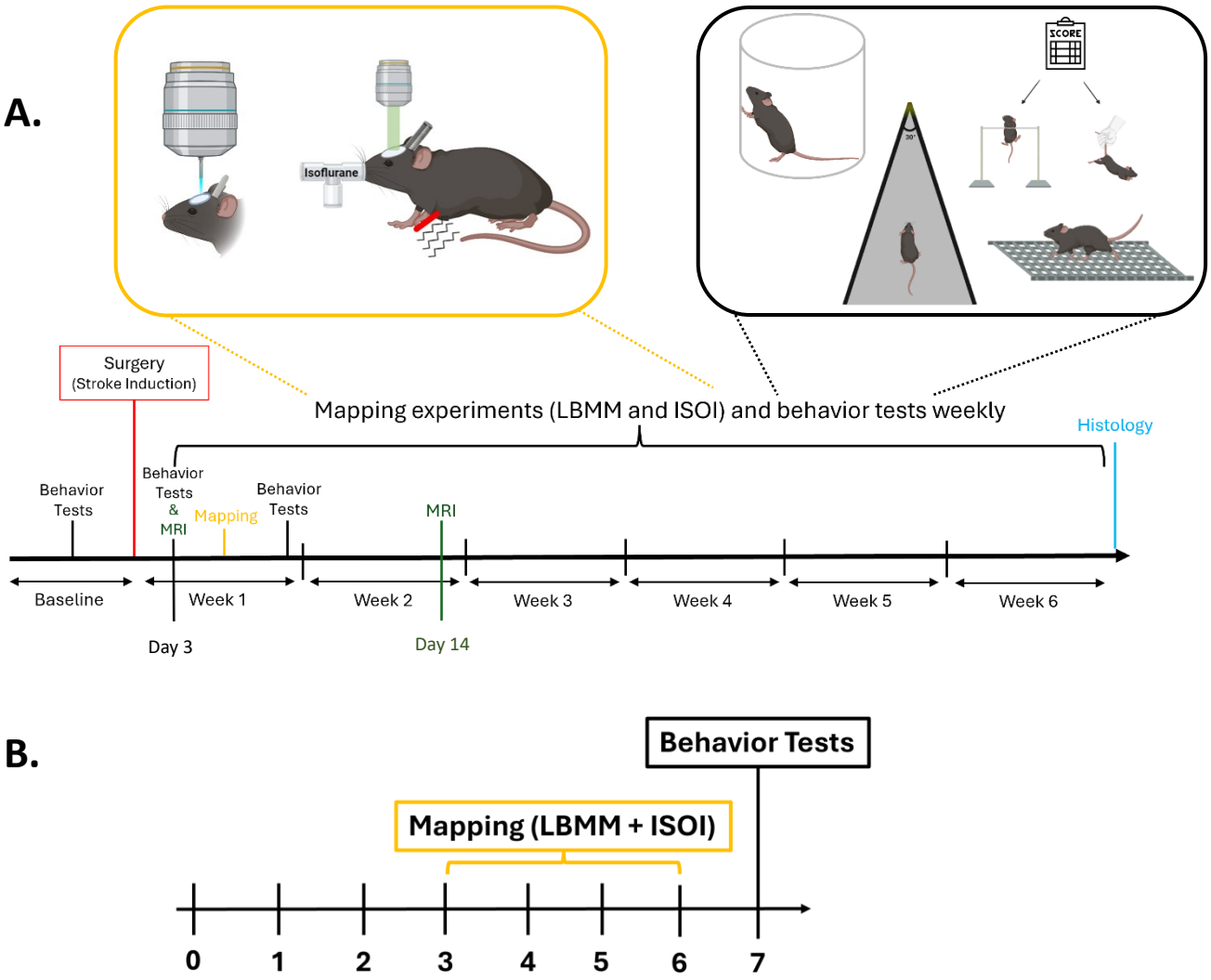

Figure 1. Experimental Timeline: A: A battery of behavioral tests (the cylinder test, the grid walking test, neurological deficit score and the corner turn test) was completed before surgery for a baseline measure. ICH was induced during surgery. At post-ICH day 3, mice repeated the same behavior tests followed by MRI imaging. Mapping experiments (LBMM and ISOI) and behavioral testing was then conducted weekly for 6 weeks. MRI imaging was repeated on post-ICH day 14. After the 6^{th} week, animals were sacrificed and brain tissue processed for histology. **B.** Weekly timeline for the post-ICH weeks in which each ticks represents the day relative to ICH surgery. Mapping experiments lasted 4 days followed by behavior on the last day of the week.

2.2 Surgical Procedures

ICH was induced by injecting collagenase (sigma C2399, 0.15u/µL saline) in the right dorsolateral striatum. The mice were anesthetized using 4% isoflurane to begin and kept at 2-3%-1L/min oxygen until the end of the procedure. Carprofen (10mg/mL, 20mg/kg) was subcutaneously injected

followed by subcutaneous injection of 1mL of saline. The scalp of the animal's head was shaved and cleaned with iodine. Ophthalmic ointment was applied to both eyes and anesthetic gel was administered inside both ears to prevent irritation from stereotaxic ear bars. The head was secured in a stereotactic frame and a rectal probe regulated a thermal blanket underneath the animal to keep the mice at normothermia (36.5-37.4°) during surgery. The skull was exposed by removing the scalp over both hemispheres, and using a variable speed drill, a burr hole was made in the cranial bone 3mm lateral to the right and 1mm anterior relative to bregma (Fig 2A). With a 5µL Hamilton syringe, 0.05µL of collagenase was delivered 3mm deep in the brain parenchyma at a 10° angle over 5 minutes (0.01µL/min) using a standard infusion pump (Pump 11 Elite, Harvard Apparatus). The needle was left in position 5 minutes after the end of the injection to prevent backflow. Once the needle was retracted, the skull was cleaned and dental cement (C&B Metabond L-Powder, S399, Parkell Edgewood NY) was applied on the skull as previously described (118). A circular glass coverslip (deckgläser 8mm diameter, Thomas Scientific) was placed on the dental cement and a head-fixing nylon screw was fixed at the posterior end of the window with additional dental cement (Fig 2B). Mice were kept anesthetized until the cement solidified (around 20 minutes) and were then allowed to recover in an incubator. Sham mice underwent the same procedures but were injected with 0.05µL of saline instead of collagenase.

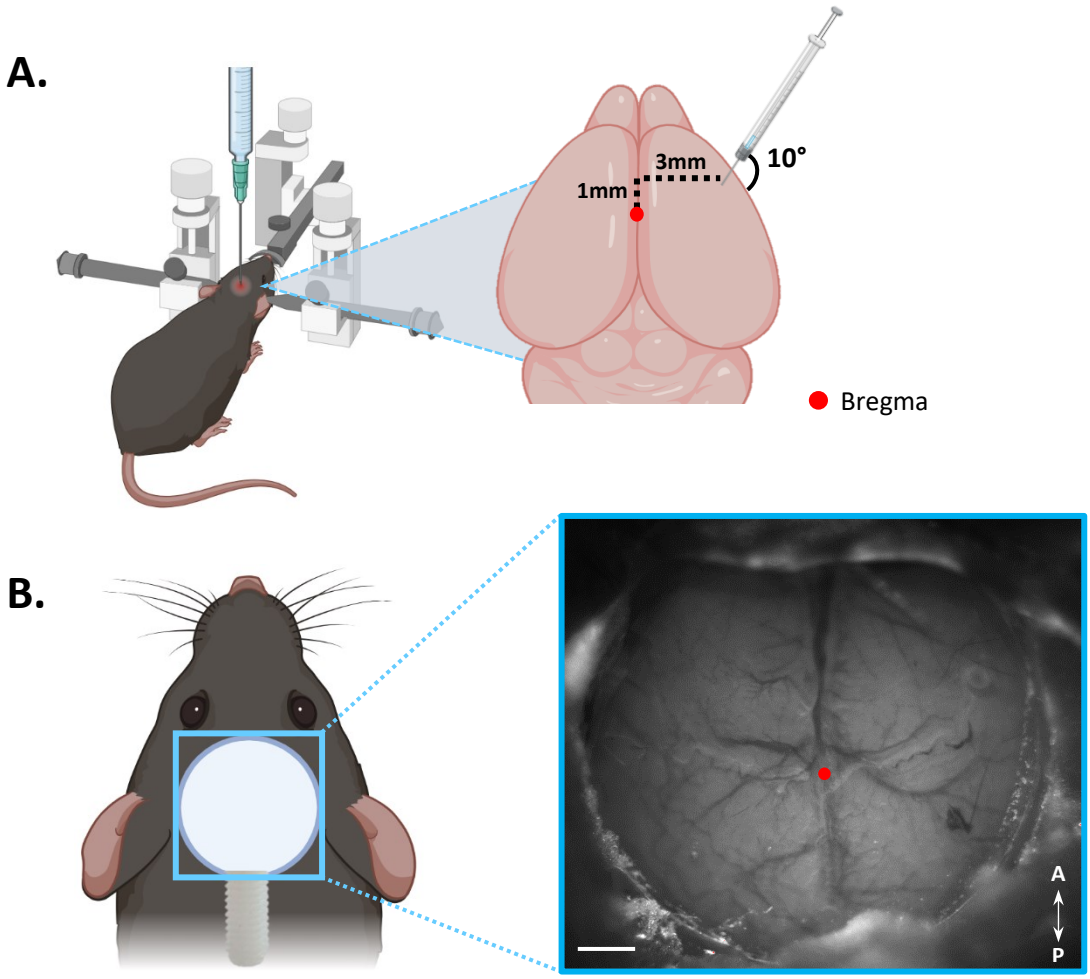

Figure 2. Intracerebral Hemorrhagic Stroke Surgery and Transcranial Window Implantation: A: Surgery of intracranial collagenase injection in the mouse striatum. The mouse was head fixed on a stereotaxic apparatus. Injection was delivered 3mm lateral and 1mm anterior from bregma at a 10° angle. **B.** Representative figure of a transcranial window implanted on top of the mouse skull following collagenase injection. A nylon screw was glued on top of the head for imaging purposes. Scale bar represents 1mm and anterior (A) – posterior (P) axis is labelled at the right bottom.

2.3 Behavioral Tests

Four different spontaneous behavioral tests were used to assess unilateral injury of sensory and motor functions. The cylinder test allowed analysis of lateralized sensorimotor impairments of the limbs. Front limbs' locomotion and coordination were examined in the grid walking test. The corner turn test helped evaluate turning asymmetry, and the neurological deficit score measured forelimb

sensorimotor deficits on a scale from 0-3. All behavioral tests, except the corner turn test, were conducted twice before surgery, at post-ICH day 3, and then weekly for 6 weeks (Fig. 1A). The corner turn test was done only once at baseline to prevent habituation to the test.

2.3.1 Cylinder Test

The mice were placed inside a plexiglass cylinder of 20.5cm height x 9.5cm diameter in an enclosed isolated space. The cylinder was illuminated from the side and below to allow visualization of the forelimb movements (Fig 8A). A raspberry-pi camera positioned under the cylinder recorded the test. The mice explored in the cylinder for 7 minutes. If less than 10 bouts of exploration were accomplished within the 7 minutes, the mice stayed in the cylinder until completion of 10 bouts, or for a maximum of 15 minutes. A full bout was characterized by the forelimbs leaving the ground and touching the wall at least once before landing back. The videos were analyzed manually. Different parameters were scored within a bout: the forelimb used to push off, the forelimb that touched the wall first, the total number of wall contacts with each forelimb and the forelimb used to land first. If both forelimbs were touching the surface simultaneously, it was assigned to the "both forelimb" category. The following equation was used to calculate contralesional forelimb preference:

$$\frac{Ipsilesional\ Forelimb}{(Ipsilesional\ Forelimb + Contralesional\ Forelimb + (0.5 * Both\ Forelimbs))}$$

2.3.2 Grid Walking

A 33cm x 20.5cm meshed wire grid, with 1cm square opening, elevated above the floor in an enclosed isolated space was used for this test (Fig 6A). The mice were positioned on the grid and allowed to walk freely on the surface for 5 minutes. Sessions were recorded below the grid on the side at a 45° angle with a cell phone camera (Pixel 6; 1080p at 30 fps) for visualization of missteps from the side perspective. Videos were analyzed by manually counting total steps and missteps for each forelimb. A misstep was characterized by a slip of the forelimb with the wrist passing through the grid. Contralesional forelimb missteps were calculated using the following equation:

$$\frac{Contralesional\ Forelimb}{(Ipsilesional\ Forelimb\ +\ Contralesional\ Forelimb)}$$

2.3.3 Neurological Deficit Score

Forelimb sensorimotor deficits were evaluated on a score from 0-3 using three subtests: forelimb wire hanging, forelimb outstretching and forelimb extension (Fig 7A). The extension test looks at the movement of the forelimbs and their extension amplitude when the animal is lifted by the base of the tail. On the other hand, the outstretching test allows observation of walking behavior of the upper limbs on a flat surface and limb outstretching when the mouse is dragged backward by the base of its tail. Finally, during wire hanging test, the mouse is suspended with both its forelimbs on a metal wire (25cm long x 20cm height) and let go. Difficulties to use the injured forelimb and compensation behavior were assessed during the test. The latency to fall was also measured. A score from 0-3 (0 = normal behavior, 3 = severe deficits, Table 1) based on the Garcia scale deficit score (146) was set for each subtest.

2.3.4 Corner Turn Test

Mice were allowed to enter an apparatus corner and explore it. When reaching the end of the corner, overstimulation of the whiskers made the mice turn in either the left or right direction (Fig 7A). The apparatus corner consisted of two pieces of hard plastic (45cm long x 20cm height) that were held together in a 30° corner by 3D-printed braces. The two walls did not join completely, leaving a narrow slit (~3mm) that allowed ambient light to enter the apparatus. Two other pieces of hard plastic covered the top to restrict any distractions. Only the base of the apparatus was open to allow observation of the mouse walking on the table surface. For each trial, the mouse was placed at the open end of the corner and allowed to walk freely toward the slit. A minimum of 6 trials was required to end the task. When immobile for more than 1 minute, the mouse would be returned to the start position. The number of turns in either direction was recorded to analyze turning asymmetry.

2.4 Mapping Experiments

2.4.1 Intrinsic Signaling Optical Imaging

ISOI was utilized to visualize forelimb sensory representations within the cortex. Brain activity was recorded by measuring the hemodynamic response to a vibrotactile stimulus delivered to the forelimbs. The animals were anesthetized with isoflurane in an induction chamber (4%-1.5L/min) and kept on the imaging rig at 1%-1L/min (light anesthesia). The head of the mouse was stabilized with the nylon screw attached to an articulating arm (Fig 3A). Optixcare eye lubricant was applied to the eyes to prevent cornea drying. Body temperature of the mice was maintained at normothermia (36.5-37.4°) with a heating pad. The forelimb was secured on a vibrating haptic-motor and fixed using poly-wax (Fig 3A). The cortical surface of the brain was imaged with a ThorLab Scientific Cmos camera and the LabeoTech LightTrack Modular Optical Imaging System (OiS200) using 630nm (red) and 530nm (green) light pulses at 10Hz (5Hz respectively). Exposure time of the camera was set at 1 millisecond and images were binned 2x2 to reduce file size and increase sensitivity. The vibrotactile stimulus was provided by powering the vibrating motor with a 5V stimulation with a pulse period of 19.8ms and pulse width of 20ms. Each forelimb received 20 stimulation repetitions every 30 seconds for a total of 610 seconds. Each repetition consisted of a 3 second baseline period, followed by a 3 second stimulation period and a post-stimulation phase of 24 seconds (Fig 3B). Once the image acquisition was done, the mice were transferred to a heated recovery cage until they fully woke up.

Analysis of ISOI was conducted with UmIToolBox, a custom script provided by LabeoTech that was used as a plugin within MatLab (R2021a). Both red and green light illumination data were acquired, but following analysis, evoked responses in the red channel were unreliably observed in a number of mice. Therefore, only the green channel data will be presented. Cortical images were aligned to bregma and scaled with the 8mm window. A high cut-off filter of 1Hz was applied to eliminate high frequency noise. Within each stimulation trial, responses were separated and averaged in two groups, pre-stimulation (baseline) and post-stimulation (up to 8 seconds after stimulation) to complete baseline normalization. The relative signal change (ΔR/R(t)) was extracted using the following equation:

$$\Delta R/R(t) = \frac{S_i(t) - bsln_i}{bsln_i}$$

Where $S_i(t)$ is the pixel value for a given *t* time and $bsln_i$ is the baseline value (retrieved from *https://labeotech.github.io/Umit/documentation/userDocs/fcns/normalizeBSLN.html*). A custom mask of the cranial window was then created and the peak response was manually selected for thresholding. The response was thresholded at two standard deviations of pixels intensities and any regions of interests (ROIs) smaller than 25 pixels were excluded. The size and amplitude of the evoked cortical response was quantified within anatomical regions of the Allen Mouse Brain Atlas related to sensory functions: forelimb and hindlimb somatosensory field and the primary motor cortex (147; Fig. 3C). Thresholded ROIs were crossed with the anatomical regions ROIs and any response outside the sensorimotor regions were excluded. For group visualisation, the peak amplitude and the map area were subsequently calculated and averaged within groups (Fig. 3D). Averaged sensory maps were created based on the average of the maximum cortical response in each mouse.

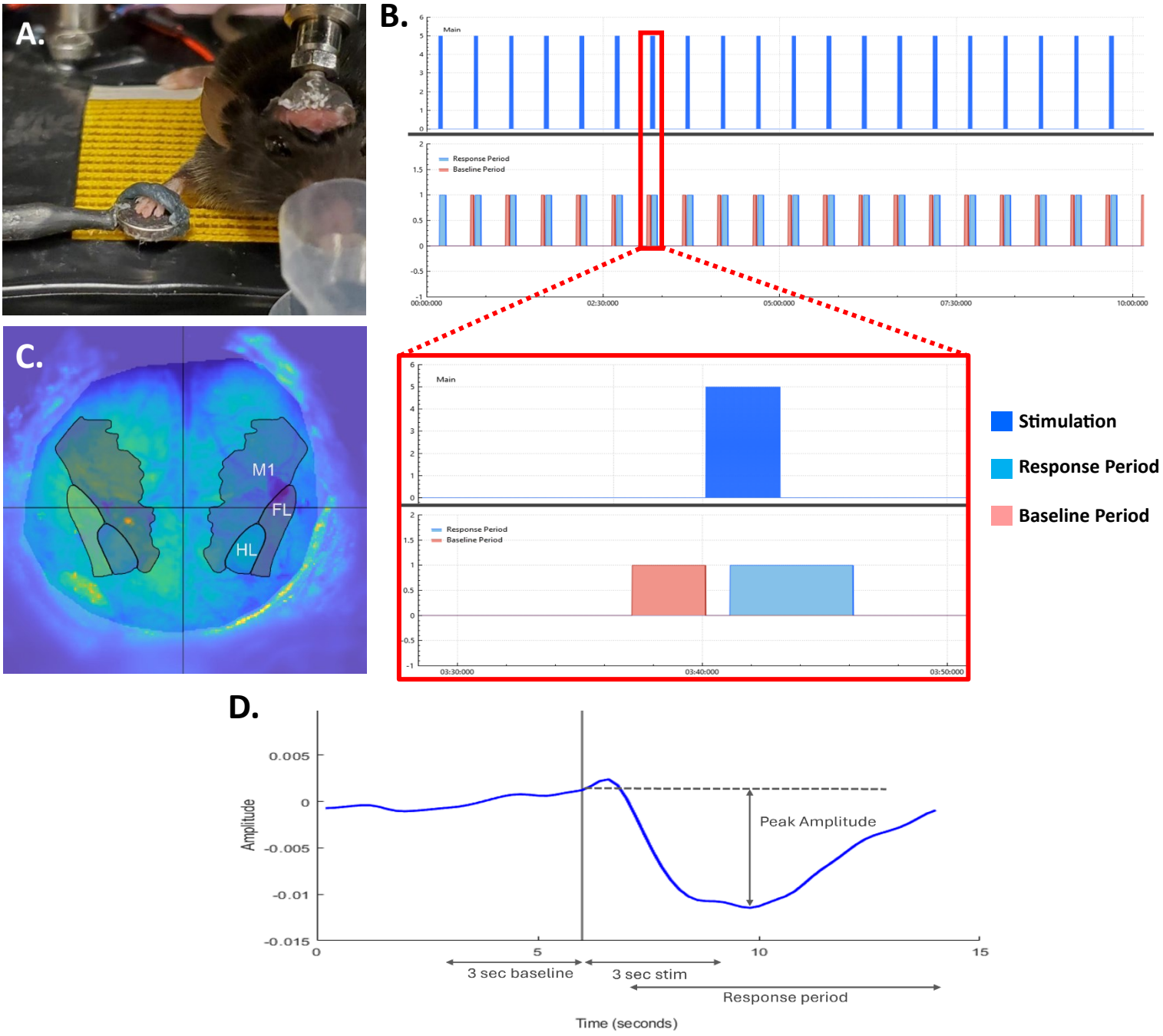

Figure 3. Intrinsic Signaling Optical Imaging Characterization: A: The mouse was head-fixed on the imaging rig and kept anesthetized with isoflurane. A vibrotactile stimulus was delivered to the forelimb using a vibro-motor apparatus. The wrist was fixed to the motor using poly wax. **B.** 20 stimulations trials were delivered every 30 seconds for a total of 610 seconds (top). A trial consisted of a 3 second pre-stimulation period (orange) followed by vibration train lasting 3 seconds (blue) and a post-stimulation period of 24 seconds (light blue; bottom). **C.** The sensory maps were aligned relative to bregma and superimposed on the Allen Mouse Brain Atlas anatomical areas related to sensory functions: forelimb (FL) and hindlimb (HL) somatosensory field as well as the primary motor cortex (M1). **D.** The signal trace during a stimulation trial. The vertical solid line delineates the stimulation initiation. Peak amplitude was calculated during the post-stimulation period.

2.4.2 Light-Based Motor Mapping

Optogenetics was used as a light-based motor mapping (LBMM) tool to assess longitudinal motor response changes from cortical stimulation following ICH. The animals were briefly anesthetized in an induction chamber with isoflurane (4%, 3L/min oxygen) and injected intraperitoneally with a cocktail of xylazine (3mg/kg) and ketamine (30mg/kg) afterwards. Optixcare eye lubricant was applied to the eyes to prevent cornea drying. The mouse head was then stabilized underneath a custom macroscope with the nylon screw attached to an articulating arm. Body temperature of the mice was maintained at normothermia (36.5-37.4°) with a heating pad. The animals were positioned under the overhead camera with the cranial window perpendicular to the imaging plane and aligned with the medial line. The forelimbs were placed symmetrically in front of the behavioral camera at the platform edge, hanging freely from the shoulder (Fig 4A). During data acquisition, the mice were kept anesthetized with constant infusion of ketamine through an indwelling needle placed intraperitoneally. A standard infusion pump (Pump 11 Elite, Harvard Apparatus) delivered ketamine (10mg/mL) at a rate of 3µL/min through a 27Gx1/2” winged needle (SURFLO, Terumo, ON, Canada) fixed to an insulin syringe.

For LBMM, the lowest laser power to evoke reliable movements in the relevant brain regions (CFA and RFA) was evaluated to generate comparable maps between mice. The resting motor threshold was established by stimulating different points in the motor cortex using a range of laser intensities (1-5mW, blue light 450nm, 5ms duration, 50µm diameter). Once the threshold was determined, an array of stimulation points spaced by 300µm was manually set over both hemispheres covering the sensorimotor cortex (Fig 4c). Blue light stimulation was then randomly delivered at a 500ms inter-stimulus interval two times for every stimulation point. The two stimulation repetitions together lasted for approximately 7 minutes. Evoked movements from the cortical stimulation were captured with a high frame-rate video camera (900Hz, 0.1ms exposure time; Fig 4B). A two-repetition map session could be repeated if the anesthesia plane was observed to fluctuate during the map acquisition. Resting motor threshold was re-evaluated after each map completion. If the mice became too light during an experiment, a brief delivery of isoflurane (4%, 3L/min) was administered to bring the mouse back to a proper anesthesia plane. A complete mapping sequence lasted on

average 120 minutes. Once finished, the mice were transferred to a heated recovery cage until they were fully awake.

Evoked movement amplitude and movement latency were analyzed to evaluate cortical response to stimulation. The two map repetitions were averaged for each stimulation point and expressed as an averaged maximum movement amplitude heatmap over the cortex for both forelimbs using a custom MatLab (R2021a) script (Fig 4C). The maximum movement amplitude is described as the maximum linear distance reached by the forelimb. Movement latency was quantified as the time (relative to the laser pulse) for the forelimb to reach the farthest position. Movement latency was calculated for each stimulation site and presented as latency maps. Group data was generated by averaging individual mouse maps within groups using a second custom MatLab script. Different motor map dimensions were further examined. The map size was calculated with the number of pixels activated. Average movement amplitude and sum were determined by the mean and addition of all pixels values respectively within the cortical map.

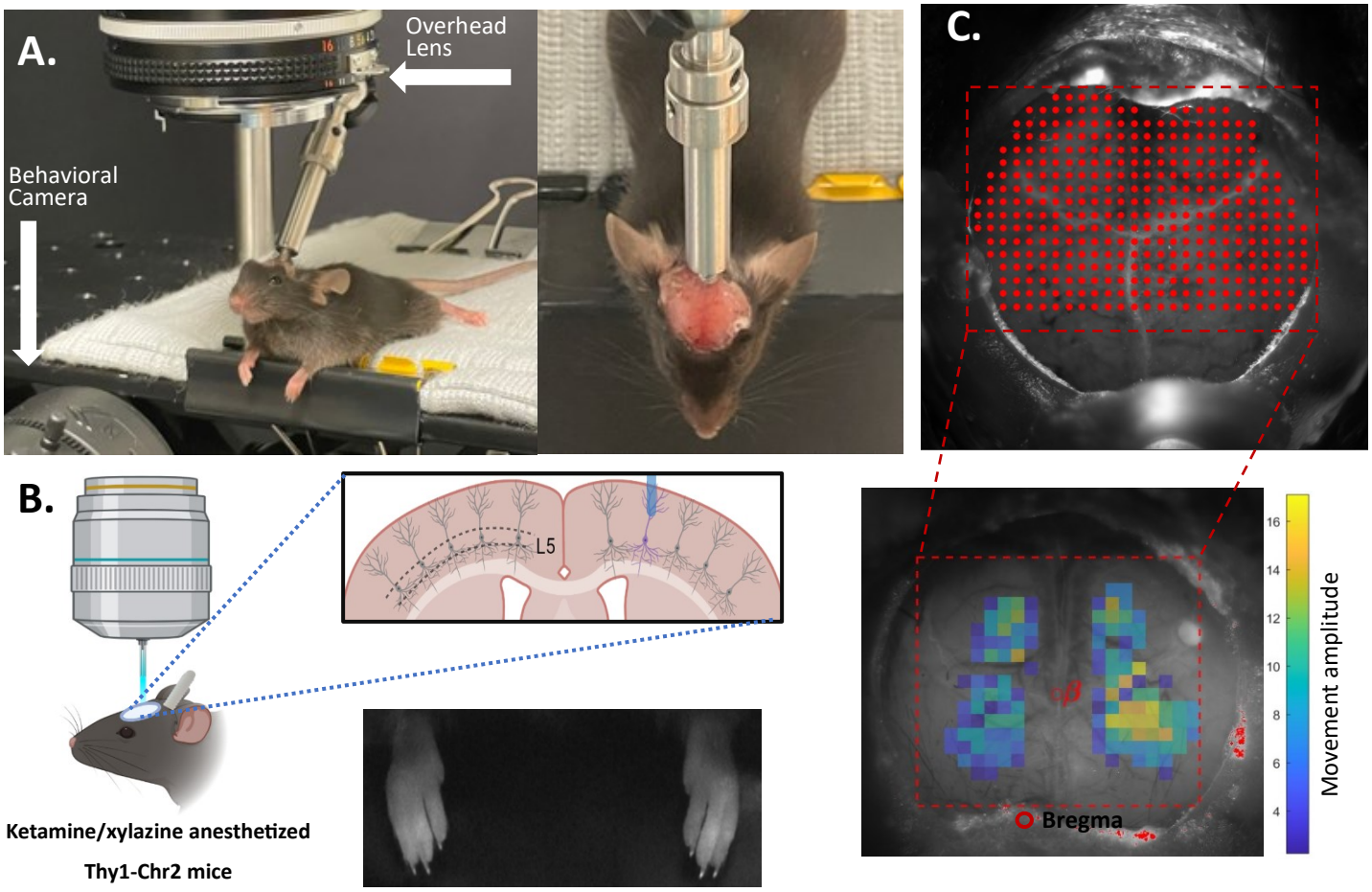

Figure 4. Motor Maps Characterization: A. The mouse was head-fixed using a nylon screw on the optogenetic rig and positioned under the overhead lens (left). Forelimbs were placed on the platform edge hanging freely from the shoulder. Behavioral camera located in front of the limbs recorded the evoked forelimb movements. A heating pad under the mouse maintained it at normothermia. The transcranial window was positioned perpendicular to the overhead lens and aligned with the medial line (right). **B.** A 5ms blue laser (450nm) pulse was delivered through the overhead lens to activate layer 5 pyramidal neurons within the cortex of anesthetized Thy1-Chr2 mice. When motor regions were activated, forelimb movements were visible and were recorded through behavioral camera. **C.** A grid of stimulation point was drawn over the mouse cortex covering the motor cortex (top). Each stimulation point was activated twice randomly, and the evoked forelimb movements amplitudes were averaged for each activation point to create a heated map (bottom).

2.5 MRI

Images of ICH lesions were acquired *in-vivo* at 3 and 14 days post-ICH using a high-field small-animal MRI (7.0T, Agilent MR901, General Electric, USA). The mice were anesthetized using isoflurane (2-4%-1.5L/min oxygen) during the procedure and kept at normothermia with a heating pad.

Respiratory rate and body temperature were monitored with a small animal monitoring and gating system (Small Animal Instruments Inc., Strony Brook, USA). Imaging was completed using a T2 fast spin echo sequence with the following parameters: slice thickness = 300 or 500 microns, 19-28 axial transverse slices, spin echo = 8, echo time = 4500ms, scan time = 5:15 to 8:00 minutes. Lesion area was outlined manually with ImageJ and lesion volume was calculated by multiplying the area for all coronal sections by the slice thickness.

2.6 Histology

Following post-ICH week 6, mice were sacrificed and the brain collected for histology. The animals were deeply anesthetized with intraperitoneal injection of euthanyl (65mg/mL, 10mL/kg). Responsiveness was examined by toe-pinch reflex. The mice were transcardially perfused with 10x PBS solution followed by 4% formaldehyde solution (Fischer Chemical, USA) at a rate of 3.2mL/min for 8 minutes each. Brains were extracted and stored in 4% formaldehyde solution at 4°C until slicing (minimum 48 hours). 100 µm coronal slices were generated using a vibratome and were mounted on 1% gelatin-coated glass slides. Sections were then stained with cresyl violet according to the procedure done by Sirkin D.W., 1983 (148).

Slides were imaged using a flatbed scanner (CanoScan 9000F Mark II, Canon) at 1200 dpi. Brain slices were compared to the Allen Mouse Brain Atlas to determine the anterior-posterior coordinates relative to bregma. Lesion and atrophy volume were measured manually within ImageJ following MacLellan et al., (146) protocol (Fig 5C):

$$V_{lost} = (V_{intact} - V_{lesion}) \times N \times T$$

Where:

V_{lost} is the volume of tissue lost
V_{intact} is the volume of the intact hemisphere
V_{lesion} is the volume of the lesioned hemisphere
N is the number of sections
T is the volume thickness

Volume of intact and lesioned hemisphere were calculated as such:

$$V_{intact\ hemisphere\ adjusted} = V_{intact\ hemisphere} - V_{intact\ ventricle}$$

$$V_{lesioned\ hemisphere\ adjusted} = V_{lesioned\ hemisphere} - V_{lesioned\ ventricle} - V_{lesion}$$

2.7 Statistical Analysis

All data were evaluated for heterogeneity and normality by plotting model residuals in a qqplot with the addition of the Levene's and Shapiro-Wilk test. For parametric data, a repeated measure ANOVA followed by a Tukey's HSD multiple comparisons post-hoc test was used. Part of ISOI and motor maps post-hoc analysis applied the Kenward-Roger degrees-of-freedom correction test. For dataset following a non-normal distribution, data was fitted in a generalized linear mixed model (GLMM) with gamma distribution and analyzed using the Tukey's HSD multiple comparisons test. The Mann-Whitney U test with FDR correction was utilized within each individual day for corner turn test analysis. After log transformation of the data, a T test with Welch's correction was executed to compare atrophy between the sham and ICH groups. All models except the corner turn test and atrophy comparison had mouse as a random effect. Statistical models of motor map amplitude and size considered mouse and hemisphere interaction as a random effect. A p-value of <0.05 was considered significant in all cases. All analyses and graphs were completed using R (Version 4.3.1, windows) in RStudio (Version 2024.04.02-764, windows) unless indicated otherwise. All singular analysis will be specified in the result sections.

3. Results

3.1 ICH was delivered in the right striatum and led atrophy of the injured hemisphere

Following ICH induction, MRI images were acquired on days 3 and 14 post-ICH. Hematoma was confirmed subcortically in the right hemisphere of all ICH mice 3 days after surgery as indicated by a

white lesion contrasting with the darker tissue (Fig. 5A). One sham mouse was also imaged to optimize MRI sequence, and no lesion was observed (data not shown). Considerable variability was observed in the lesion volume across mice, ranging from 3.13 to 17.32 mm^3, with nearly half the animals (n = 5) over 10 mm^3 and the remaining half (n = 6) falling below (Fig. 5B). On day 14, a resolution of hematoma was observed. However, three mice showed an increase in lesion volume compared to day 3 (0.42 – 2.845mm^3; 5B). A Tukey's HSD pairwise multiple comparison showed significant difference between the two timepoints (p = 0.0044)

Histological analysis revealed an atrophy of the lesioned hemisphere in ICH. A Welsh T test showed significant difference between sham and ICH group in atrophy measurements (p = 0.001, Prism v.8.2.1; Fig. 5D). Similar to day 3 MRI measures, ICH mice had a large range of atrophy, the smallest having 0.77mm^3 difference between the injured and uninjured hemisphere and the largest 11.5mm^3. Sham mice also showed atrophy, with some individuals exhibiting larger non-lesioned hemisphere and others with greater lesioned hemisphere volume (Fig. 5D). Strikingly, a number of sham mice (n = 3) had more atrophy in the injured hemisphere compared to the smallest ICH mouse atrophy. Further analysis of the anterior-posterior distribution of ICH lesions showed the maximal lesion volume close to 1mm anterior to bregma, corresponding to the anterior-posterior coordinate of the collagenase injection (Fig. 5E). Overall, these results demonstrated that ICH was successfully induced in the right striatum, with resolution of hematoma volume over time producing significant atrophy in the lesion hemisphere.

Differences in stroke lesions have been observed between males and females in previous studies (146). As such, sex difference was analyzed, but no significant differences were found between male and female lesion volumes in MRI or histology (data not shown).

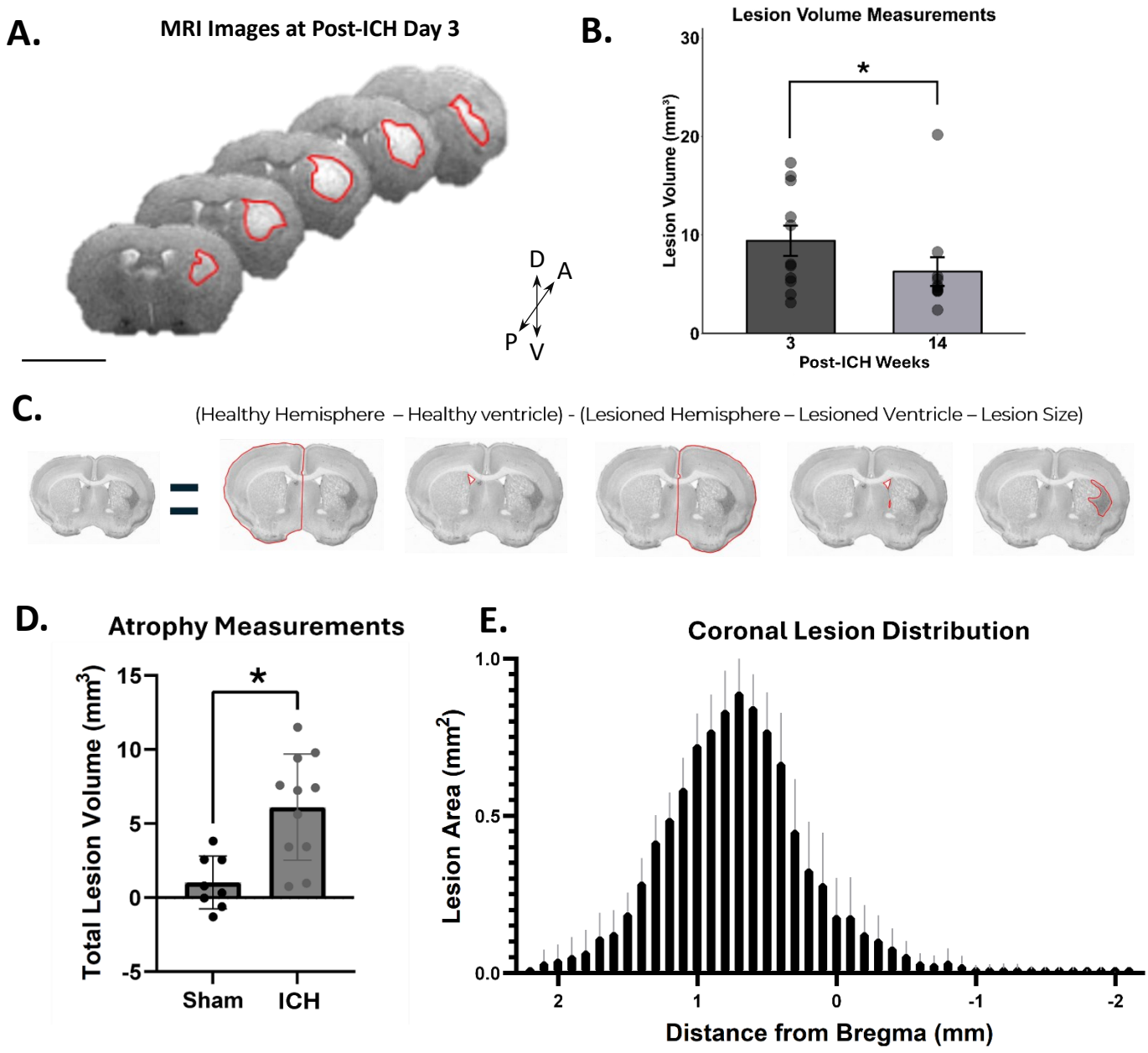

Figure 5. Lesion Volume Measurements Performed Through MRI and Histology: MRI images (500µm thickness) of one mouse at post-ICH day 3 showing lesions in the right striatum. Scale bar represents 5mm and D (dorsal) – V (ventral), A (anterior) – P (posterior) axes are displayed at the bottom right. **B.** Lesion volume (mm^3) calculated from MRI images acquired at post-ICH day 3 and post-ICH day 14. **C.** Workflow used to calculate atrophy of the injured hemisphere from the extracted brains after the 6 post-ICH weeks. Brains were sliced at 100 microns using a vibrotome, stained with Cresyl Violet and then imaged. Atrophy was measured by subtracting healthy tissue of the uninjured hemisphere to the healthy tissue of the injured hemisphere. **D.** Atrophy measurements (mm^3) compared between sham and ICH groups. **E.** Anterio-posterior distribution of the lesion relative to bregma after 6 weeks post-ICH.

3.2 Acute sensorimotor deficits were identified following ICH induction

Different behavioral tests were performed for evaluation of sensorimotor deficits after generating striatal injury. Forelimb sensorimotor coordination was assessed using the grid walking test. A forelimb misstep score was calculated for each forelimb. Three days following ICH induction, the ICH group showed a slightly higher missteps score compared to the sham group, indicating a larger number of impaired forelimb missteps (Fig. 6B). However, at the end of the first week, scores were similar between the two groups and stayed constant until week 4. Unexpectedly, sham animals expressed an increase of impaired paw forelimb missteps starting week 4 until week 6. A Tukey's HSD pairwise multiple comparison fitted with a generalized linear mixed model showed significant interaction effect between groups and timepoints (week 4: $p = 0.025$, week 6: $p = 0.034$).

Further investigation of the normalized missteps count to the total count of steps was completed (Fig. 6D). The ICH animals demonstrated a progressive increase of impaired forelimb missteps following ICH induction, presuming an enhanced difficulty to move on the grid with this forelimb. On the other hand, the sham group exhibited a similar increase of impaired forelimb missteps starting week 3 (Fig. 6D). Looking at the unimpaired forelimb, the ICH and sham mice missteps slowly increased over time. Additionally, the total number of steps was not different between sham and ICH groups at any timepoints, with a slight decrease of total steps for both groups starting on week 2 and lasting until the end of behavioral testing, suggesting a reduction of activity in the test (Fig. 6D). A Tukey's HSD multiple comparison test fitted with a generalized linear mixed model demonstrated a significant effect of time between baseline and weeks post-ICH in the ICH group (week 1-3: $p < 0.003$, week 5-6: $p \leq 0.0004$; Fig. 6D). A significant effect was also found in the sham group when comparing baseline with other timepoints (week 3: $p = 0.039$, week 4-6: $p < 0.005$). The same test found significant group effect in the impaired forelimb on week 4 ($p = 0.011$). The unimpaired forelimb had a significant effect of time between baseline and weeks post-ICH in both sham and ICH groups (ICH: week 5: $p = 0.012$, week 6: $p = 0.0002$; sham: week 5: $p < 0.0001$, week 6: $p = 0.0022$).

A.

B.

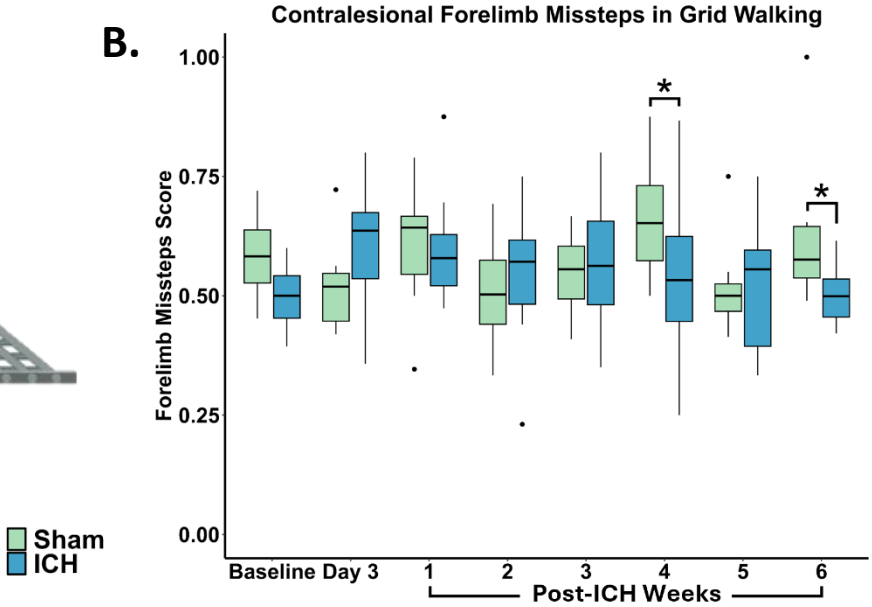
Contralesional Forelimb Missteps in Grid Walking
Forelimb Missteps Score
1.00
0.75
0.50
0.25
0.00
*
*
Baseline Day 3
1
2
3
4
5
6
Post-ICH Weeks
Sham
ICH

C.

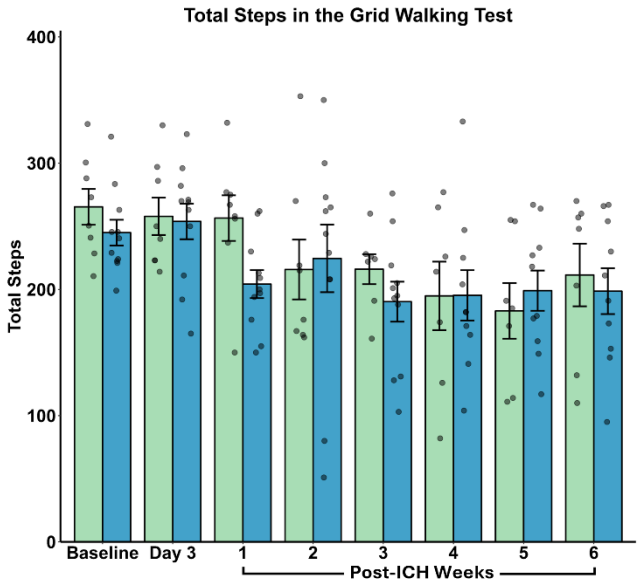
Total Steps in the Grid Walking Test
Total Steps
400
300
200
100
0
Baseline
Day 3
1
2
3
4
5
6
Post-ICH Weeks

D.

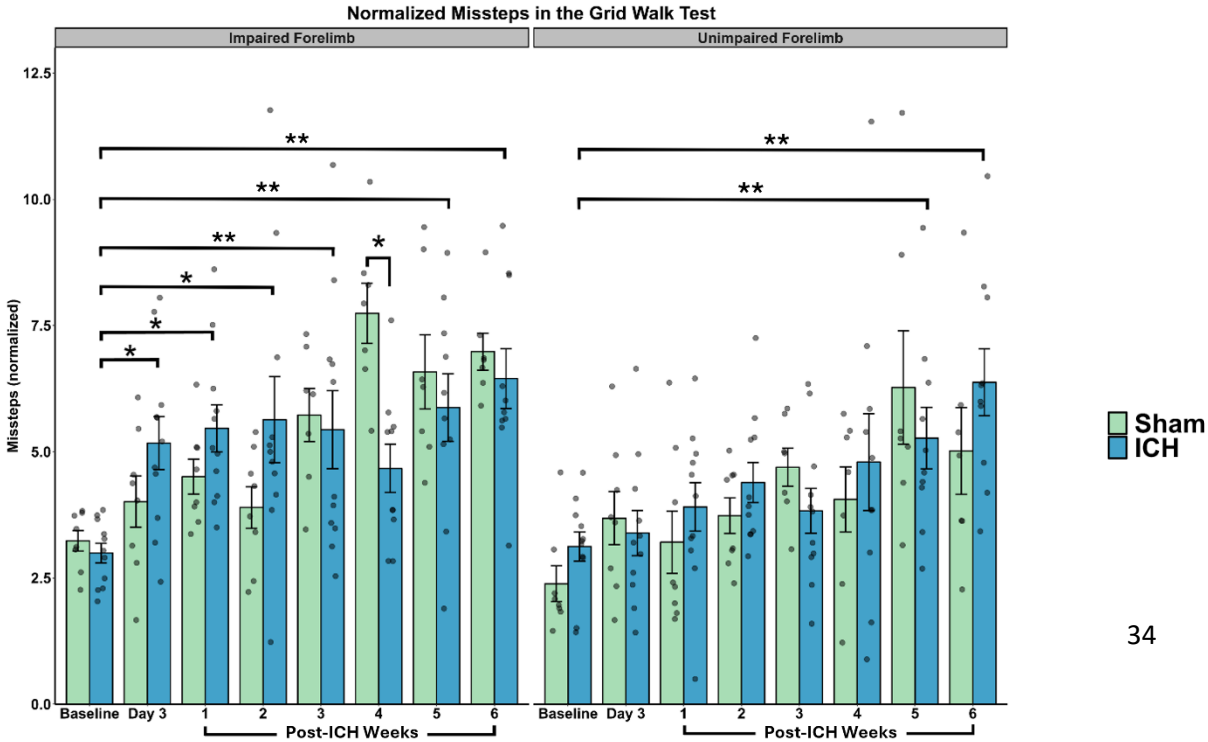
Normalized Missteps in the Grid Walk Test
Impaired Forelimb
Unimpaired Forelimb
Missteps (normalized)
12.5
10.0
7.5
5.0
2.5
0.0
**
**
**
*
*
*
*
**
**
Baseline
Day 3
1
2
3
4
5
6
Post-ICH Weeks
Sham
ICH

Figure 6. Grid Walking Test: A. In the grid walking test, the mouse is placed on a meshed grid and is allowed to walk on it. Every misstep with either the left or right forelimb was recorded. **B.** Box plot displaying the rate of missteps for the contralesional (impaired) forelimb relative to total steps with that forelimb. A higher score indicates more missteps of the impaired forelimb. **C.** Total number of steps. **D.** Total count of missteps normalized to the total steps for both the impaired and unimpaired forelimb. Stars (*) indicates significant difference, two stars (**) indicates significant difference between days in both sham (green) and ICH (blue) group. Measurements were done at baseline, post-ICH day 3 and over the 6 post-ICH weeks.

In the corner turn test, sensory and orientation asymmetries were measured longitudinally. The percentage of turns executed toward the lesioned side was calculated. A similar percentage of ipsilesional turns was observed at baseline in the sham and ICH group (Fig. 7A). A large increase of ipsilesional turn in ICH mice was observed on the first week, with individuals making 100% turn toward their lesioned side. The impairment diminished in ICH mice by week 2 and kept decreasing weekly, suggesting a recovery of turning asymmetry. Conversely, ipsilesional turn percentages were quantitively constant over all timepoints in sham mice. A Tukey's HSD pairwise multiple comparison demonstrated effect between baseline and other timepoints in ICH group (day 3: $p = 0.0011$, week 1: $p = 0.0144$) and between groups (day 3: $p = 0.0134$; Fig. 7A). Overall, following striatal ICH, a decrease of skilled walking ability with affected forelimb and sensory asymmetry were captured at early timepoints, recovering by the third week.

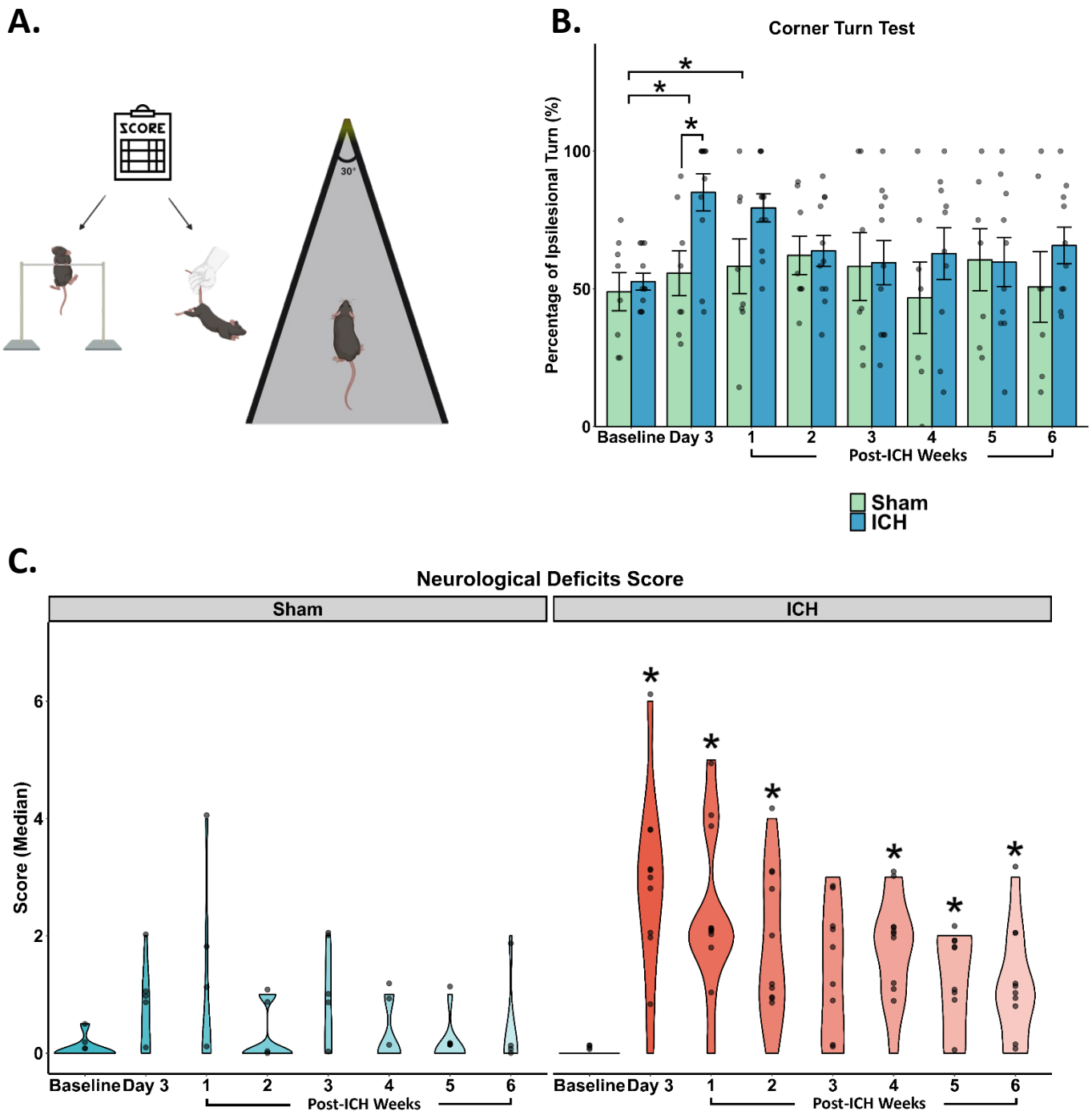

Figure 7. Neurological Deficit Score and Corner Turn Test: The neurological deficit score (NDS) and the corner turn test. The NDS assessments consisted of the wire hanging test, the forelimb asymmetry test and the forelimb outstretching test. The corner turn test helped evaluating turning asymmetry after ICH. **B.** Percentage of ipsilesional turns in the corner turn test, with higher percentage indicating mouse preference to turn right. Stars (*) indicates significant difference between sham (green) and ICH (blue) groups. **C.** NDS score in which a higher score represents larger forelimb motor deficits. Stars (*) indicates significant difference between sham (left) and ICH (right) groups.

3.3 Cylinder test and NDS found long-lasting forelimb impairments in ICH animals

Grip strength, balance and locomotor functions of the forelimbs were evaluated and scored on a scale from 0-3 in a neurological deficit score (Table 1). The baseline measurements showed no deficits in both groups with a median score of 0 (Fig. 7C). ICH mice demonstrated an increase in their score starting day 3 and lasting until the end of data acquisition, revealing impaired forelimb deficits after surgery that lasted for multiple weeks. A Mann-Whitney U test showed significance difference between groups at multiple timepoints (day 3: $p = 0.0042$, week 1: $p = 0.0277$, week 2: $p = 0.0035$, week 4: $p = 0.004$, week 5: $p = 0.0097$, week 6: $p = 0.0497$; Fig. 7C).

The cylinder test evaluated spontaneous forelimb use when exploring in a cylinder. A contralesional forelimb preference score was determined to examine which forelimb was most used during rearing behavior. ICH and sham mice score were equivalent during baseline measurements and stayed similar on day 3 (Fig. 8B). Interestingly, ICH animals showed a substantial drop of their contralesional preference score at the end of week 1. This reduction of impaired forelimb use stayed similar until the 6th week. A Tukey's HSD multiple comparison test fitted with a generalized linear mixed model showed significant effect of group (week 1: $p = 0.0035$, week 4-5: $p < 0.035$) and time (baseline-week1: $p = 0.012$, day 3-week 1: p 0.0012).

Following these results, the forelimb used to pushoff and the total wall contacts were measured in all rears. In both metrics, the percentage of impaired forelimb utilisation at baseline was similar for the sham and ICH groups (Fig. 8C-D). ICH mice showed reduced use of the impaired forelimb to pushoff themselves on day 3 (Fig. 8D). This reduction stayed similar until week 6 post-ICH, when the percentage returned near baseline, suggesting a recovery of the impaired forelimb use in the last week (Fig. 8D). In contrast, percentage of pushoff impaired forelimb of sham animals were kept constant throughout behavioral assessments. The percentage of total wall contacts from the impaired forelimb, on the other hand, did not immediately changed after ICH induction. A decrease of impaired forelimb use in the ICH group was observed starting at the end of week 1 and lasted until week 6 (Fig. 8C). Comparatively to the pushoff forelimb, the sham group had a constant use of their impaired forelimb for wall contacts throughout the weeks (Fig. 8C). A repeated measure ANOVA found significant effect in the pushoff forelimb for time and group ($p = 0.004$, $p = 0.0141$ respectively). The Tukey's HSD pairwise multiple comparison post-hoc found significant difference

between baseline and week 2 (p = 0.0312) and between groups on the same week (p = 0.0353, Kenward-Roger test). For the total wall contact, same tests were used and found significant effect of group and time interaction (p = 0.0117) with significant difference between baseline and week 1 (p = 0.0214) and between groups (week 1: p = 0.0028, week 5: p = 0.039). In summary, these results indicates that the impaired forelimb sensory and locomotor functions were altered longitudinally after inducing ICH and did not completely recovery after 6 weeks post-ICH.

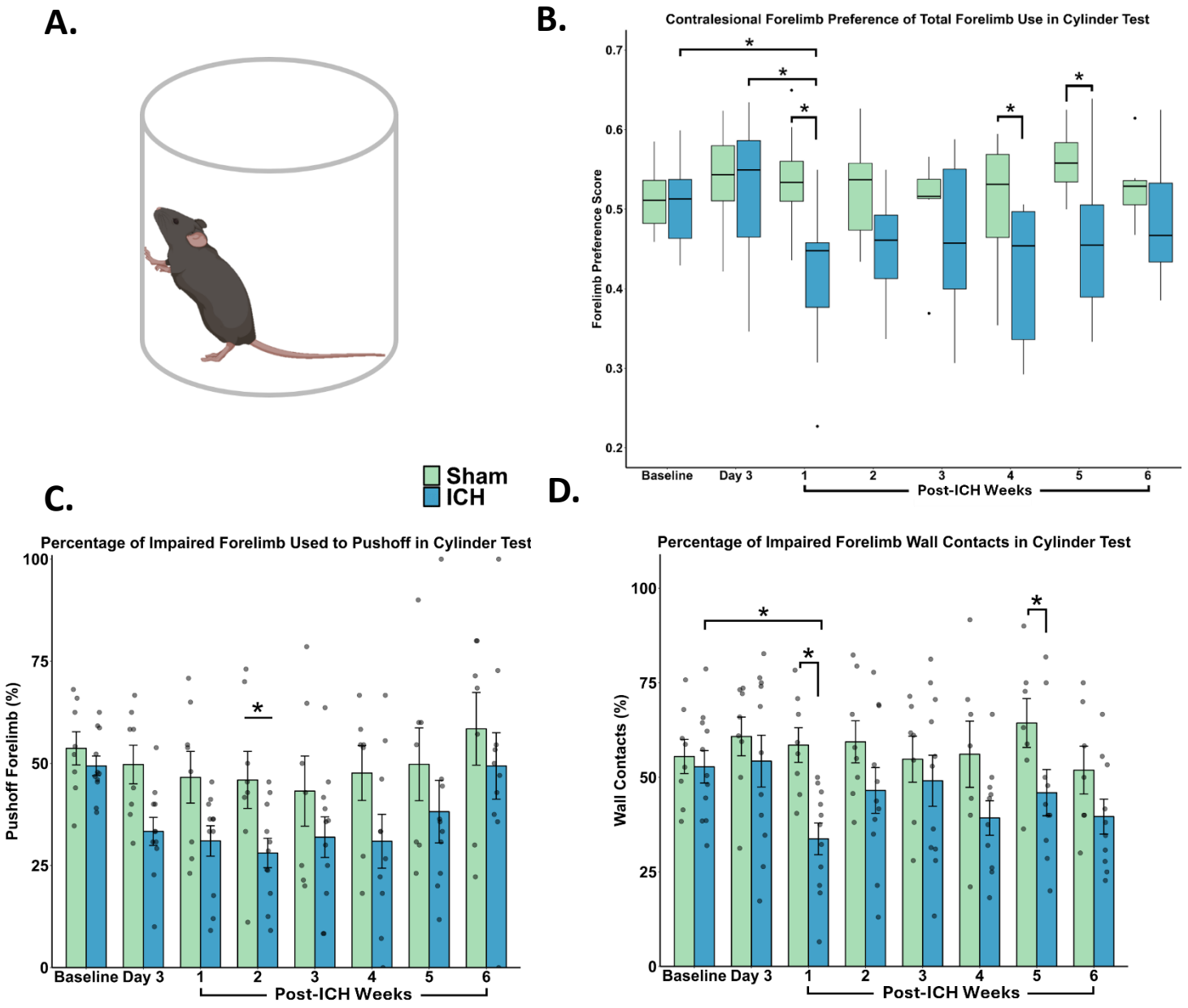

Figure 8. Cylinder Test: A. For assessment in the cylinder test, each mouse is placed inside a plexiglass cylinder in which it naturally rears up and touches the wall to explore its environment. Each time the mouse used either its left or right forelimb within a rear was scored. **B.** Box plot displaying the animals' preference to use their contralesional (impaired) forelimb. A lower score indicates less usage of the impaired forelimb. **C.** Percentage of the overall count the animals utilized their impaired forelimb to push themselves off. **D.** Percentage of the total wall contacts using the impaired forelimb. Sham group is represented in green and ICH in blue. Stars (*) indicate significant different. Measurements were done at baseline, post-ICH days 3 and over the 6 post-ICH weeks.

3.4 Striatal ICH did not alter cortical responses from sensory stimulation

Completed weekly, ISOI measurements allowed longitudinal visualization of blood flow responses in the sensory cortex following forelimb vibro-tactile stimulus. The average response evoked for both the impaired and unimpaired forelimb did not differ between sham and stroke mice (Fig. 9A, Fig. S2A). On week 2, the response appeared smaller i.e lighter in gray contrast, in the injured hemisphere when stimulating the impaired forelimb compared to the other timepoints (Fig. 9A) However, when quantifying the stimulus evoked area size, no significant difference was found in either group (Fig. S1A). Consistently, the non-impaired forelimb demonstrated no changes over time in area size and maximum amplitude for both groups (Fig. S1A/C, Fig. S1B/D). A small number of mice had bilateral responses in both forelimbs (Fig S1).

Further investigation of the evoked responses in sensorimotor-related Allen Mouse Brain Atlas areas was performed to evaluate changes within functional regions. Evoked area and maximum amplitude have been assessed within M1 as well as the FL and HL sensorimotor cortex. Response size of the impaired forelimb in its contralateral hemisphere demonstrated no changes over time in any anatomical regions (Fig. 9B). Surprisingly, the non-impaired forelimb evoked area in sham mice presented an increase on week 6 (Tukey's HSD: $p = 0.017$; Fig. S2B). Being the most activated region, average traces of evoked signal were generated for the FL anatomical region. Looking in the contralateral hemisphere of both forelimbs, no changes were detected over time (Fig. 10A, Fig S2A). The trace peak amplitude within the injured hemisphere of ICH mice impaired forelimb on week 2 seemingly decreased in comparison to week 1 (Fig. 10A). Nonetheless, when assessing the measure of evoked peak amplitude, no significant difference was found in the ICH group (Fig. 10B). Taken

together, these results suggest that the sensorimotor cortex had no activation alterations from sensory stimulation following subcortical ICH.

A.

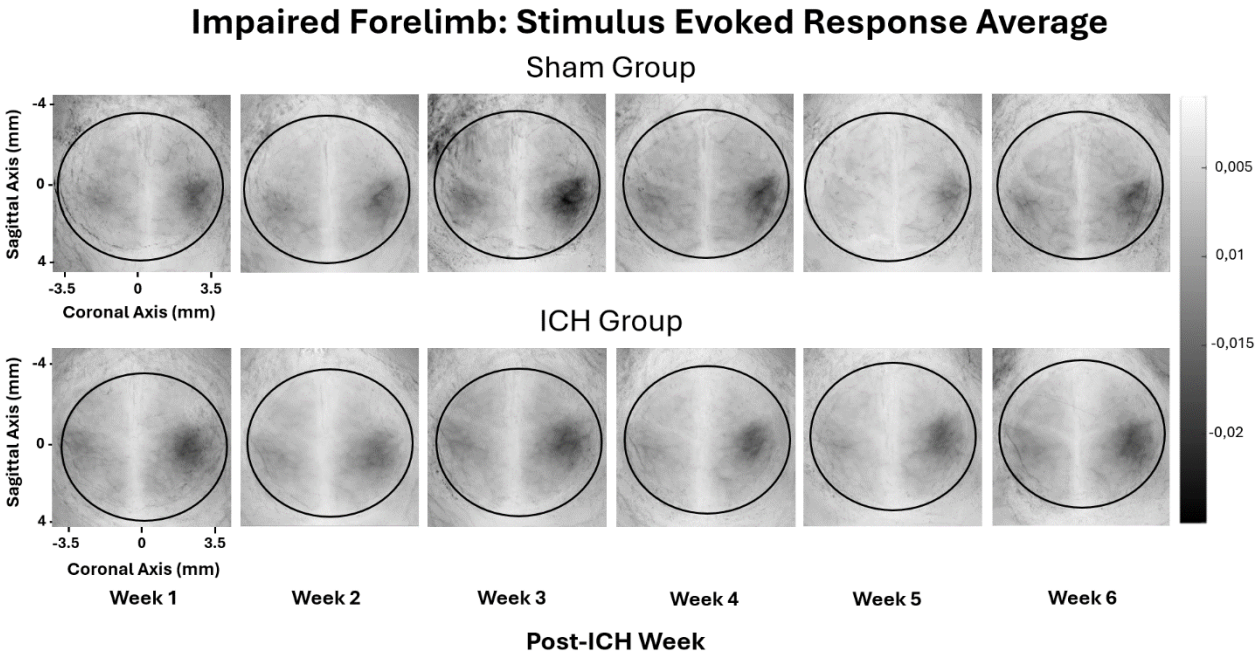

B.

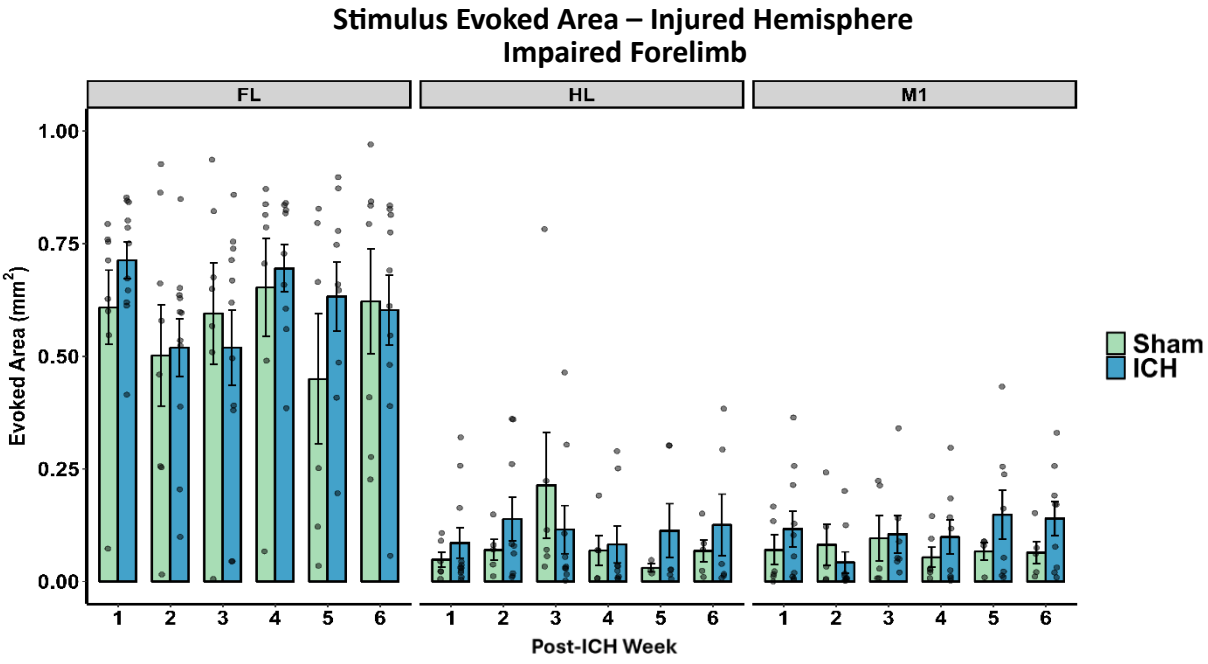

Figure 9. ISOI: Evoked Area in Impaired Forelimb: A. Evoked blood volume response following sensory stimulation in both sham (top) and ICH (bottom) groups over the 6 post-ICH weeks for the impaired forelimb. **B.** Size of the response area (mm^2) from forelimb stimulation within Allen Mouse Brain Atlas anatomical regions of the injured brain hemisphere in both sham (green) and ICH (blue) groups over the 6 post-ICH weeks for the impaired forelimb.

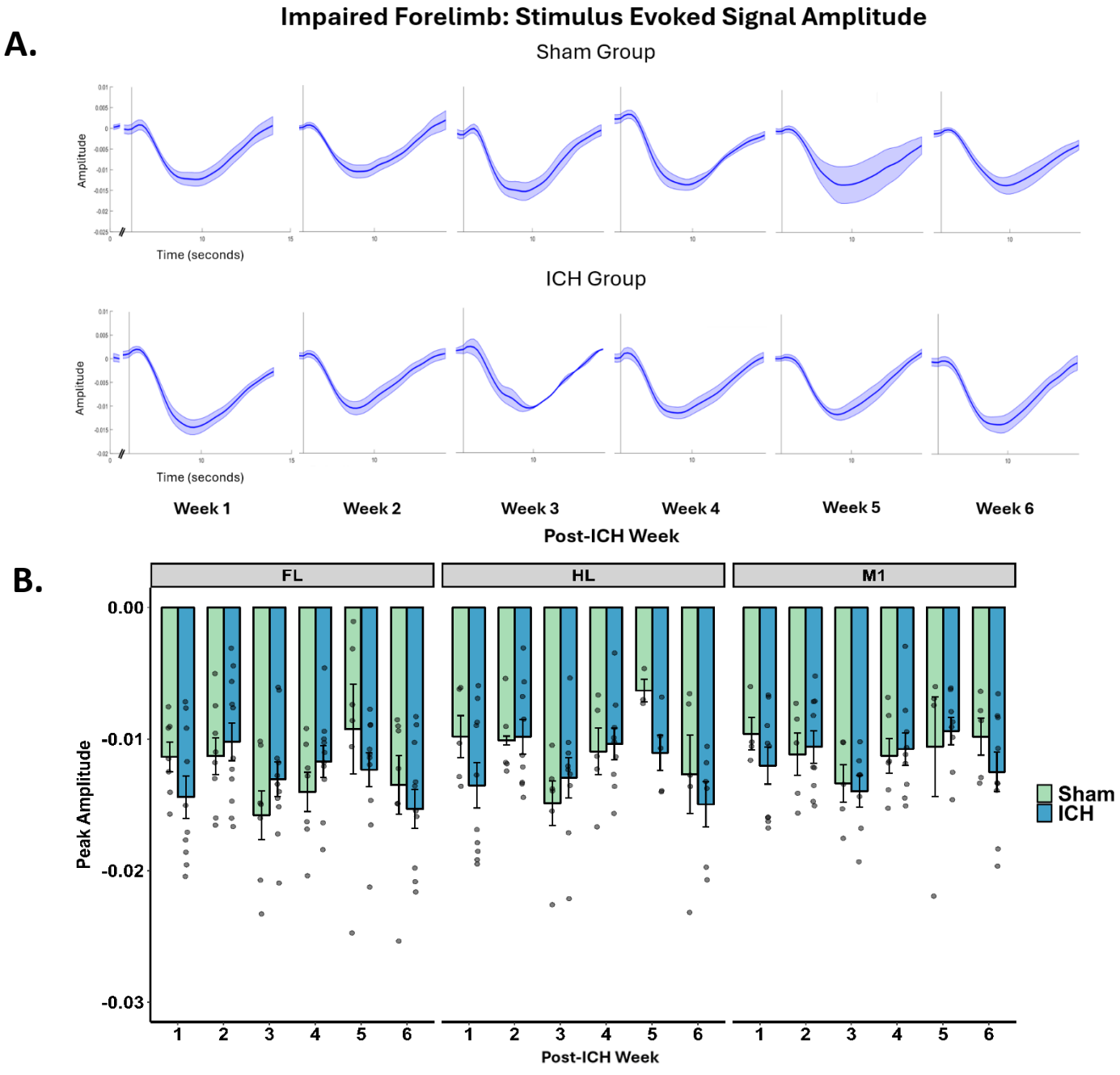

Figure 10. ISOI: Evoked Peak Amplitude in Impaired Forelimb: A. Average stimulus evoked signal traces in FL area within sham (top) and ICH (bottom) groups over the 6 post-ICH weeks for the impaired forelimb. The vertical solid line indicates the vibrotactile stimulus onset. **B.** Peak amplitude of evoked response within the Allen Mouse Brain Atlas anatomical areas in the injured brain hemisphere for both sham (green) and ICH (blue) groups over the 6 post-ICH weeks for the impaired forelimb.

3.5 Motor maps showed bilateral decrease in size and amplitude after striatal injury

Measurements of forelimb movements resulting from cortical activation using LBMM was used to longitudinally evaluate the impact of subcortical ICH on motor representations in the brain. Motor maps for the impaired forelimb of ICH mice showed differences compared to the sham animals from week 1 until the end of data acquisition on week 6 (Fig. 11A). The maximum movement amplitude of ICH mice was localized primarily in the ipsilateral hemisphere of the impaired forelimb with the injured hemisphere evoking smaller forelimb movement. Conversely, the sham group showed contralateral motor representations with larger evoked movement in the contralateral hemisphere (Fig. 11B). The uninjured hemisphere showed no changes following ICH induction. In contrast to the impaired forelimb, the non-impaired forelimb of the ICH group presented larger evoked movements in the contralateral hemisphere (Fig. S4A). Interestingly, peak movement amplitudes were smaller in the ICH group compared to the sham throughout the LBMM experiments (Fig. S4B), suggesting a negative impact to the non-impaired forelimb as well. A Tukey's HSD multiple comparison test fitted with a generalized linear mixed model found significant difference between groups for peak amplitude in the impaired paw (injured hemisphere: week 1-3: $p < 0.005$, week5: $p = 0.035$) and the unimpaired paw (week 5:$p = 0.026$, week 6: $p = 0.019$).

Further investigation of different parameters of evoked movement amplitudes showed similar results. The mean and sum of the maximum amplitude were assessed in both forelimbs. The amplitude sums of the impaired forelimb in ICH mice were disrupted throughout the 6 weeks (Fig. 11E). Comparably, when stimulating the injured hemisphere, the movement amplitude average showed a significant decrease compared to sham animals (Fig. 11D). The non-impaired forelimb demonstrated low average and sum of movement amplitude in ICH mice (Fig. S4E). There were no changes in the uninjured hemisphere on any weeks for both amplitude measurements. For the sum of evoked movements, a Tukey's HSD multiple comparison test fitted with a generalized linear mixed

model was used for both forelimbs. An effect was found for the impaired forelimb in hemisphere (week 1: $p = 0.0023$, week 1-2: $p = 0.01$, week 6: $p = 0.034$) and group (week 1-3: $p < 0.0015$, week 4-6: $p \leq 0.02$). The unimpaired forelimb had significant difference between hemisphere (week 1-2: $p < 0.004$, week 3: $p = 0.024$) and groups (week 1: $p = 0.014$, week 2: $p = 0.023$, week 4: $p = 0.041$) A repeated measure ANOVA was used for the evoked movement average and demonstrated an effect in time and group interaction for the impaired forelimb ($p = 0.0036$). A Tukey's HSD pairwise multiple comparison showed significant difference between groups (week 1-3 & 5: $p < 0.015$, Kenward-Roger test).

The average evoked movement of each sagittal coordinates were analyzed to visualize the amplitude distribution within specific regions. Anterior to posterior distribution of the mean evoked amplitude revealed larger evoked movements within the injured hemisphere in sham group compared to ICH mice around bregma point (Fig. 12) At both acute (week 1-3) and chronic (week 4-6) timepoints, sham animals displayed greater averaged movements amplitude in the coordinates representing the CFA region (0.3mm to -1.5mm relative to bregma) from the impaired forelimb (Fig. 12A). A similar trend is observable in the non-impaired forelimb, but only for the chronic timepoints across a smaller distribution (0.3mm to -0.5mm; Fig. 12B).

The size of the motor maps has been analyzed to evaluate changes in the evoked movements area following ICH induction. The injured hemisphere map size of ICH mice presented impairment with a smaller area that lasted until week 6 post-ICH (Fig. 11C). A similar disruption was shown in the unimpaired forelimb (Fig. S4C). No changes were observed in the uninjured hemisphere of both forelimbs. A Tukey's HSD multiple comparison test fitted with a generalized linear mixed model was used for both forelimbs. Significant effect was found for hemisphere (week 1-3: $p < 0.015$, week 6: $p = 0.019$) and group (week 1/3: $p < 0.03$, week 2/4: $p \leq 0.006$, week 5: $p = 0.039$) in the impaired forelimb. The non impaired forelimb also had significant effect for hemisphere (week 1/3: $p \leq 0.0035$, week 2: $p = 0.0058$) and group (week 1-2: $p < 0.05$, week 4: $p = 0.19$). To summarize, both forelimb motor representations in unilateral lesioned mice decreased in size and peak amplitude when stimulating the motor cortex bilaterally.

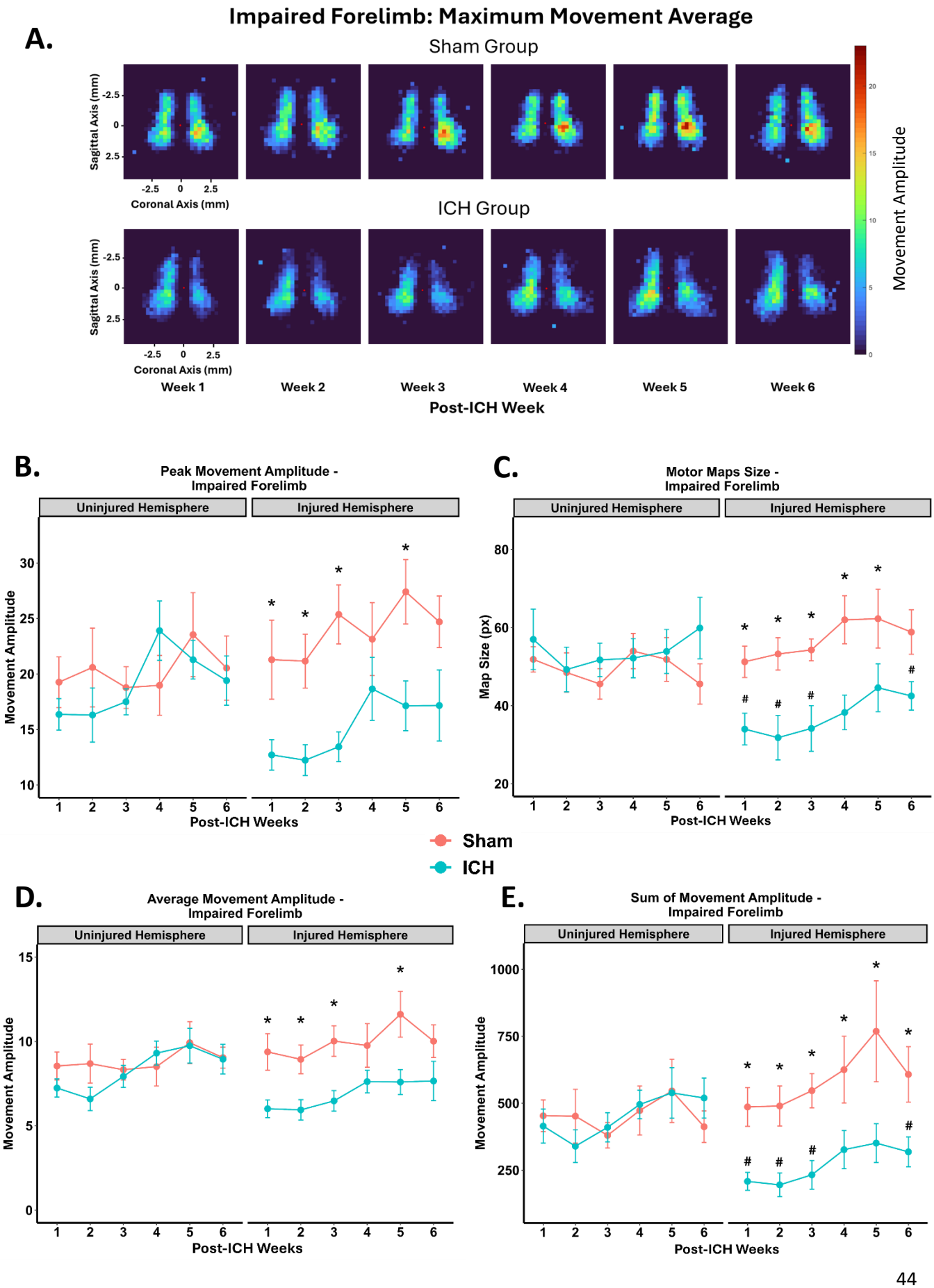
A.
Impaired Forelimb: Maximum Movement Average
Sham Group
ICH Group
Sagittal Axis (mm)
Coronal Axis (mm)
Movement Amplitude
Week 1
Week 2
Week 3
Week 4
Week 5
Week 6
Post-ICH Week
B.
Peak Movement Amplitude - Impaired Forelimb
C.
Motor Maps Size - Impaired Forelimb
Uninjured Hemisphere
Injured Hemisphere
Movement Amplitude
Map Size (px)
Post-ICH Weeks
Sham
ICH
D.
Average Movement Amplitude - Impaired Forelimb
E.
Sum of Movement Amplitude - Impaired Forelimb

Figure 11. Motor Maps Amplitude and Motor Maps Size for Impaired Forelimb: A. Motor maps of the impaired forelimb representing the averaged movement amplitude per activation point within both sham (top) and ICH (bottom) groups over the 6 post-ICH weeks. **B-C-D-E.** Different map analysis compared between sham (orange) and ICH (blue) groups within both hemispheres for the impaired forelimb. Stars (*) indicate significant difference between groups and dash (#) indicates significant difference between hemispheres. **B.** Maximum movement amplitude. **C.** Averaged map size calculated by the number of pixels activated. **D.** Movement amplitude average. **E.** Sum of total movement amplitude

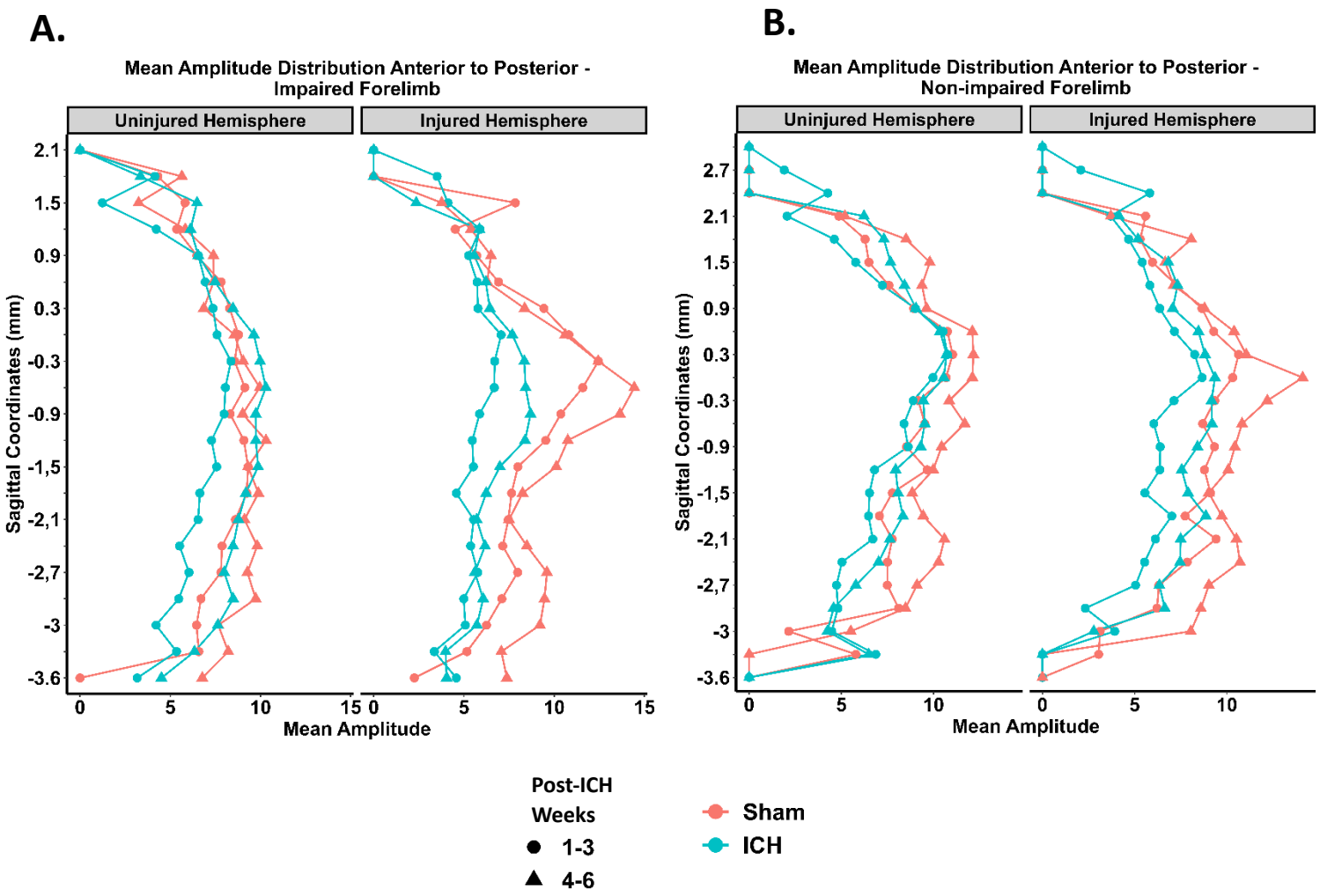

Figure 12. Motor Maps Sagittal Coordinates Distribution of Mean Amplitude: A-B Mean amplitude averaged for each sagittal coordinate showing movement amplitude anterior-to-posterior distribution on the cortex between sham (orange) and ICH (blue) groups for both the impaired (**A**) and unimpaired (**B**) forelimbs. Post-ICH weeks were combined in two groups: week 1 to 3 (circle; acute phase) and week 4 to 6 (triangle; chronic phase).

3.6 Larger movement latencies were observed in ICH mice

Analysis of an evoked movement time to reach its farthest position following cortical stimulation allowed to investigate temporal modifications of forelimb movements after ICH. Both the sham and ICH groups exhibited constant movement latencies over time in the uninjured hemisphere of the unimpaired forelimb (Fig. 13C). The ICH mice demonstrated larger latencies as opposed to sham animals in the injured hemisphere for both forelimb with a trend toward recovery on week 6 (Fig. 13B-C). In both forelimbs, ICH animals had larger latencies closer to the edges of the forelimb representations, which was not as prominent in sham maps (Fig. 13A/D). Interestingly, although not significant, the uninjured hemisphere of the impaired paw had an increase in latencies around week 3 (Fig. 13B). A Tukey's HSD multiple comparison test fitted with a generalized linear mixed model was used for both forelimbs. Significant differences between group in the impaired (week 2: $p = 0.0454$, week 3: $p = 0.0205$, week 4: $p = 0.0079$, week 5: $p = 0.0447$) and unimpaired forelimb (week 2: $p = 0.0168$) were found. A significant effect was also observed between hemisphere in the impaired forelimb (week 2: $p = 0.0479$).

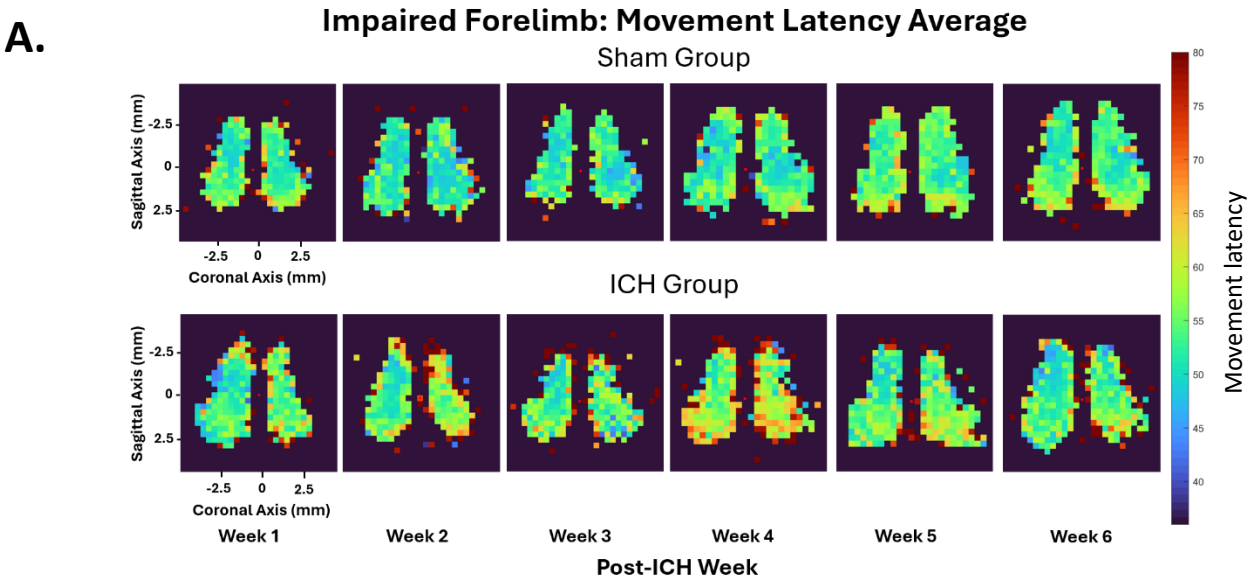
A.
Impaired Forelimb: Movement Latency Average
Sham Group
ICH Group
Sagittal Axis (mm)
Coronal Axis (mm)
Movement latency
Week 1
Week 2
Week 3
Week 4
Week 5
Week 6
Post-ICH Week

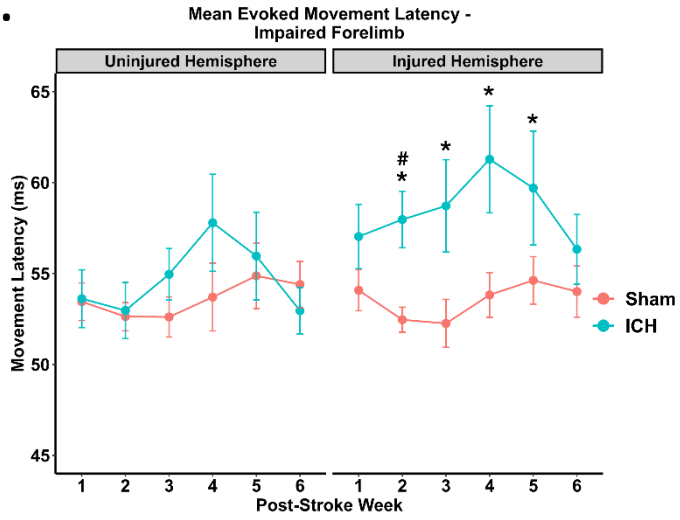
B.
Mean Evoked Movement Latency - Impaired Forelimb
Uninjured Hemisphere
Injured Hemisphere
Movement Latency (ms)
Post-Stroke Week
Sham
ICH

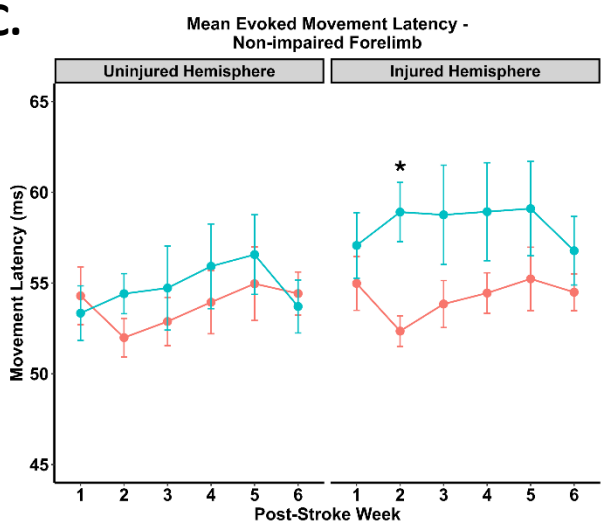
C.
Mean Evoked Movement Latency - Non-impaired Forelimb
Uninjured Hemisphere
Injured Hemisphere
Movement Latency (ms)
Post-Stroke Week

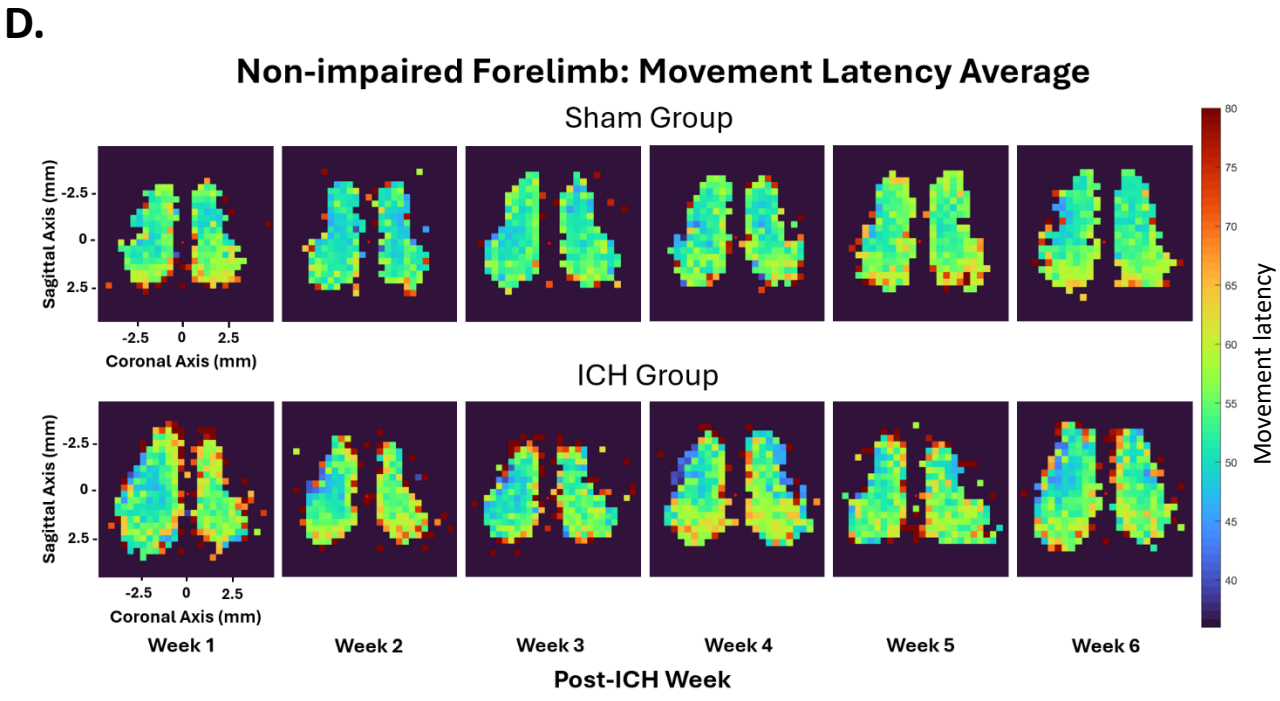
D.
Non-impaired Forelimb: Movement Latency Average
Sham Group
ICH Group
Sagittal Axis (mm)
Coronal Axis (mm)
Movement latency
Week 1
Week 2
Week 3
Week 4
Week 5
Week 6
Post-ICH Week

Figure 13. Latency of Peak Movement Amplitude Maps: A & D. Average latency for evoked movements to reach their peak displacement within both sham (top) and ICH (bottom) groups over the 6 post-ICH weeks for the impaired forelimb (**A**) and unimpaired forelimb (**D**). **B-C.** Mean evoked movement latency compared between sham (orange) and ICH (blue) groups within each hemisphere for the impaired (**B**) and unimpaired (**C**) forelimb. Stars (*) indicate significant difference between groups and dash (#) significant difference between weeks within a group.

4. Discussion

The results of this thesis revealed acute and chronic behavioral impairments over 6 weeks following ICH induction in the dorsolateral striatum of mice. The first weeks were marked by impaired locomotion, a decrease of spontaneous use of the impaired forelimb and turning asymmetry in response to vibrissae stimulation. While some recovery was observed in earlier timepoints for turning asymmetry and locomotion, the ICH animals showed long-lasting deficits in forelimb use. These behavioral deficits were associated with disruption of the forelimb motor representations, showing a decrease in evoked movement amplitude and map size. Evoked movement latency presented similar time course of impairment. Our longitudinal mapping revealed some reorganization within motor representations as both forelimbs showed an increase in map size and amplitude overtime. Conversely, the sensory responses were not impacted by ICH, as no difference was found between the sham and ICH groups. To our knowledge, this is the first study to evaluate the relationship between behavioral recovery and bilateral sensorimotor map reorganization following striatal ICH in the rodent brain.

4.1 Collagenase injection induced ICH leading to an atrophy of the lesioned hemisphere

To induce a striatal ICH, we used the collagenase model which enzymatically disrupts the blood vessel wall leading to a subsequent haemorrhage. In our results, the lesion volume we measured from T2 images exhibited an initial large lesion in subcortical regions on the third day post-ICH that had significantly reduced by day 14, similar to what other studies have shown (144; Fig. 5A-B). The collagenase rodent model has previously shown to generate a hematoma within the initial hours after collagenase injection, followed by significant edema that gradually resolved in the ensuing weeks (144). This injury progression is also comparable to what has been observed in ICH patients (149). Moreover, the large variability in lesion volume that we observed in our ICH group, with a 14.19mm^2 difference between the smallest and largest lesion (Fig 5B), is representative of ICH patients' population, in which damage irregularity is a major factor in the difficulty of finding reliable intervention. A more comprehensive understanding of the underlying mechanisms leading to lesion heterogeneity is needed, stressing the importance of having pre-clinical studies introducing lesion

variability (150,151). Surprisingly, three ICH mice showed a larger lesion at day 14 post-ICH compared to day 3. This presence of a large lesion after 2 weeks could be explained by perihemorrhagic edema. During the second phase of ICH injury, a long-lasting edema can be observed, leading to aggravated outcomes (152). Disruption of the blood brain barrier and neuroinflammation, among other processes, are thought to be the underlying factors contributing to this phenomenon. Perihemorrhagic edema has been seen to grow over a duration of up to 3 weeks in humans, with the peak occurring on the second week post-ICH (153). A similar process might have happened in our mice, leading to a prolonged edema, even 2 weeks after surgery.

In the first 2 weeks, MRI images were acquired to longitudinally assess lesion volume in ICH mice. The utilization of MRI imaging in lesion volume assessments is a common methodology in clinical and pre-clinical studies (154,155). Its prevalent application for humans patients makes MRI a good translational technique. However, doubts have been raised in the literature about the validity of MRI images compared to histological analysis. In a study evaluating ICH in a collagenase rat model, comparison of histological and MRI assessments for lesion volume showed significant variation at week 4 and 6 post-ICH (144). In a similar rat model, Liu and colleagues found a significant difference of lesion volume between histology and MRI measurements at day 14 and 56 after ICH onset (156). Interestingly, correlation analysis between the two lesion volume techniques showed a high correlation, indicating that both MRI and histology are reliable measures for lesion volume. Consistently, meta-analysis and workflow development for injury evaluation have found considerable correlation between MRI and histological lesion volume, arguing that both can be used interchangeably (155,157).

Histological quantification at the end of our experimental timeline showed atrophy of the lesioned hemisphere in all the ICH animals, with notable variability between the largest and smallest values (Fig. 5D). A reduction of brain tissue volume is a common ICH consequence that occurs from the mass effect in the early stages of the injury and appears when the edema and hematoma resolve. This loss of parenchyma has been correlated with an increase density of neuronal cells and a reduction of cell body size, potentially linked to abnormal neuronal activity (158). The resulting atrophy is thought to be associated with the initial hematoma size, which could explain the variation

observed in our atrophy volume. Intriguingly, studies have found that brain atrophy could instead be protective and reduce the mass effect in ICH, leading to favorable outcomes (159). Atrophy in the lesioned hemisphere was also observed in sham mice, with some individuals having larger atrophy compared to ICH mice. The sham procedure consists of the insertion of the needle in the brain parenchyma followed by saline injection. If the saline injection does not cause brain damage, the needle itself goes through brain tissue, disrupting potential axons, connections and blood vessels on its way down. By using a 33-gauge Hamilton syringe, the damage is limited but not completely prevented. It is thus possible that this needle insertion might have caused damage to the brain tissue resulting in some decrease of brain parenchyma volume. Many studies have used comparable sham procedures and measured brain atrophy but did not report or measured the volume changes in the sham animals (82,83). Other studies have shown atrophy in their sham animals as well (70,160,161). The use of naïve animals without any surgical intervention would be useful for future studies to control for the syringe insertion and possibly offer more insight on the atrophy presence in sham animals. Altogether, these results confirm the presence of a striatal injury in our collagenase model. The injury progression followed the initial growth of hematoma and edema seen in ICH and ultimately resulted in atrophy of the lesioned hemisphere.

4.2 Behavioral impairments followed striatal ICH with long-lasting forelimb sensorimotor functions deficits

Assessments of sensorimotor function showed some impairments in the earlier timepoints that recovered by the middle of the 6 weeks, while other test showed more chronic deficits. In the first two weeks, a significant increase of normalized impaired forelimb missteps in the grid walking test was observed in the ICH group but not in the sham animals, demonstrating a loss of coordination and movement execution for the impaired forelimb (Fig. 6B/D). The basal ganglia network has been correlated with the control of movement vigor, regulating the timing and velocity of execution. In a study that inactivated the globus pallidus in macaques (162), one of the output regions of the striatum, the speed of movement in a joystick task was greatly reduced, resulting in much slower movements. Furthermore, the timing of continuous motor events by the integration of sensorimotor information has been shown to be controlled by the basal ganglia, particularly the striatum (163). An

injury to this network could impair the rapid execution of movement showing slower responses to external stimuli. Walking on a meshed surface require the mice to constantly monitor their steps and execute timed action to avoid slipping. Following striatal injury, this capacity may be impaired, leading to an increased number of missteps (156). This movement vigor is thought to be modulated by dopamine, where dopamine input reduction in the dorsal striatum leads to a loss of velocity and fluidity of movement control, a pathophysiology commonly seen in Parkinson's disease patients (35).

In the corner turn test, the ICH group showed a considerable increase of ipsilesional turns in the corner turn test compared to baseline measurements and sham mice in the first week following ICH (Fig 7B). This spontaneous test was designed to measure sensory impairment, by examining the orientation response to stimulation of the whiskers in a tight corner, in addition to forelimb and postural asymmetries (164). Many other studies evaluating behavioral deficits in a striatal ICH rodent model have shown asymmetry of turning behavior in the corner turn test (165–167). Our results reiterate previous findings demonstrating sensorimotor deficits in the corner turn test at acute timepoints following ICH. Additionally, our ICH mice turning asymmetry displayed recovery by week 2 post-ICH. This return in turning balance is linked with the decrease of edema and hematoma shown in the MRI images, on day 14. Recovery of ipsiversive behavior in the corner turn test has been showed at similar timepoints in other studies (168,169). The association between edema and sensorimotor deficits have been assessed in ICH rodent model. The repercussion of thrombin excess and hemoglobin degradation paired with the mass effect has been shown to participate in behavioral deficits (170,171). Consequently, the progressive relief of the blood and excess water in the brain could result in partial recovery. The corner turn test results, among other behavioral tests, have been correlated with brain edema 24 and 72 hours after ICH induction in a collagenase mice model, arguing for a role of this injury process in sensorimotor deficits (172).

While the corner turn test showed recovery on the second week post-ICH, the significant increase of normalized missteps frequency for the impaired forelimb during the grid walking test lasted over the 6 weeks post-ICH (Fig 6D). However, starting from week 3, the sham animals began to execute more normalized missteps from their impaired forelimb relative to their baseline measurement. A similar increase of normalized missteps in the unimpaired forelimb over time was displayed for both groups,

suggesting that the mice are less coordinated over time. Although not significant, analysis of the total number of steps for one forelimb showed a decrease of steps over time (Fig. 6C). By repeating the behavioral test multiple times, motivation and concentration of the mice might have decreased, leading to lower precision of movement execution. Many other kinematics are implicated in this behavioral test, such as the body position, the speed, the duration of swing phase and cadence, and have been shown to recover at different timepoints (156,173). Further evaluation of the various parameters of grid walking behavior could provide significantly more precise analysis and potentially explain discrepancy in results observed when employing a more generalized analytical approach such as missteps assessments.

While the grid walking test and corner turn test presented deficits in the earlier timepoints, the NDS and cylinder test demonstrated impairments in both the acute and chronic phases of ICH injury. A significant increase of deficit score in the NDS was exhibited by the ICH mice compared to the sham group (Fig. 7C). This significance was presented until week 6, at which point several ICH mice exhibited a score of 0 on week 6 post-ICH, while certain animals continued to display deficits. This NDS was graded based on the Garcia scoring system, with evaluation of forelimb asymmetry in extension and walking movement as well as the balance and strength of grip on a hanging wire. Similarly to the corner turn test, in the early timepoints, a turning asymmetry was observed in ICH mice when they walked on a flat surface utilizing only their forelimb. While this asymmetry reduced over time, the use of the forelimb remained impaired for a longer period of time. More specifically, wire grasping in the wire hanging task presented prolonged deficits. The implication of the striatum in skilled forelimb movement has been assessed in many studies (146,174,175). In a study from MacLellan and colleagues (146), the kinematics of a skilled reaching task were analyzed in ICH-induced rats. By examining the different components of the reaching movement, they were able to observe abnormal retrieving movements where the rats had trouble closing their digits around the food pellet and rotate their forelimb to retrieve it. This apparent difficulty to execute finer motor behavior might explain the increased score of our ICH mice in the wire hanging test where they showed impairment to grasp the wire. Compensatory mechanisms were taken in account during the scoring in which the use of the impaired forelimb wrist or shoulder to hold on the wire were considered as deficits.

Similar to NDS deficits during the chronic phase, the cylinder test showed a significant forelimb preference in the ICH mice until week 5 post-ICH (Fig. 8B). A preference to use the unimpaired paw was observed in comparison to sham mice who exhibited no discernible preference; this effect was evident during the first week and persisted for 5 weeks. Strikingly, no significant difference of paw preference score was observed on the third day post-ICH. When looking at the components of the rearing behavior executed in the cylinder, a reduction of impaired forelimb utilization to push itself off the ground was observed starting day 3, whereas the total wall contacts made with the impaired forelimb only began to decrease later in week 1 (Fig. 8C-D). The accomplishment of pushing its body off the ground involves movement execution and control from the distal forelimb, which was shown to be impacted in our other behavioral tests. The forelimb utilization to touch the wall, on the other hand, results from large unprecise movements that can use proximal forelimb action to compensate. It is possible that following a reduction in their impaired forelimb use, ICH mice demonstrated maladaptive learning initiated later in the week, reinforcing the utilization of their unimpaired paw only. Maladaptive learning is a mechanism well known in stroke injury in which deficit of the impaired limb are exacerbated by a reduction of its utilization (95). With a decrease in sensorimotor neuronal activity early after stroke onset, the use of the impaired limb becomes difficult, forcing the utilization of the other limb. By doing so, reinforcement of the motor activity from the unimpaired limb occurs, which further depresses the impaired limb neuronal activity, resulting in inefficient movement execution of the impaired limb (176). Enforcement of the impaired limb use by constraining the other limb is an effective therapy utilized for stroke injury (177,178).

All behavioral deficits demonstrated recovery over the weeks, implying a compensatory mechanism for the loss of striatal functions from ICH. With its role in sensorimotor functions and its many connections with the striatum, the motor cortex could be part of this recovery process. Motor cortex input is thought to play an important role in determining motor commands where the striatum would be critical in the subsequent information modulation (179). This raises the possibility that the motor cortex might have taken over some of the functional loss observed in ICH mice. A study from Tamakoshi and others (83) has found an increase of neuronal activation and plasticity marker in the bilateral sensorimotor cortex following motor skill training in rats lesioned by striatal ICH. In another study replicating similar experiments (180), marker for plasticity were found in both trained and non-

trained rat motor cortex, suggesting that some recovery process is proceeding in this brain region after striatal injury. Overall, the various behavioral tests used to assess sensorimotor impairments following striatal ICH in a collagenase mouse model exhibited both acute and chronic deficits and recovered throughout the 6 experimental weeks.

4.3 Stimulus-evoked sensory responses are not impaired by striatal ICH

ISOI was used to assess the impact of a striatal injury on sensory representations in the sensorimotor cortex. The stimulation of the impaired forelimb did not show any significant difference between sham and ICH groups at any timepoints for both the peak amplitude and area size of the evoked response (Fig. 9A, Fig. 10A, Fig. S1). Further examination of the ISOI response within anatomical brain regions did not present any differences as well (Fig. 9B, Fig. 10B). Surprisingly, ICH animals showed a larger evoked response, although not significant, in the first week compared to sham mice. This unexpected result could be explained by neurovascular coupling disruption in the early stage following stroke (136).

The striatum has been shown to share connections with the sensory cortex and participates in the integration of sensory information (43,181,182). Studies have illustrated that sensory stimulation induces neuronal activation within the striatum, demonstrating a relay of sensory information from the sensory cortex to the basal ganglia network (183,184). Direct stimulation or inhibition of corticostriatal projections using optogenetics disrupted the performance of rats in a vibrotactile task, implying a significant role of the striatum in vibrotactile information modulation (185). Moreover, injury to the basal ganglia has shown to affect sensory responses in the brain (186–188). Nonetheless, if the striatum participates in the modulation of sensory information, the somatosensory pathway initiates outside of the striatum (189). Sensory information from the forelimbs, for example, is received by hindbrain which relays it to the thalamus in the ventroposterior nucleus. Thalamocortical axons are then sent to the neocortex by the internal capsule and innervate S1. This functional circuit has likely not been impacted, or only minimally, by our striatal lesion as preliminary investigations of the collagenase mouse model for this work revealed minimal damage of the thalamus and internal capsule (data not shown). Additionally,

similar results were found in a study from Bauer and colleagues (190). The sensory representations were evaluated in an ischemic stroke mouse model that produced damage in different locations. One group demonstrated exclusively subcortical damage, whereas two other groups showed both subcortical and various cortical damage. Electrical forelimb stimulation revealed only a slight reduction of the evoked response amplitude in the subcortical infarct group compared to the other groups, with most of the sensory representation still present. This difference of sensory responses from a subcortical stroke compared to stroke in both subcortical and cortical regions suggests that damaging only subcortical regions impacts minimally the sensory representations in the sensorimotor cortex. By injuring exclusively the modulator of sensorimotor cortex output, the initial response coming from deeper brain regions may remain present in the cortex. The exact role of the striatum in sensory functions is still not completely understood but our results suggest that damaging the striatal structure does not lead to sensory representation disruption.

4.4 LBMM showed motor map alterations

The use of LBMM allowed us to evaluate the motor representations following ICH and how they change over time. Sham animals demonstrated comparable motor maps to what has been previously shown in the same mouse line (52; Fig. 11A, Fig. S4A). Contralateral activation with a well-defined CFA on the posterior side and a smaller RFA positioned anteriorly are displayed throughout the 6 weeks. On the first week, a noticeable change was observed in the ICH group compared to the sham group (Fig. 11A). Evoked movements from the impaired paw exhibited ipsilateral maps as opposed to sham mice that presented larger amplitude in the contralateral hemisphere. The striking difference appears in the contralateral hemisphere of the ICH animal maps, where a considerable shrinkage of the representation is observed. This change was confirmed by a significant difference of movement amplitude and motor map size between the sham and ICH animals in the injured hemisphere (Fig. 11B-E). A similar pattern was shown for latency of evoked movements where a significant difference was displayed in the injured hemisphere of the impaired forelimb between both groups (Fig. 13). Moreover, the unimpaired forelimb also showed damage in the injured hemisphere (Fig. S4) The decrease evoked amplitude in motor maps could not be related to a major power reduction used to elicit movement as the experiments were done based on motor resting threshold and the range of

power was similar between sham and ICH animals (1-4mW). This study is not the first one to report damage of motor maps from non-M1 injury. A reduction of contralateral-to-injured forelimb motor maps after subcortical stroke has been reported by Gharbawie *et al.* study (142). Moreover, damage in the lateral neocortex leaving M1 intact has also demonstrated reduction of motor map size (141,191).

A first explanation for this functional motor impairment is distal injury from the acute inflammation present in ICH. It has been shown in both humans and rodents that following ICH in deeper brain regions, secondary injury represented by reduction of dendritic spine density and integrity lost of white matter was observed in regions distal from the stroke site (192,193). Injury processes present in remote regions from the initial stroke site brings the possibility of damage to cortical neurons. Assessment of neuronal damage in the cortex in future studies would allow further analysis of cortical neuron disruptions.

Injury to cortical connections with downstream target could be another justification for the impairment of motor representations seen in our ICH mice. Indirect corticospinal connections going through the basal ganglia regulate the processing of motor information (194,195). By inducing ICH in the striatum, these connections might have been damaged. In both humans and rodents, the loss of cortico-striatal projections following subcortical ICH was demonstrated (70,196,197). Injury of these connections could possibly disrupt the afferent pathway to the spinal cord, resulting in a form of M1 deafferentation. Studies looking at M1 deafferentation through spinal cord injury have found similar reduction of cortical motor representations (198–201). Using LBMM, Hilton and colleagues measured evoked movements in mice after lesioning pyramidal tracts (199). An almost complete ablation of the map was observed early after the injury and showed recovery by the second week. Similar functional damage was observed as well in humans (202). In this study, TMS was used to measure brain activity when participants with spinal cord injury contracted their hand muscles. While the motor map area of control participants increased after muscle contraction, the map area of spinal cord injured subjects reduced in size, demonstrating that M1 deafferentation led to abnormal functional representations of their hands. The impact of corticospinal tracts damage on motor maps is similar to what we observed in our ICH mice. It is important to note that a large

portion of indirect corticospinal connections are situated in the internal capsule (203). However, as mentioned earlier, the internal capsule was not, or minimally, damaged by our striatal stroke, indicating that the possible damage to corticospinal afferent pathways would originate from the striatum.

Most of the changes observed in our ICH mice motor maps were situated in the CFA. The sagittal distribution of mean evoked amplitude showed a substantial difference between sham and ICH animals in the coordinates related to the CFA (Fig. 12). Interestingly, a similar decrease pattern was demonstrated in rats with pyramidal tract lesions, demonstrating further correlation with M1 deafferentation (200). The prominent damage in the CFA region of the motor maps follows the topographical distribution of their connections with the striatum. RFA connections to the striatum have been found to be denser and cover a larger part of the striatum compared to CFA inputs (204). Projections from the CFA are restricted to the lateral and dorsolateral part of the striatum whereas RFA innervations are found in most of the striatum with higher density in the ventral subregion. The coordinates we used to induce ICH aimed the dorsolateral striatum with minimum damage to the ventral part. With larger damage to the dorsolateral zone, most CFA connections would be damaged compared to the RFA inputs where many projections in the ventral striatum would be largely intact.

The reduction of motor maps in the first week of LBMM experiments lasted for 5 weeks before showing an initiation of recovery. While the injured hemisphere generated smaller evoked movements in ICH mice, the uninjured hemisphere showed no difference compared to sham animal. This ipsilateral activity of the impaired paw displays the importance of both hemisphere in the recovery process following ICH and will be discussed in the next section.

4.5 Bilateral sensorimotor representations with no recovery over time

Bilateral activity for both forelimbs was observed during LBMM experiments and sensory mapping. The sham animals showed motor maps with strong contralateral activity but stimulation of the ipsilateral hemisphere evoked movements as well (Fig. 11, Fig. S4). Moreover, presence of bilateral response when stimulating a single forelimb was observed in ISOI results (Fig. S1). Evidence of ipsilateral implication in unilateral movements has been shown in the past years (205–207).

Moreover, bilateral motor representations have been previously generated with a similar dominance for contralateral activity as seen in our maps (118,208). The sensorimotor cortices are joined by the corpus callosum, a large tract of white-matter fibers composed of excitatory axons that innervate inhibitory and excitatory neurons on the opposite hemisphere (209–211). This connection between hemispheres is thought to participate in regulating unilateral activity via interhemispheric inhibition, suggesting an important role for bilateral activity in motor control (212–215).

If the sham mice demonstrated contralateral motor maps, the ICH animals on the other side showed greater ipsilateral activity compared to the opposite hemisphere in the impaired forelimb (Fig. 11A-E). Significant difference between movement amplitude and map size of both groups was observed for the 5 first weeks following ICH onset (Fig. 11B-E). This disbalance of hemispherical activity is commonly seen following stroke injury. A common concept across the mammalian brain is that with a reduction of intrahemispheric connectivity comes an increase of interhemispheric connections (216,217). By injuring cortical projections within one hemisphere, a stroke can lead to increased use of transcallosal connections. Indeed, damage caused in the lesioned hemisphere have been shown to consolidate and create new connections with the opposite hemisphere, and is also paired with an increase of ipsilateral activity (73,94,218). Similar processes have been observed following subcortical ICH as well (219–221).

The ipsilateral dominance in our ICH animals' motor maps were present for a prolonged period of time (6 weeks post-ICH; Fig, 11A). Although the enhanced activity of the contralesional hemisphere is thought to act as a compensation mechanism, many studies argue that this compensation can lead to maladaptive plasticity (222–225). As discussed earlier, the increased use of the unimpaired forelimb can lead to a depression of the other forelimb motor control. The interhemispheric imbalance observed after stroke injury can exacerbate the inactivation of the lesioned hemisphere (226). In accordance with the interhemispheric inhibition concept, augmented activity in the contralesional hemisphere may result in an increase inhibition of the lesioned hemisphere, potentially worsening the loss of activity already present. In a clinical study by Murase *et al.* (227), they demonstrated that patients injured with chronic subcortical stroke had an unusual high interhemispheric inhibition when using their impaired hand. Moreover, inhibition of the

contralesional hemisphere in humans injured by a stroke led to facilitation in using their impaired hand (96). The persistent ipsilateral activity in our ICH mice motor representations might result from this maladaptive plasticity. By not forcing any constraint on their unimpaired forelimb, the animals were free to use any forelimb they preferred. It is possible that the increase utilization of the unimpaired forelimb exhibited in the behavioral tests have led to greater activity of the non-lesioned hemisphere, inducing abnormal interhemispheric inhibition.

However, an initiation of recovery seems to occur by week 6. The significance between sham and ICH groups in the motor map size and movement amplitude disappears by week 6 where a reduction trend is shown in the values (Fig. 11. B-D). This recovery is similar to the behavioral deficits improvements observed in the cylinder test and NDS. While the mice were left with the opportunity to employ any forelimb they want, the behavioral test used weekly may have functioned as a form of rehabilitation therapy. The rigorous enforcement and practice of utilising the impaired limb is a prevalent rehabilitation program employed with stroke patients (96). The training and enhance use of the impaired forelimb could overcome the maladaptive plasticity. The spontaneous behavioral tests we used were not specialized for such therapy, but they did engage the mice in weekly testing of the forelimbs. This has potentially contributed to an improvement of the impaired paw use, slowly resulting in functional cortical recovery.

Another explanation for this recovery observed in motor maps is the idea that there is transcallosal excitation instead of inhibition. Studies have debated the hypothesis of interhemispheric inhibition (228). The stimulation of both hemispheres in the brain showed an ipsilateral excitability with a decrease of activity in the contralateral hemisphere (229). Moreover, Waters and colleagues (230) have tested the connections between both hemispheres by evaluating cortical activity during motor learning. They found that both hemispheres participated in better results of a skilled task without any reduction of performance when stimulating the ipsilateral cortex, arguing for an interhemispheric cooperation. Interestingly, and in concordance with this process, the non-impaired forelimb showed recovery in the injured hemisphere earlier than the impaired paw (Fig. S4), suggesting that the increased utilization of the unimpaired forelimb in acute timepoints might have helped in the recovery of its ipsilateral hemisphere by coordinated excitation. The possible

excitability collaboration between both hemispheres could have helped in the recovery of our ICH animals' motor maps over time by facilitating the lesioned hemisphere activity.

5. Conclusion

5.1 Significance

The understanding of the recovery progression following ICH is still incomplete in the literature. The aim of this study was to provide a better comprehension of the injury and recovery process following a striatal ICH by assessing functional and behavioral changes. Although many studies have looked at behavioral deficits and connectivity alterations following a striatal ICH, we were the first one to investigate the longitudinal impact on bilateral sensorimotor maps in relation to behavioral deficits.

Striatal ICH in the collagenase mouse model demonstrated a variety of outcomes in lesion damage which correlated with the heterogeneity of ICH injury observed in the human population. We reiterated the evidence of acute and chronic motor behavioral impairments with progressive recovery shown in previous studies. By following a novel experimental timeline utilizing non-invasive LBMM and ISOI in ICH mice, we showed that striatal ICH impaired motor representations in the cortex without damaging sensory maps. While similar findings have been demonstrated in the past, this study was the first one to evaluate the sensorimotor functions in both hemispheres. To compensate for the loss of functions in the ipsilesional hemisphere, larger contralesional activity in the injured mice was seen after ICH induction. This contralesional dominance lasted for 5 weeks before demonstrating a trend toward recovery. This recovery initiation was paired with a recovery of impaired forelimb utilization. Additionally, the unimpaired forelimb motor representations recovery preceded the impaired forelimb. Overall, LBMM, ISOI and behavioral testing highlighted the complex injury progression occurring after ICH and the brain capacity to undergo plasticity to overcome the resulting deficits.

5.2 Limitations and future direction

5.2.1 Isoflurane neuroprotection

One limitation of this study is the use of isoflurane during surgery. Although surgeries were done efficiently, within a limited timeframe and utilizing the lowest isoflurane settings possible, the animal remained under anesthesia for approximately an hour. Isoflurane has been studied as a neuroprotective agent regulating inflammation and reducing apoptosis in brain injuries with benefits observed when used as a pre- or post-conditioning treatment (231–233). In an ICH mouse model, exposure to isoflurane for a duration of one hour post-surgery resulted in a marked reduction of brain edema and cellular apoptosis which was related to better behavioral outcome (234). These studies suggest that using isoflurane during ICH induction may introduce a confounding variable in the injury consequences by acting as a protective agent. The utilization of different anesthetics, such as xylazine and ketamine, could overcome this limitation in the future.

5.2.2 Anesthesia-induced LBMM and ISOI

Another limitation is the weekly use of anesthesia in our sensorimotor data acquisition. Isoflurane and a cocktail of ketamine and xylazine were administered to the mice to keep them under an anesthetized state during experiments. Although the repetitive use of xylazine and ketamine is not known to induce any long-term behavioral changes, ketamine displayed synaptic plasticity when administered in subanesthetic dose (235,236). Conversely, multiple use of isoflurane has been shown to cause mild distress with changes in exploratory behavior and food intake (237). However, these effects were exhibited after multiple anesthesia sessions within a day and repeated every 3-4 days. Our mice were induced once a week for approximately an hour, possibly limiting the negative effect of isoflurane. Nevertheless, in future studies, the experiment could be done in awake mice, preventing the utilization of anesthesia, and providing a more comprehensive understanding of ICH progression by replicating the awake state of the brain.

5.2.3 Baseline measurements

In this study, we used a chronic cranial window to allow longitudinal and minimally invasive evaluation of cortical functions. A limitation of this technique came when we paired it with the collagenase model, preventing baseline measurements acquisition. Since our ICH mouse model involved an intracranial injection, the chronic window could not be implanted prior to ICH induction, preventing LBMM and ISOI before the surgery. While sham animals were used as a control for the sensorimotor maps experiments, the baseline assessments would have provided a comprehensive and complete evaluation of striatal ICH impact on sensorimotor functions within the groups. Moreover, sham mice received an injection as well, leading to the disruption of brain parenchyma by the needle tract. The use of a naïve group of mice, with only the transcranial window implantation, could allow control for needle damage in brain tissue.

5.2.4 Spontaneous behavioral task for a motor skilled-related brain region

While the striatum participates in movement control and decision-making behavior, it also plays a major role in skilled motor movement (18,34). The utilization of spontaneous behavioral test enabled the evaluation of behavior without any training needed, providing no confound of motor learning on the ICH recovery. However, utilizing a skilled motor task in future research could further assess the impact of striatal injury in this functional component. Additionally, the striatum is also thought to store learned motor skills once they are acquired, but this remains a debate in the literature (238). It would be interesting to examine the impact of a striatal injury at different period of a skilled-task training in ICH rodents to provide additional evidence on the striatum role within motor learning.

5.2.5 Neurovascular coupling disruption and ISOI

ISOI assessment uses neurovascular coupling as a measurement of the sensory response. However, neurovascular coupling has been demonstrated to be impaired following an ischemia episode in the brain (136,239). In a study by Sunil *et al.* (240), neuronal response were examined simultaneously with hemodynamic response. The neurovascular coupling showed a high correlation with neuronal firing in healthy conditions but induction of a stroke led to a disconnection between the two

measurements in the first week after injury onset. This dysregulation of the hemodynamic response early after stroke indicate that acute ISOI measurements could inaccurately represent sensory response.

5.2.6 Individual correlation between sensorimotor mapping, behavior and ICH lesion size

By utilizing non-invasive imaging and stimulation techniques, longitudinal assessments within the same animals were completed, allowing for investigation of recovery over time. Additionally, using mice as an animal model provides for individual identification of each subject. Nonetheless, no correlation measurements were achieved in this study. Since there is a still an uncomplete knowledge of the lesion size impact on stroke recovery (241), analysing the correlation between the sensorimotor mapping experiments, the behavioral deficits and the lesion size could provide a better understanding of the recovery process.

5.2.7 Age group in ICH

The prevalence and incidence of ICH in humans is greater in the older population (<70 years old) (2). To reliably study ICH injury, old mice should be utilized in order to mimic the natural changes occurring in aging brain (242). The mice in our study were relatively young (3-4 months old), but their faster recovery and larger resilience to complications after brain injury facilitated the evaluation of spontaneous recovery. Regardless, the results of this study contribute to the understanding of recovery in a healthy population, which is not conforming to the global ICH incidence.

6. Supplemental Figures

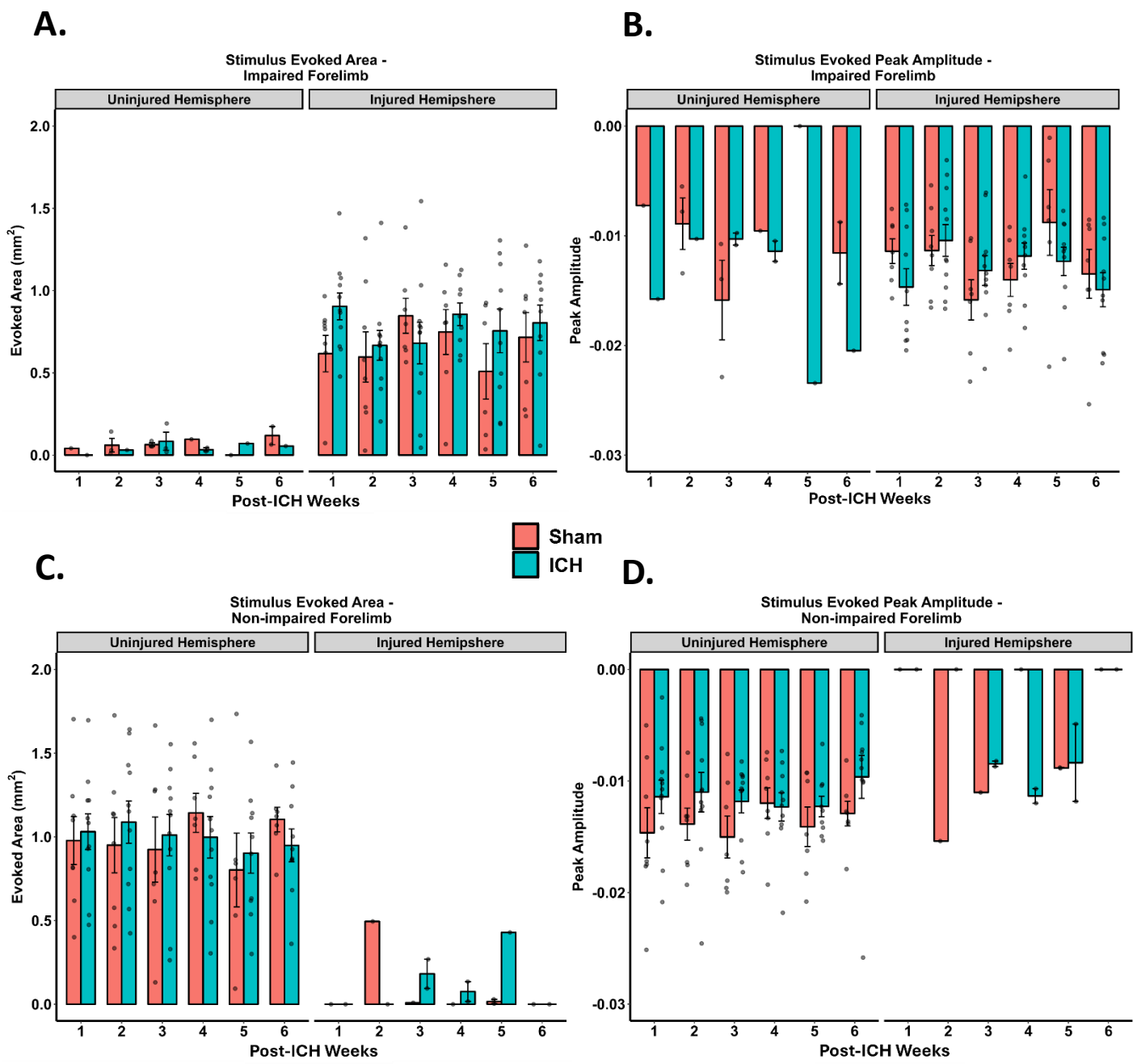

Figure S1. ISOI Evoked Response from Sensory Stimulation in Both Hemispheres: A-D. Evoked response within each hemisphere for both sham (orange) and ICH (blue) group over the 6 post-ICH weeks. Area size of evoked response in both impaired (**A**) and non-impaired (**C**) forelimb. Response peak amplitude in both impaired (**B**) and non-impaired (**D**) forelimb.

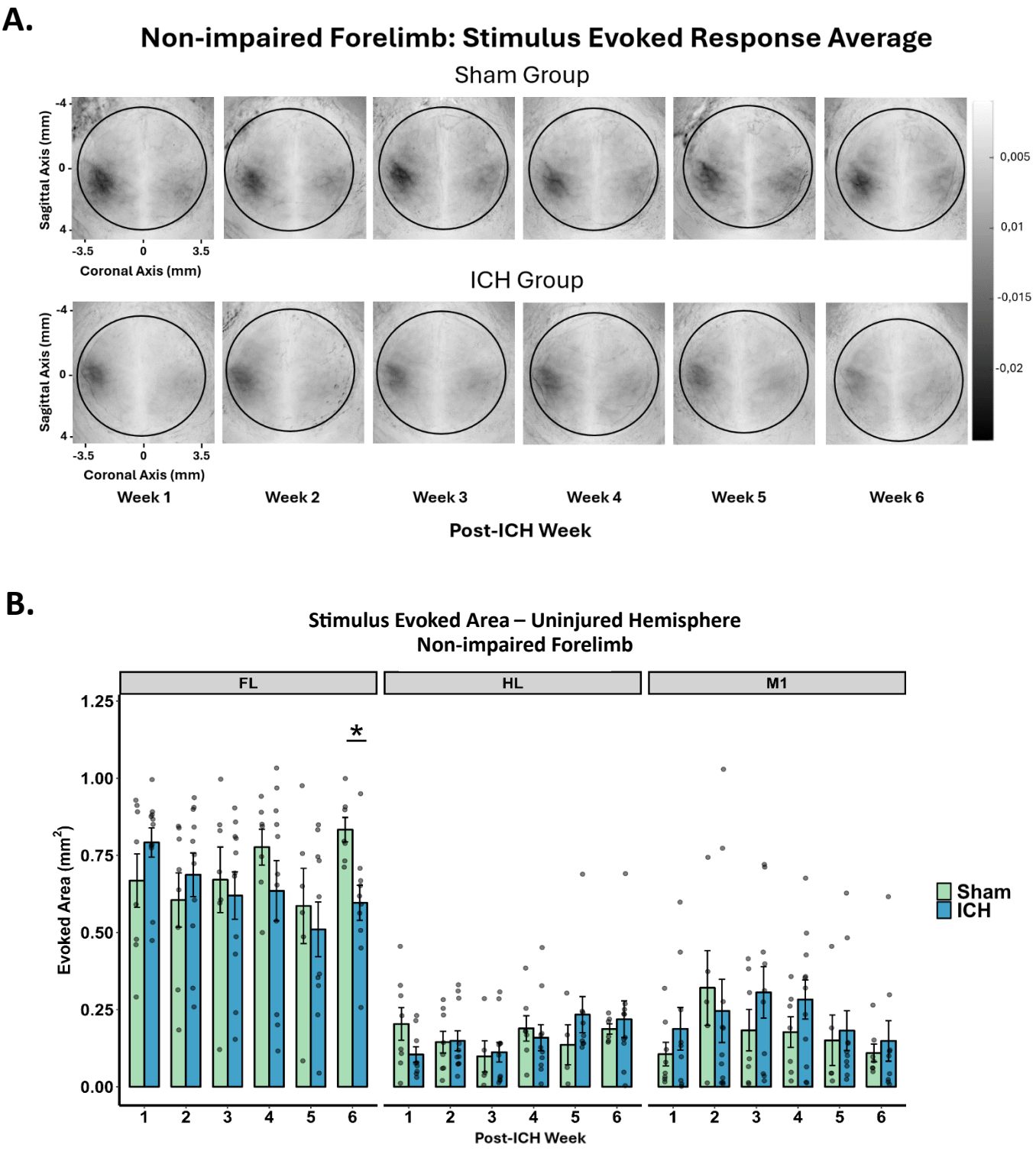

Figure S2. ISOI: Evoked Area in Non-Impaired Forelimb: A. Evoked sensory maps in both sham (top) and ICH (bottom) groups over the 6 post-ICH weeks for the non-impaired forelimb. **B.** Size of the response area (mm^2) from forelimb stimulation within Allen Mouse Brain Atlas anatomical regions of the uninjured brain hemisphere in both sham (green) and ICH (blue) groups over the 6 post-ICH weeks for the unimpaired forelimb.

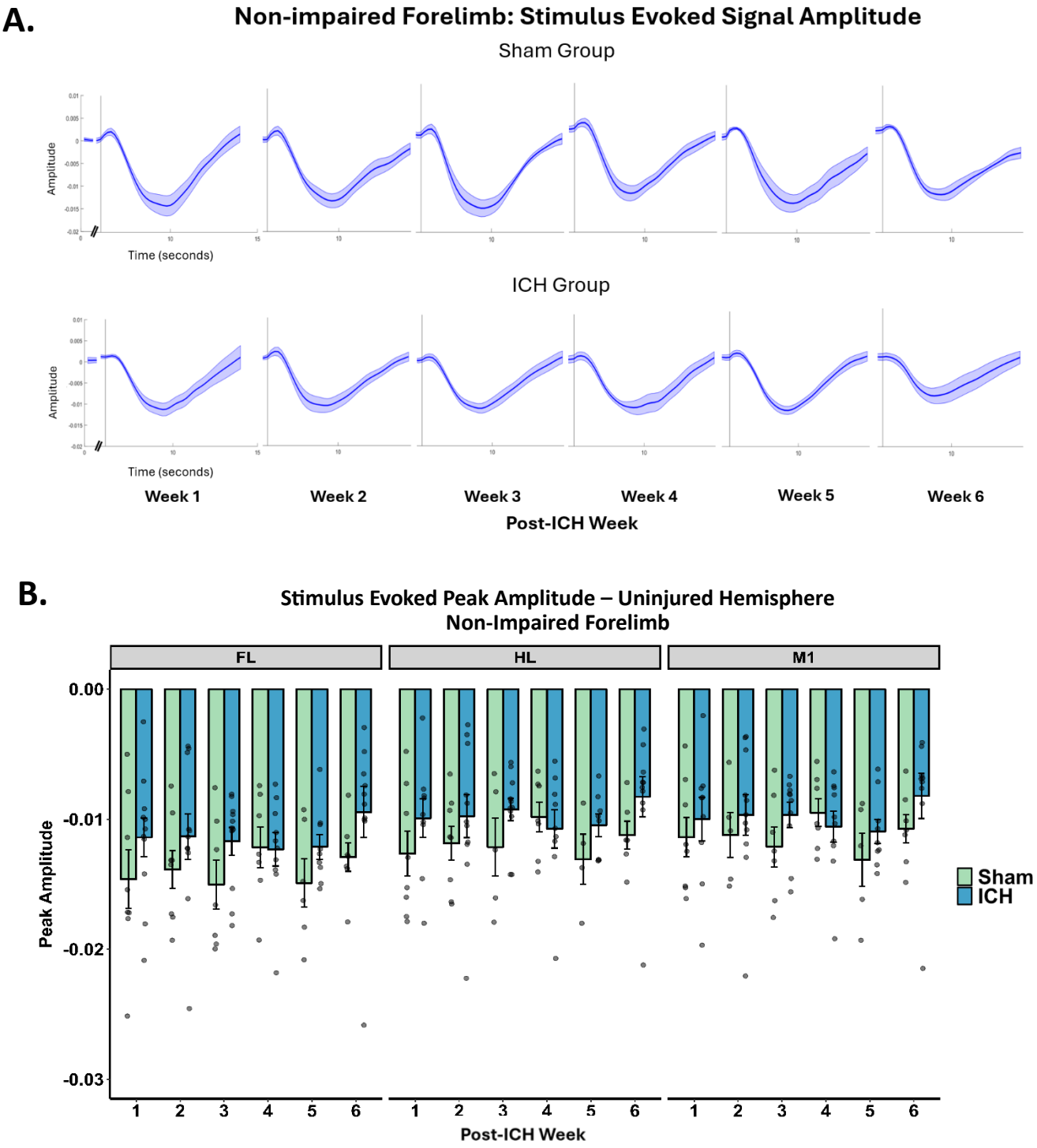

Figure S3. ISOI: Evoked Peak Amplitude in Non-Impaired Forelimb: A. Average traces of the evoked response in FL area within sham (top) and ICH (bottom) groups over the 6 post-ICH weeks for the unimpaired forelimb. The vertical solid line indicates the onset of the vibrotactile stimulus. **B.** Peak amplitude from evoked signal within the Allen Mouse Brain Atlas anatomical areas in the uninjured brain hemisphere for both sham (green) and ICH (blue) groups over the 6 post-ICH weeks for the unimpaired forelimb.

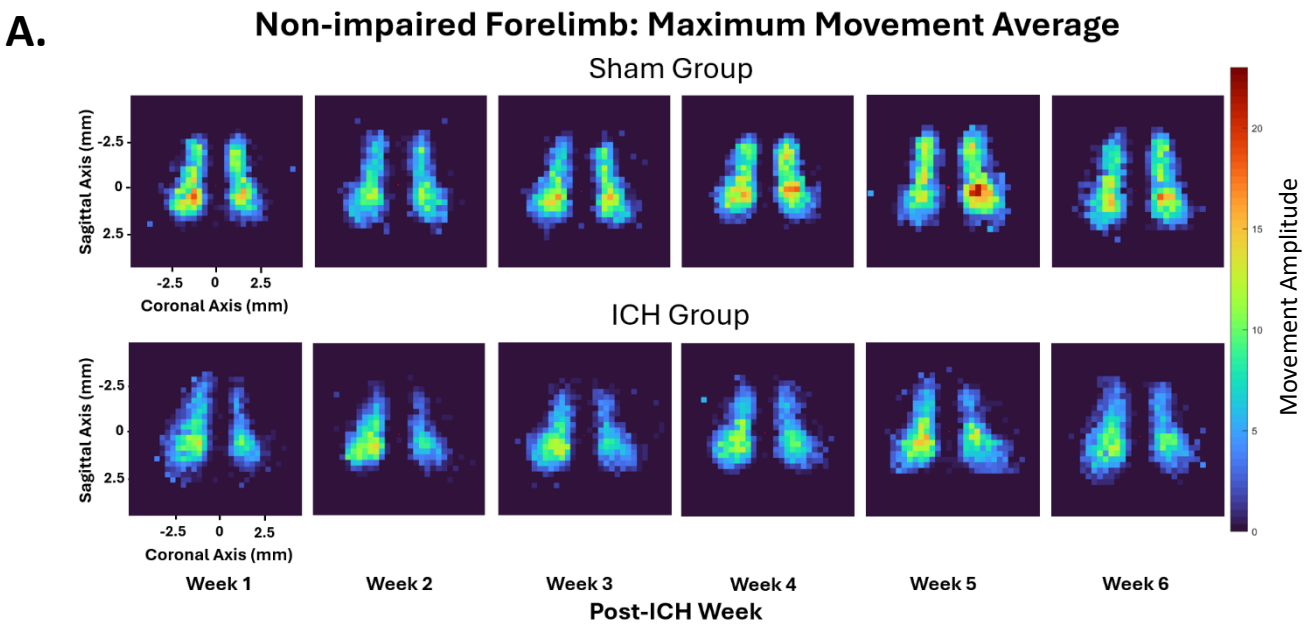
A.
Non-impaired Forelimb: Maximum Movement Average
Sham Group
ICH Group
Sagittal Axis (mm)
Coronal Axis (mm)
Movement Amplitude
Week 1
Week 2
Week 3
Week 4
Week 5
Week 6
Post-ICH Week

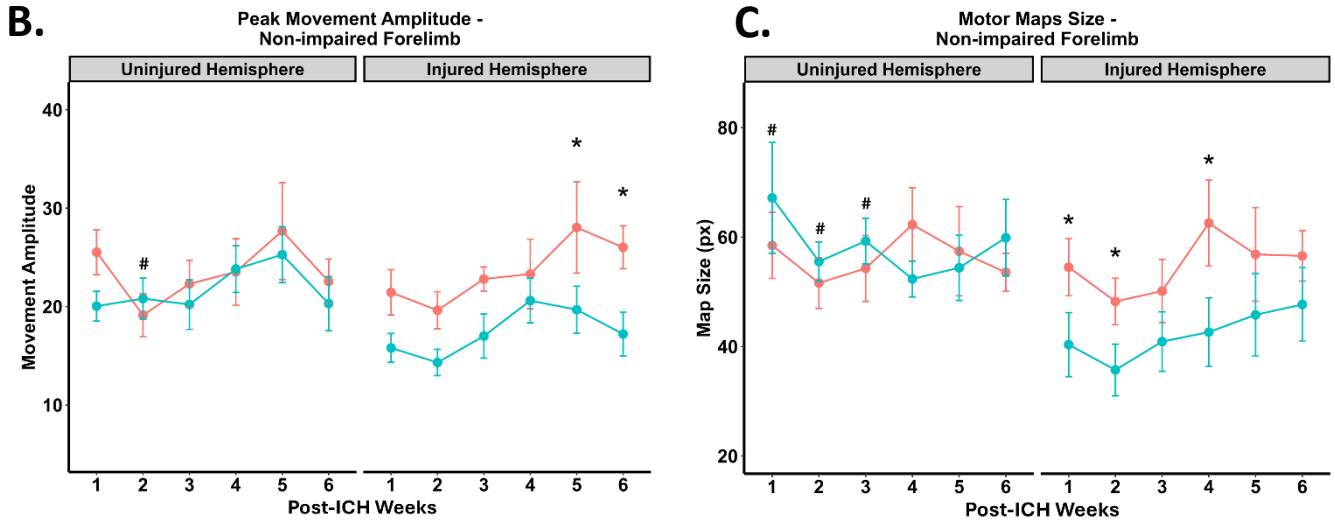
B.
Peak Movement Amplitude - Non-impaired Forelimb
C.
Motor Maps Size - Non-impaired Forelimb
Uninjured Hemisphere
Injured Hemisphere
Movement Amplitude
Map Size (px)
Post-ICH Weeks
Sham
ICH

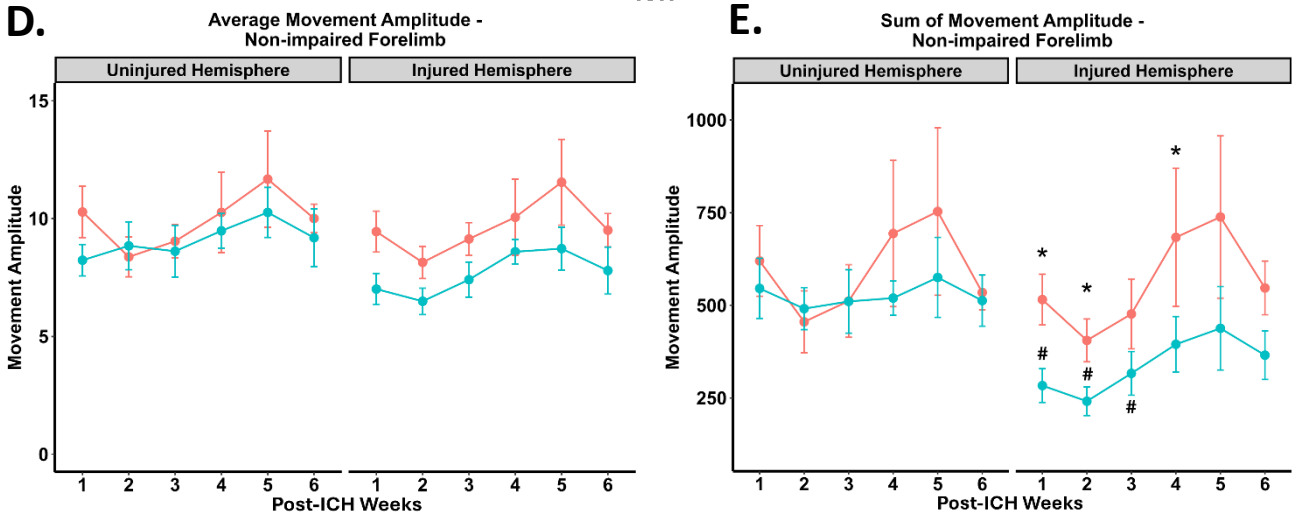
D.
Average Movement Amplitude - Non-impaired Forelimb
E.
Sum of Movement Amplitude - Non-impaired Forelimb
Uninjured Hemisphere
Injured Hemisphere
Movement Amplitude
Post-ICH Weeks

Figure S4. Motor Maps Amplitude and Map Size for Unimpaired Forelimb: A. Averaged motor maps for the unimpaired forelimb representing the movement amplitude per stimulation point within both sham (top) and ICH (bottom) groups over the 6 post-ICH weeks. **B-C-D-E.** Different map interpretations compared between sham (orange) and ICH (blue) group within both hemispheres for the unimpaired forelimb. Stars (*) indicate significant differences between groups and dash (#) represents significant differences between hemispheres. **B.** Peak movement amplitude. **C.** Average map size calculated by the number of pixels activated. **D.** Movement amplitude average. **E.** Sum of total movement amplitude.

Subtests	**Score**			
	0	**1**	**2**	**3**
Forelimb Extension	Forelimbs are symmetrical	Impaired forelimb does not extend as much as unimpaired side	Impaired forelimb held close to body and minimal movement	Impaired forelimb does not move at all
Forelimb Outstretching	Walks in straight line and forelimbs are outstretched	Walks toward impaired side and forelimbs are outstretched	Walks heavily toward impaired side and impaired forelimb does not outstretch well	Impaired forelimb does not move or outstretch
Forelimb Wire Hanging	Both forelimbs grab the wire	Impaired forelimb grabs but not able to support weight	Grabs with wrist of impaired forelimb	Can't grab the wire with the impaired forelimb

Table 1. Neurological Deficit Score: Scoring scale description of the three NDS subtests. Subtests are scored on a scale of 0-3, 0 representing normal behavior and 3 showing severe deficits in the mouse.

7. Bibliography

1. Shoamanesh (Co-chair) A, Patrice Lindsay M, Castellucci LA, Cayley A, Crowther M, de Wit K, et al. Canadian stroke best practice recommendations: Management of Spontaneous Intracerebral Hemorrhage, 7th Edition Update 2020. International Journal of Stroke. 2021 Apr 1;16(3):321–41.

2. Feigin VL, Brainin M, Norrving B, Martins S, Sacco RL, Hacke W, et al. World Stroke Organization (WSO): Global Stroke Fact Sheet 2022. International Journal of Stroke. 2022 Jan 1;17(1):18–29.

3. Grefkes C, Fink GR. Recovery from stroke: current concepts and future perspectives. Neurological Research and Practice. 2020 Jun 16;2(1):17.

4. Aronowski J, Zhao X. Molecular Pathophysiology of Cerebral Hemorrhage: Secondary Brain Injury. Stroke. 2011 Jun;42(6):1781–6.

5. Schlunk F, Greenberg SM. The Pathophysiology of Intracerebral Hemorrhage Formation and Expansion. Transl Stroke Res. 2015 Aug 1;6(4):257–63.

6. Jiang C, Guo H, Zhang Z, Wang Y, Liu S, Lai J, et al. Molecular, Pathological, Clinical, and Therapeutic Aspects of Perihematomal Edema in Different Stages of Intracerebral Hemorrhage. Oxidative Medicine and Cellular Longevity. 2022 Sep 17;2022:e3948921.

7. Keep RF, Hua Y, Xi G. Intracerebral haemorrhage: mechanisms of injury and therapeutic targets. Lancet Neurol. 2012 Aug;11(8):10.1016/S1474-4422(12)70104-7.

8. Wan S, Cheng Y, Jin H, Guo D, Hua Y, Keep RF, et al. Microglia Activation and Polarization After Intracerebral Hemorrhage in Mice: the Role of Protease-Activated Receptor-1. Transl Stroke Res. 2016 Dec;7(6):478–87.

9. Ironside N, Chen CJ, Ding D, Mayer SA, Connolly ES. Perihematomal Edema After Spontaneous Intracerebral Hemorrhage. Stroke. 2019 Jun;50(6):1626–33.

10. Skriver EB, Olsen TS. Tissue Damage at Computed Tomography following Resolution of Intracerebral Hematomas. Acta Radiologica Diagnosis. 1986 Sep;27(5):495–500.

11. Hartman R, Lekic T, Rojas H, Tang J, Zhang JH. Assessing functional outcomes following intracerebral hemorrhage in rats. Brain Research. 2009 Jul 14;1280:148–57.

12. Foster NN, Barry J, Korobkova L, Garcia L, Gao L, Becerra M, et al. The mouse cortico–basal ganglia–thalamic network. Nature. 2021;598(7879):188–94.

13. Balleine BW, O'Doherty JP. Human and Rodent Homologies in Action Control: Corticostriatal Determinants of Goal-Directed and Habitual Action. Neuropsychopharmacol. 2010 Jan;35(1):48–69.

14. Valjent E, Gangarossa G. The Tail of the Striatum: From Anatomy to Connectivity and Function. Trends in Neurosciences. 2021 Mar;44(3):203–14.

15. Parent A. Extrinsic connections of the basal ganglia. Trends in Neurosciences. 1990 Jul 1;13(7):254–8.

16. Parent A, Hazrati LN. Functional anatomy of the basal ganglia. I. The cortico-basal ganglia-thalamo-cortical loop. Brain Research Reviews. 1995 Jan;20(1):91–127.

17. Balsters JH, Zerbi V, Sallet J, Wenderoth N, Mars RB. Primate homologs of mouse cortico-striatal circuits. Wassum KM, Kahnt T, Laubach M, White S, editors. eLife. 2020 Apr 16;9:e53680.

18. Woolley DG, Laeremans A, Gantois I, Mantini D, Vermaercke B, Op de Beeck HP, et al. Homologous involvement of striatum and prefrontal cortex in rodent and human water maze learning. Proceedings of the National Academy of Sciences. 2013 Feb 19;110(8):3131–6.

19. Guo Q, Wang D, He X, Feng Q, Lin R, Xu F, et al. Whole-Brain Mapping of Inputs to Projection Neurons and Cholinergic Interneurons in the Dorsal Striatum. Arenkiel B, editor. PLoS ONE. 2015 Apr 1;10(4):e0123381.

20. Collins AL, Saunders BT. Heterogeneity in striatal dopamine circuits: Form and function in dynamic reward seeking. J Neurosci Res. 2020 Jun;98(6):1046–69.

21. Chuhma N, Oh SJ, Rayport S. The dopamine neuron synaptic map in the striatum. Cell Reports. 2023 Mar;42(3):112204.

22. Katthagen T, Kaminski J, Heinz A, Buchert R, Schlagenhauf F. Striatal Dopamine and Reward Prediction Error Signaling in Unmedicated Schizophrenia Patients. Schizophr Bull. 2020 Apr 22;46(6):1535–46.

23. Kalmbach A, Winiger V, Jeong N, Asok A, Gallistel CR, Balsam PD, et al. Dopamine encodes real-time reward availability and transitions between reward availability states on different timescales. Nat Commun. 2022 Jul 1;13:3805.

24. Menegas W, Babayan BM, Uchida N, Watabe-Uchida M. Opposite initialization to novel cues in dopamine signaling in ventral and posterior striatum in mice. eLife. 6:e21886.

25. Chen AP, Chen L, Kim TA, Xiong Q. Integrating the Roles of Midbrain Dopamine Circuits in Behavior and Neuropsychiatric Disease. Biomedicines. 2021 Jun 7;9(6):647.

26. Ikemoto S. Dopamine reward circuitry: two projection systems from the ventral midbrain to the nucleus accumbens-olfactory tubercle complex. Brain Res Rev. 2007 Nov;56(1):27–78.

27. Salvatore MF. Dopamine Signaling in Substantia Nigra and Its Impact on Locomotor Function—Not a New Concept, but Neglected Reality. Int J Mol Sci. 2024 Jan 17;25(2):1131.

28. Zamora-Ursulo MA, Perez-Becerra J, Tellez LA, Saderi N, Carrillo-Reid L. Reversal of pathological motor behavior in a model of Parkinson's disease by striatal dopamine uncaging. PLoS One. 2023 Aug 18;18(8):e0290317.

29. Dudman JT, Krakauer JW. The basal ganglia: from motor commands to the control of vigor. Current Opinion in Neurobiology. 2016 Apr;37:158–66.

30. Pan WX, Mao T, Dudman JT. Inputs to the Dorsal Striatum of the Mouse Reflect the Parallel Circuit Architecture of the Forebrain. Front Neuroanat. 2010 Dec 27;4:147.

31. Kreitzer AC, Malenka RC. Striatal plasticity and basal ganglia circuit function. Neuron. 2008 Nov 26;60(4):543–54.

32. Hunnicutt BJ, Jongbloets BC, Birdsong WT, Gertz KJ, Zhong H, Mao T. A comprehensive excitatory input map of the striatum reveals novel functional organization. eLife. 2016 Nov 28;5:e19103.

33. Hintiryan H, Foster NN, Bowman I, Bay M, Song MY, Gou L, et al. The mouse cortico-striatal projectome. Nat Neurosci. 2016 Aug;19(8):1100–14.

34. Phillips CD, Myers CC, Leventhal DK, Burgess CR. Striatal dopamine contributions to skilled motor learning.

35. Panigrahi B, Martin KA, Li Y, Graves AR, Vollmer A, Olson L, et al. Dopamine Is Required for the Neural Representation and Control of Movement Vigor. Cell. 2015 Sep;162(6):1418–30.

36. Kim N, Barter JW, Sukharnikova T, Yin HH. Striatal firing rate reflects head movement velocity. Eur J of Neuroscience. 2014 Nov;40(10):3481–90.

37. Forstmann BU, Anwander A, Schäfer A, Neumann J, Brown S, Wagenmakers EJ, et al. Cortico-striatal connections predict control over speed and accuracy in perceptual decision making. Proceedings of the National Academy of Sciences. 2010 Sep 7;107(36):15916–20.

38. Markowitz JE, Gillis WF, Beron CC, Neufeld SQ, Robertson K, Bhagat ND, et al. The Striatum Organizes 3D Behavior via Moment-to-Moment Action Selection. Cell. 2018 Jun 28;174(1):44-58.e17.

39. Vink M, Kahn RS, Raemaekers M, van den Heuvel M, Boersma M, Ramsey NF. Function of striatum beyond inhibition and execution of motor responses. Human Brain Mapping. 2005;25(3):336–44.

40. Robertson CL, Ishibashi K, Mandelkern MA, Brown AK, Ghahremani DG, Sabb F, et al. Striatal D1- and D2-type Dopamine Receptors Are Linked to Motor Response Inhibition in Human Subjects. J Neurosci. 2015 Apr 15;35(15):5990–7.

41. Zandbelt BB, Vink M. On the Role of the Striatum in Response Inhibition. PLOS ONE. 2010 Nov 4;5(11):e13848.

42. Lee CR, Yonk AJ, Wiskerke J, Paradiso KG, Tepper JM, Margolis DJ. Opposing Influence of Sensory and Motor Cortical Input on Striatal Circuitry and Choice Behavior. Curr Biol. 2019 Apr 22;29(8):1313-1323.e5.

43. Reig R, Silberberg G. Multisensory Integration in the Mouse Striatum. Neuron. 2014 Sep 3;83(5):1200–12.

44. Hidalgo-Balbuena AE, Luma AY, Pimentel-Farfan AK, Peña-Rangel T, Rueda-Orozco PE. Sensory representations in the striatum provide a temporal reference for learning and executing motor habits. Nat Commun. 2019 Sep 9;10:4074.

45. Wiesendanger M, Hummelsheim H, Bianchetti M, Chen DF, Hyland B, Maier V, et al. Input and output organization of the supplementary motor area. Ciba Found Symp. 1987;132:40–62.

46. Barthas F, Kwan AC. Secondary motor cortex: where 'sensory' meets 'motor' in the rodent frontal cortex. Trends Neurosci. 2017 Mar;40(3):181–93.

47. Lemon RN. Descending Pathways in Motor Control. Annu Rev Neurosci. 2008 Jul 1;31(1):195–218.

48. Bakken TE, Jorstad NL, Hu Q, Lake BB, Tian W, Kalmbach BE, et al. Comparative cellular analysis of motor cortex in human, marmoset and mouse. Nature. 2021 Oct;598(7879):111–9.

49. Brecht M, Krauss A, Muhammad S, Sinai-Esfahani L, Bellanca S, Margrie TW. Organization of rat vibrissa motor cortex and adjacent areas according to cytoarchitectonics, microstimulation, and intracellular stimulation of identified cells. J of Comparative Neurology. 2004 Nov 22;479(4):360–73.

50. Neafsey EJ, Sievert C. A second forelimb motor area exists in rat frontal cortex. Brain Research. 1982 Jan;232(1):151–6.

51. Tennant KA, Adkins DL, Donlan NA, Asay AL, Thomas N, Kleim JA, et al. The Organization of the Forelimb Representation of the C57BL/6 Mouse Motor Cortex as Defined by Intracortical Microstimulation and Cytoarchitecture. Cerebral Cortex. 2011 Apr;21(4):865–76.

52. Tennant KA, Kerr AL, Adkins DL, Donlan N, Thomas N, Kleim JA, et al. Age-dependent reorganization of peri-infarct "premotor" cortex with task-specific rehabilitative training in mice. Neurorehabil Neural Repair. 2015 Feb;29(2):193–202.

53. Brown AR, Teskey GC. Motor Cortex Is Functionally Organized as a Set of Spatially Distinct Representations for Complex Movements. J Neurosci. 2014 Oct 8;34(41):13574–85.

54. Kunori N, Takashima I. High-order motor cortex in rats receives somatosensory inputs from the primary motor cortex via cortico-cortical pathways. Barbas H, editor. Eur J of Neuroscience. 2016 Dec;44(11):2925–34.

55. Deffeyes JE, Touvykine B, Quessy S, Dancause N. Interactions between rostral and caudal cortical motor areas in the rat. J Neurophysiol. 2015 Jun;113(10):3893–904.

56. Hira R, Ohkubo F, Tanaka YR, Masamizu Y, Augustine GJ, Kasai H, et al. In vivo optogenetic tracing of functional corticocortical connections between motor forelimb areas. Front Neural Circuits. 2013 Apr 1;7:55.

57. Rouiller EM, Moret V, Liang F. Comparison of the Connectional Properties of the Two Forelimb Areas of the Rat Sensorimotor Cortex: Support for the Presence of a Premotor or Supplementary Motor Cortical Area. Somatosensory & Motor Research. 1993 Jan;10(3):269–89.

58. Brus-Ramer M, Carmel JB, Martin JH. Motor Cortex Bilateral Motor Representation Depends on Subcortical and Interhemispheric Interactions. Journal of Neuroscience. 2009 May 13;29(19):6196–206.

59. Dolbakyan E, Hernandez-Mesa N, Bures˘ J. Skilled forelimb movements and unit activity in motor cortex and caudate nucleus in rats. Neuroscience. 1977 Feb 1;2(1):73–80.

60. Soma S, Saiki A, Yoshida J, Ríos A, Kawabata M, Sakai Y, et al. Distinct Laterality in Forelimb-Movement Representations of Rat Primary and Secondary Motor Cortical Neurons with Intratelencephalic and Pyramidal Tract Projections. J Neurosci. 2017 Nov 8;37(45):10904–16.

61. Touvykine B, Elgbeili G, Quessy S, Dancause N. Interhemispheric modulations of motor outputs by the rostral and caudal forelimb areas in rats. Journal of Neurophysiology. 2020 Apr;123(4):1355–68.

62. Zuo S, Pan P, Li Q, Chen Y, Feng H. White Matter Injury and Recovery after Hypertensive Intracerebral Hemorrhage. BioMed Research International. 2017;2017(1):6138424.

63. Katsuki H, Hijioka M. Intracerebral Hemorrhage as an Axonal Tract Injury Disorder with Inflammatory Reactions. Biological & Pharmaceutical Bulletin. 2017;40(5):564–8.

64. Hijioka M, Anan J, Matsushita H, Ishibashi H, Kurauchi Y, Hisatsune A, et al. Axonal dysfunction in internal capsule is closely associated with early motor deficits after intracerebral hemorrhage in mice. Neuroscience Research. 2016 May 1;106:38–46.

65. Moxon-Emre I, Schlichter LC. Neutrophil Depletion Reduces Blood-Brain Barrier Breakdown, Axon Injury, and Inflammation After Intracerebral Hemorrhage. Journal of Neuropathology & Experimental Neurology. 2011 Mar 1;70(3):218–35.

66. Matsushita H, Hijioka M, Hisatsune A, Isohama Y, Shudo K, Katsuki H. Natural and synthetic retinoids afford therapeutic effects on intracerebral hemorrhage in mice. European Journal of Pharmacology. 2012 May 15;683(1):125–31.

67. Pinho J, Costa AS, Araújo JM, Amorim JM, Ferreira C. Intracerebral hemorrhage outcome: A comprehensive update. Journal of the Neurological Sciences. 2019 Mar 15;398:54–66.

68. Qureshi AI, Mendelow AD, Hanley DF. Intracerebral haemorrhage. The Lancet. 2009 May;373(9675):1632–44.

69. Clarke J, Ploughman M, Corbett D. A qualitative and quantitative analysis of skilled forelimb reaching impairment following intracerebral hemorrhage in rats. Brain Research. 2007 May;1145:204–12.

70. Barratt HE, Lanman TA, Carmichael ST. Mouse Intracerebral Hemorrhage Models Produce Different Degrees of Initial and Delayed Damage, Axonal Sprouting, and Recovery. J Cereb Blood Flow Metab. 2014 Sep;34(9):1463–71.

71. Cassidy JM, Cramer SC. Spontaneous and Therapeutic-Induced Mechanisms of Functional Recovery After Stroke. Transl Stroke Res. 2017 Feb 1;8(1):33–46.

72. Jones TA, Schallert T. Use-dependent growth of pyramidal neurons after neocortical damage. J Neurosci. 1994 Apr 1;14(4):2140–52.

73. Benowitz LI, Carmichael ST. Promoting axonal rewiring to improve outcome after stroke. Neurobiol Dis. 2010 Feb;37(2):259.

74. Jones TA, Kleim JA, Greenough WT. Synaptogenesis and dendritic growth in the cortex opposite unilateral sensorimotor cortex damage in adult rats: a quantitative electron microscopic examination. Brain Research. 1996 Sep 9;733(1):142–8.

75. Mestriner RG, Pagnussat AS, Boisserand LSB, Valentim L, Netto CA. Skilled reaching training promotes astroglial changes and facilitated sensorimotor recovery after collagenase-induced intracerebral hemorrhage. Exp Neurol. 2011 Jan;227(1):53–61.

76. Cramer SC. Repairing the human brain after stroke: I. Mechanisms of spontaneous recovery. Annals of Neurology. 2008;63(3):272–87.

77. Kwakkel G, Wagenaar RC, Twisk JW, Lankhorst GJ, Koetsier JC. Intensity of leg and arm training after primary middle-cerebral-artery stroke: a randomised trial. The Lancet. 1999 Jul;354(9174):191–6.

78. Saulle MF, Schambra HM. Recovery and Rehabilitation after Intracerebral Hemorrhage. Semin Neurol. 2016 Jun;36(3):306–12.

79. Lee KB, Kim JS, Hong BY, Kim YD, Hwang BY, Lim SH. The Motor Recovery Related with Brain Lesion in Patients with Intracranial Hemorrhage. Behav Neurol. 2015;2015:258161.

80. Kwakkel G, Kollen B, Lindeman E. Understanding the pattern of functional recovery after stroke: Facts and theories. :19.

81. Zhu W, Gao Y, Wan J, Lan X, Han X, Zhu S, et al. Changes in motor function, cognition, and emotion-related behavior after right hemispheric intracerebral hemorrhage in various brain regions of mouse. Brain, Behavior, and Immunity. 2018 Mar 1;69:568–81.

82. Liu Y, Lu G, Su XW, Ding T, Wang WL, Li YM, et al. Characterization of Axon Damage, Neurological Deficits, and Histopathology in Two Experimental Models of Intracerebral Hemorrhage. Front Neurosci. 2018 Dec 11;12:928.

83. Tamakoshi K, Ishida A, Takamatsu Y, Hamakawa M, Nakashima H, Shimada H, et al. Motor skills training promotes motor functional recovery and induces synaptogenesis in the motor cortex and striatum after intracerebral hemorrhage in rats [Internet]. [cited 2022 Nov 7].

84. Kolb B, Brown R, Witt-Lajeunesse A, Gibb R. Neural Compensations After Lesion of the Cerebral Cortex. Neural Plasticity. 2001 Jan;8(1–2):1–16.

85. Brown CE, Wong C, Murphy TH. Rapid Morphologic Plasticity of Peri-Infarct Dendritic Spines After Focal Ischemic Stroke. Stroke. 2008 Apr;39(4):1286–91.

86. Brown CE, Li P, Boyd JD, Delaney KR, Murphy TH. Extensive Turnover of Dendritic Spines and Vascular Remodeling in Cortical Tissues Recovering from Stroke. J Neurosci. 2007 Apr 11;27(15):4101–9.

87. Tombari D, Loubinoux I, Pariente J, Gerdelat A, Albucher JF, Tardy J, et al. A longitudinal fMRI study: in recovering and then in clinically stable sub-cortical stroke patients. NeuroImage. 2004 Nov 1;23(3):827–39.

88. Li S, Overman JJ, Katsman D, Kozlov SV, Donnelly CJ, Twiss JL, et al. An age-related sprouting transcriptome provides molecular control of axonal sprouting after stroke. Nat Neurosci. 2010 Dec;13(12):1496–504.

89. Nguyen A, Huynh H, Sjovold S, Colbourne F. Progressive Brain Damage and Alterations in Dendritic Arborization after Collagenase-Induced Intracerebral Hemorrhage in Rats. CNR. 2008 Aug 1;5(3):171–7.

90. Papadopoulos CM, Tsai SY, Guillen V, Ortega J, Kartje GL, Wolf WA. Motor Recovery and Axonal Plasticity With Short-Term Amphetamine After Stroke. Stroke. 2009 Jan;40(1):294–302.

91. Carmichael ST, Chesselet MF. Synchronous Neuronal Activity Is a Signal for Axonal Sprouting after Cortical Lesions in the Adult. J Neurosci. 2002 Jul 15;22(14):6062–70.

92. Cuadrado ML, Egido JA, González-Gutiérrez JL, Varela-de-Seijas E. Bihemispheric Contribution to Motor Recovery after Stroke: A Longitudinal Study with Transcranial Doppler Ultrasonography. Cerebrovascular Diseases. 1999 Oct 15;9(6):337–44.

93. Netz J, Lammers T, Hömberg V. Reorganization of motor output in the non-affected hemisphere after stroke. Brain. 1997 Sep 1;120(9):1579–86.

94. Biernaskie J, Szymanska A, Windle V, Corbett D. Bi-hemispheric contribution to functional motor recovery of the affected forelimb following focal ischemic brain injury in rats. European Journal of Neuroscience. 2005;21(4):989–99.

95. Jones TA, Adkins DL. Motor System Reorganization After Stroke: Stimulating and Training Toward Perfection. Physiology. 2015 Sep;30(5):358–70.

96. Takeuchi N, Izumi SI. Maladaptive plasticity for motor recovery after stroke: mechanisms and approaches. Neural Plast. 2012;2012:359728.

97. Fritsch G, Hitzig E. Electric excitability of the cerebrum (Über die elektrische Erregbarkeit des Grosshirns). Epilepsy & Behavior. 2009 Jun;15(2):123–30.

98. Kallioniemi E, Könönen M, Julkunen P. Repeatability of functional anisotropy in navigated transcranial magnetic stimulation – coil-orientation versus response. NeuroReport. 2015 Jun 17;26(9):515–21.

99. Fautrelle L, Gueugnon M, Barbieri G, Bonnetblanc F. Inter-hemispheric remapping between arm proprioception and vision of the hand is disrupted by single pulse TMS on the left parietal cortex. Brain and Cognition. 2013 Jul 1;82(2):146–51.

100. Hussin AT, Boychuk JA, Brown AR, Pittman QJ, Teskey GC. Intracortical Microstimulation (ICMS) Activates Motor Cortex Layer 5 Pyramidal Neurons Mainly Transsynaptically. Brain Stimulation. 2015 Jul;8(4):742–50.

101. Thompson FJ, Fernandez JJ. Patterns of cortical projection to hindlimb muscle motoneurone pools. Brain Research. 1975 Oct;97(1):33–46.

102. Murphy JT, Wong YC, Kwan HC. Afferent-efferent linkages in motor cortex for single forelimb muscles. Journal of Neurophysiology. 1975 Jul 1;38(4):990–1014.

103. Bonazzi L, Viaro R, Lodi E, Canto R, Bonifazzi C, Franchi G. Complex Movement Topography and Extrinsic Space Representation in the Rat Forelimb Motor Cortex as Defined by Long-Duration Intracortical Microstimulation. J Neurosci. 2013 Jan 30;33(5):2097–107.

104. Overduin SA, d'Avella A, Carmena JM, Bizzi E. Microstimulation Activates a Handful of Muscle Synergies. Neuron. 2012 Dec 20;76(6):1071–7.

105. Graziano MSA, Taylor CSR, Moore T. Complex Movements Evoked by Microstimulation of Precentral Cortex. Neuron. 2002 May 30;34(5):841–51.

106. Nishibe M, Urban ETR, Barbay S, Nudo RJ. Rehabilitative Training Promotes Rapid Motor Recovery but Delayed Motor Map Reorganization in a Rat Cortical Ischemic Infarct Model. Neurorehabil Neural Repair. 2015 Jun;29(5):472–82.

107. Nudo RJ, Milliken GW. Reorganization of movement representations in primary motor cortex following focal ischemic infarcts in adult squirrel monkeys.

108. Frost SB, Barbay S, Friel KM, Plautz EJ, Nudo RJ. Reorganization of Remote Cortical Regions After Ischemic Brain Injury: A Potential Substrate for Stroke Recovery. Journal of Neurophysiology. 2003 Jun;89(6):3205–14.

109. Dancause N, Barbay S, Frost SB, Zoubina EV, Plautz EJ, Mahnken JD, et al. Effects of Small Ischemic Lesions in the Primary Motor Cortex on Neurophysiological Organization in Ventral Premotor Cortex. Journal of Neurophysiology. 2006 Dec;96(6):3506–11.

110. Starkey ML, Bleul C, Zörner B, Lindau NT, Mueggler T, Rudin M, et al. Back seat driving: hindlimb corticospinal neurons assume forelimb control following ischaemic stroke. Brain. 2012 Nov;135(11):3265–81.

111. Murphy TH, Corbett D. Plasticity during stroke recovery: from synapse to behaviour. Nat Rev Neurosci. 2009 Dec;10(12):861–72.

112. Touvykine B, Mansoori BK, Jean-Charles L, Deffeyes J, Quessy S, Dancause N. The Effect of Lesion Size on the Organization of the Ipsilesional and Contralesional Motor Cortex. Neurorehabil Neural Repair. 2016 Mar;30(3):280–92.

113. Okabe N, Shiromoto T, Himi N, Lu F, Maruyama-Nakamura E, Narita K, et al. Neural network remodeling underlying motor map reorganization induced by rehabilitative training after ischemic stroke. Neuroscience. 2016 Dec 17;339:338–62.

114. Nagel G, Szellas T, Huhn W, Kateriya S, Adeishvili N, Berthold P, et al. Channelrhodopsin-2, a directly light-gated cation-selective membrane channel. Proc Natl Acad Sci USA. 2003 Nov 25;100(24):13940–5.

115. Wang H, Peca J, Matsuzaki M, Matsuzaki K, Noguchi J, Qiu L, et al. High-speed mapping of synaptic connectivity using photostimulation in Channelrhodopsin-2 transgenic mice. Proc Natl Acad Sci USA. 2007 May 8;104(19):8143–8.

116. Pan ZH, Ganjawala TH, Lu Q, Ivanova E, Zhang Z. ChR2 Mutants at L132 and T159 with Improved Operational Light Sensitivity for Vision Restoration. PLOS ONE. 2014 juin;9(6):e98924.

117. Harrison TC, Murphy TH. Motor maps and the cortical control of movement. Current Opinion in Neurobiology. 2014 Feb;24:88–94.

118. Silasi G, Xiao D, Vanni MP, Chen ACN, Murphy TH. Intact skull chronic windows for mesoscopic wide-field imaging in awake mice. J Neurosci Methods. 2016 Jul 15;267:141–9.

119. Harrison TC, Silasi G, Boyd JD, Murphy TH. Displacement of Sensory Maps and Disorganization of Motor Cortex After Targeted Stroke in Mice. Stroke. 2013 Aug;44(8):2300–6.

120. Harding-Forrester S, Feldman DE. Somatosensory maps. In: Handbook of Clinical Neurology [Internet]. Elsevier; 2018 [cited 2024 Sep 19]. p. 73–102. Available from: https://linkinghub.elsevier.com/retrieve/pii/B9780444636225000048

121. Donoghue JP, Parham C. Afferent connections of the lateral agranular field of the rat motor cortex. J of Comparative Neurology. 1983 Jul 10;217(4):390–404.

122. Veinante P, Deschênes M. Single-cell study of motor cortex projections to the barrel field in rats. J of Comparative Neurology. 2003 Sep 8;464(1):98–103.

123. Hooks BM. Sensorimotor Convergence in Circuitry of the Motor Cortex. Neuroscientist. 2017 Jun;23(3):251–63.

124. Hall RD, Lindholm EP. Organization of motor and somatosensory neocortex in the albino rat. Brain Research. 1974 Jan;66(1):23–38.

125. Halley AC, Baldwin MKL, Cooke DF, Englund M, Krubitzer L. Distributed Motor Control of Limb Movements in Rat Motor and Somatosensory Cortex: The Sensorimotor Amalgam Revisited. Cereb Cortex. 2020 Jul 20;30(12):6296–312.

126. Ayling OGS, Harrison TC, Boyd JD, Goroshkov A, Murphy TH. Automated light-based mapping of motor cortex by photoactivation of channelrhodopsin-2 transgenic mice. Nat Methods. 2009 Mar;6(3):219–24.

127. Wolpert DM, Ghahramani Z, Jordan MI. An Internal Model for Sensorimotor Integration. Science. 1995 Sep 29;269(5232):1880–2.

128. Mathis MW, Mathis A, Uchida N. Somatosensory Cortex Plays an Essential Role in Forelimb Motor Adaptation in Mice. Neuron. 2017 Mar 22;93(6):1493-1503.e6.

129. Tseng Y weng, Diedrichsen J, Krakauer JW, Shadmehr R, Bastian AJ. Sensory Prediction Errors Drive Cerebellum-Dependent Adaptation of Reaching. Journal of Neurophysiology. 2007 Jul;98(1):54–62.

130. Winship IR, Murphy TH. Remapping the Somatosensory Cortex after Stroke: Insight from Imaging the Synapse to Network. Neuroscientist. 2009 Oct 1;15(5):507–24.

131. Devor A, Dunn AK, Andermann ML, Ulbert I, Boas DA, Dale AM. Coupling of Total Hemoglobin Concentration, Oxygenation, and Neural Activity in Rat Somatosensory Cortex. Neuron. 2003 Jul 17;39(2):353–9.

132. Grinvald A, Lieke E, Frostig RD, Gilbert CD, Wiesel TN. Functional architecture of cortex revealed by optical imaging of intrinsic signals. Nature. 1986 Nov;324(6095):361–4.

133. Bélanger S, Oliveira Ferreira de Souza B, Casanova C, Lesage F. Correlation of hemodynamic and fluorescence signals under resting state conditions in mice's barrel field cortex. Neuroscience Letters. 2016 Mar 11;616:177–81.

134. Guinto MC, Haruta M, Kurauchi Y, Saigo T, Kurasawa K, Ryu S, et al. Modular head-mounted cortical imaging device for chronic monitoring of intrinsic signals in mice. J Biomed Opt. 2022 Feb;27(2):026501.

135. Winship IR, Plaa N, Murphy TH. Rapid Astrocyte Calcium Signals Correlate with Neuronal Activity and Onset of the Hemodynamic Response In Vivo. J Neurosci. 2007 Jun 6;27(23):6268–72.

136. Bo B, Li Y, Li W, Wang Y, Tong S. Neurovascular Coupling Impairment in Acute Ischemic Stroke by Optogenetics and Optical Brain Imaging. In: 2020 42nd Annual International Conference of the IEEE Engineering in Medicine & Biology Society (EMBC) [Internet]. Montreal, QC, Canada: IEEE; 2020 [cited 2024 Sep 19]. p. 3727–30. Available from: https://ieeexplore.ieee.org/document/9176641/

137. Malonek D, Grinvald A. Interactions Between Electrical Activity and Cortical Microcirculation Revealed by Imaging Spectroscopy: Implications for Functional Brain Mapping. Science. 1996 Apr 26;272(5261):551–4.

138. Hayley P, Tuchek C, Dalla S, Borrell J, Murphy M, Nudo R, et al. Post-Ischemic Reorganization of Sensory Responses in Cerebral Cortex [Internet]. Neuroscience; 2023 Jan [cited 2023 Feb 22]. Available from: http://biorxiv.org/lookup/doi/10.1101/2023.01.18.524583

139. Clarkson AN, López-Valdés HE, Overman JJ, Charles AC, Brennan K, Carmichael ST. Multimodal Examination of Structural and Functional Remapping in the Mouse Photothrombotic Stroke Model. J Cereb Blood Flow Metab. 2013 May 1;33(5):716–23.

140. Brown CE, Aminoltejari K, Erb H, Winship IR, Murphy TH. In Vivo Voltage-Sensitive Dye Imaging in Adult Mice Reveals That Somatosensory Maps Lost to Stroke Are Replaced over Weeks by New Structural and Functional Circuits with Prolonged Modes of Activation within Both the Peri-Infarct Zone and Distant Sites. J Neurosci. 2009 Feb 11;29(6):1719–34.

141. Gharbawie OA, Gonzalez CLR, Williams PT, Kleim JA, Whishaw IQ. Middle cerebral artery (MCA) stroke produces dysfunction in adjacent motor cortex as detected by intracortical microstimulation in rats. Neuroscience. 2005 Jan 1;130(3):601–10.

142. Gharbawie OA, Williams PTJA, Kolb B, Whishaw IQ. Transient middle cerebral artery occlusion disrupts the forelimb movement representations of rat motor cortex. European Journal of Neuroscience. 2008;28(5):951–63.

143. Kathirvelu B, Carmichael ST. Intracerebral hemorrhage in mouse models: therapeutic interventions and functional recovery. Metab Brain Dis. 2015 Apr;30(2):449–59.

144. MacLellan CL, Silasi G, Poon CC, Edmundson CL, Buist R, Peeling J, et al. Intracerebral Hemorrhage Models in Rat: Comparing Collagenase to Blood Infusion. J Cereb Blood Flow Metab. 2008 Mar;28(3):516–25.

145. Ward NS. Neural plasticity and recovery of function. In: Laureys S, editor. Progress in Brain Research [Internet]. Elsevier; 2005 [cited 2022 Nov 30]. p. 527–35. (The Boundaries of Consciousness: Neurobiology and Neuropathology; vol. 150). Available from: https://www.sciencedirect.com/science/article/pii/S0079612305500360

146. MacLellan CL, Gyawali S, Colbourne F. Skilled reaching impairments follow intrastriatal hemorrhagic stroke in rats. Behavioural Brain Research. 2006 Nov;175(1):82–9.

147. Wang Q, Ding SL, Li Y, Royall J, Feng D, Lesnar P, et al. The Allen Mouse Brain Common Coordinate Framework: A 3D Reference Atlas. Cell. 2020 May 14;181(4):936-953.e20.

148. Sirkin DW. Critical Defatting of Frozen Brain Sections for Optimal Differentiation with the Cresyl Violet Stain. Stain Technology. 1983 Jan;58(2):121–2.

149. Wu TY, Sharma G, Strbian D, Putaala J, Desmond PM, Tatlisumak T, et al. Natural History of Perihematomal Edema and Impact on Outcome After Intracerebral Hemorrhage. Stroke. 2017 Apr;48(4):873–9.

150. Jafari M, Damani R. Blood pressure variability and outcome after acute intracerebral hemorrhage. Journal of the Neurological Sciences. 2020 Jun;413:116766.

151. Hakimi R, Garg A. Imaging of Hemorrhagic Stroke. 2016;

152. Lim-Hing K, Rincon F. Secondary Hematoma Expansion and Perihemorrhagic Edema after Intracerebral Hemorrhage: From Bench Work to Practical Aspects. Front Neurol. 2017 Apr 7;8:74.

153. Mittal MK, LacKamp A. Intracerebral Hemorrhage: Perihemorrhagic Edema and Secondary Hematoma Expansion: From Bench Work to Ongoing Controversies. Front Neurol. 2016 Nov 21;7:210.

154. Jiang Q, Zhang ZG, Chopp M. MRI of Stroke Recovery. Stroke. 2010 Feb;41(2):410–4.

155. Milidonis X, Marshall I, Macleod MR, Sena ES. Magnetic Resonance Imaging in Experimental Stroke and Comparison With Histology: Systematic Review and Meta-Analysis. Stroke. 2015 Mar;46(3):843–51.

156. Liu Y, Ao LJ, Lu G, Leong E, Liu Q, Wang XH, et al. Quantitative gait analysis of long-term locomotion deficits in classical unilateral striatal intracerebral hemorrhage rat model. Behavioural Brain Research. 2013 Nov 15;257:166–77.

157. Weber RZ. A toolkit for stroke infarct volume estimation in rodents. 2024;

158. Williamson MR, Colbourne F. Evidence for Decreased Brain Parenchymal Volume After Large Intracerebral Hemorrhages: a Potential Mechanism Limiting Intracranial Pressure Rises. Transl Stroke Res. 2017;8(4):386–96.

159. Kwon SM, Choi KS, Yi HJ, Ko Y, Kim YS, Bak KH, et al. Impact of brain atrophy on 90-day functional outcome after moderate-volume basal ganglia hemorrhage. Sci Rep. 2018 Mar 19;8:4819.

160. Puy L, Leboullenger C, Auger F, Bordet R, Cordonnier C, Bérézowski V. Intracerebral Hemorrhage-Induced Cognitive Impairment in Rats Is Associated With Brain Atrophy, Hypometabolism, and Network Dysconnectivity. Front Neurosci. 2022 Jun 30;16:882996.

161. DeBow SB, Davies MLA, Clarke HL, Colbourne F. Constraint-Induced Movement Therapy and Rehabilitation Exercises Lessen Motor Deficits and Volume of Brain Injury After Striatal Hemorrhagic Stroke in Rats. Stroke. 2003 Apr;34(4):1021–6.

162. Desmurget M, Turner RS. Motor Sequences and the Basal Ganglia: Kinematics, Not Habits. J Neurosci. 2010 Jun 2;30(22):7685–90.

163. Buhusi CV, Meck WH. What makes us tick? Functional and neural mechanisms of interval timing. Nat Rev Neurosci. 2005 Oct;6(10):755–65.

164. Zhang L, Schallert T, Zhang ZG, Jiang Q, Arniego P, Li Q, et al. A test for detecting long-term sensorimotor dysfunction in the mouse after focal cerebral ischemia. Journal of Neuroscience Methods. 2002 Jun 30;117(2):207–14.

165. Fang Y, Tian Y, Huang Q, Wan Y, Xu L, Wang W, et al. Deficiency of TREK-1 potassium channel exacerbates blood-brain barrier damage and neuroinflammation after intracerebral hemorrhage in mice. J Neuroinflammation. 2019 May 9;16:96.

166. Gao C, Meng Y, Chen G, Chen W, Chen X shi, Luo C liang, et al. Chronic restraint stress exacerbates neurological deficits and disrupts the remodeling of the neurovascular unit in a mouse intracerebral hemorrhage model. Stress. 2020 May 3;23(3):338–48.

167. Li M, Ren H, Sheth KN, Shi FD, Liu Q. A TSPO ligand attenuates brain injury after intracerebral hemorrhage. FASEB J. 2017 Aug;31(8):3278–87.

168. Hua Y, Schallert T, Keep RF, Wu J, Hoff JT, Xi G. Behavioral Tests After Intracerebral Hemorrhage in the Rat. Stroke. 2002 Oct;33(10):2478–84.

169. Li J, Song G, Jin Q, Liu L, Yang L, Wang Y, et al. The α2δ-1/NMDA receptor complex is involved in brain injury after intracerebral hemorrhage in mice. Ann Clin Transl Neurol. 2021 May 25;8(7):1366–75.

170. Lee KR, Colon GP, Betz AL, Keep RF, Kim S, Hoff JT. Edema from intracerebral hemorrhage: the role of thrombin. Journal of Neurosurgery. 1996 Jan;84(1):91–6.

171. Xi G, Hua Y, Bhasin RR, Ennis SR, Keep RF, Hoff JT. Mechanisms of Edema Formation After Intracerebral Hemorrhage. Stroke. 2001 Dec;32(12):2932–8.

172. Krafft PR, McBride DW, Lekic T, Rolland WB, Mansell CE, Ma Q, et al. Correlation between subacute sensorimotor deficits and brain edema in two mouse models of intracerebral hemorrhage. Behavioural Brain Research. 2014 May;264:151–60.

173. Barth AMI, Mody I. Novel test of motor and other dysfunctions in mouse neurological disease models. J Neurosci Methods. 2014 Jan 15;221:10.1016/j.jneumeth.2013.10.004.

174. Nicholas MA, Yttri EA. Motor cortex is responsible for motoric dynamics in striatum and the execution of both skilled and unskilled actions. Neuron. 2024 Aug;S0896627324005440.

175. Whishaw IQ, O'Connor WT, Dunnett SB. The contribution of motor cortex, nigrostriatal dopamine and caudate-putamen to skilled forelimb use in the rat. Brain. 1986;109(5):805–43.

176. Taub E, Morris DM. Constraint-induced movement therapy to enhance recovery after stroke. Curr Atheroscler Rep. 2001 Jul;3(4):279–86.

177. Wolf S, Lecraw D, Barton L, Jann B. Forced use of hemiplegic upper extremities to reverse the effect of learned nonuse among chronic stroke and head-injured patients. Experimental Neurology. 1989 May;104(2):125–32.

178. van der Lee JH, Wagenaar RC, Lankhorst GJ, Vogelaar TW, Devillé WL, Bouter LM. Forced Use of the Upper Extremity in Chronic Stroke Patients. Stroke. 1999 Nov;30(11):2369–75.

179. Guo JZ, Graves AR, Guo WW, Zheng J, Lee A, Rodríguez-González J, et al. Cortex commands the performance of skilled movement. Hausser M, editor. eLife. 2015 Dec 2;4:e10774.

180. Santos MV, Pagnussat AS, Mestriner RG, Netto CA. Motor Skill Training Promotes Sensorimotor Recovery and Increases Microtubule-Associated Protein-2 (MAP-2) Immunoreactivity in the Motor Cortex after Intracerebral Hemorrhage in the Rat. ISRN Neurol. 2013 Jul 15;2013:159184.

181. Donoghue JP, Herkenham M. Neostriatal projections from individual cortical fields conform to histochemically distinct striatal compartments in the rat. Brain Research. 1986 Feb;365(2):397–403.

182. Schulz JM, Reynolds JNJ. Pause and rebound: sensory control of cholinergic signaling in the striatum. Trends in Neurosciences. 2013 Jan;36(1):41–50.

183. Pidoux M, Mahon S, Deniau JM, Charpier S. Integration and propagation of somatosensory responses in the corticostriatal pathway: an intracellular study in vivo. J Physiol. 2011 Jan 15;589(Pt 2):263–81.

184. Sippy T, Lapray D, Crochet S, Petersen CCH. Cell-Type-Specific Sensorimotor Processing in Striatal Projection Neurons during Goal-Directed Behavior. Neuron. 2015 Oct 10;88(2):298.

185. Sun Z, Schneider A, Alyahyay M, Karvat G, Diester I. Effects of Optogenetic Stimulation of Primary Somatosensory Cortex and Its Projections to Striatum on Vibrotactile Perception in Freely Moving Rats. eNeuro. 2021 Mar 5;8(2):ENEURO.0453-20.2021.

186. Schwartze M, Stockert A, Kotz SA. Striatal contributions to sensory timing: Voxel-based lesion mapping of electrophysiological markers. Cortex. 2015 Oct;71:332–40.

187. Bray N, Burrows FE, Jones M, Berwick J, Allan SM, Schiessl I. Decreased haemodynamic response and decoupling of cortical gamma-band activity and tissue oxygen perfusion after striatal interleukin-1 injection. J Neuroinflammation. 2016 Aug 24;13(1):195.

188. de la Torre-Martinez R, Ketzef M, Silberberg G. Ongoing movement controls sensory integration in the dorsolateral striatum. Nat Commun. 2023 Feb 22;14:1004.

189. Zembrzycki A, Chou SJ, Ashery-Padan R, Stoykova A, O'Leary DDM. Sensory cortex limits cortical maps and drives top-down plasticity in thalamocortical circuits. Nature neuroscience. 2013 Aug;16(8):1060.

190. Bauer AQ, Kraft AW, Wright PW, Snyder AZ, Lee JM, Culver JP. Optical imaging of disrupted functional connectivity following ischemic stroke in mice. Neuroimage. 2014 Oct 1;99:388–401.

191. Williams PTJ, Gharbawie OA, Kolb B, Kleim JA. Experience-dependent amelioration of motor impairments in adulthood following neonatal medial frontal cortex injury in rats is accompanied by motor map expansion. Neuroscience. 2006 Jan 1;141(3):1315–26.

192. Shi E, Shi K, Qiu S, Sheth KN, Lawton MT, Ducruet AF. Chronic inflammation, cognitive impairment, and distal brain region alteration following intracerebral hemorrhage. The FASEB Journal. 2019;33(8):9616–26.

193. Song K, Liu X, Zheng Q, Zhang L, Zhang H, Yu H, et al. Secondary injury to distal regions after intracerebral hemorrhage influence neurological functional outcome. Aging (Albany NY). 2020 Mar 8;12(5):4283–98.

194. Cregg JM, Sidhu SK, Leiras R, Kiehn O. Basal ganglia–spinal cord pathway that commands locomotor gait asymmetries in mice. Nat Neurosci. 2024 Apr;27(4):716–27.

195. Grillner S, El Manira A. Current Principles of Motor Control, with Special Reference to Vertebrate Locomotion. Physiological Reviews. 2020 Jan;100(1):271–320.

196. Jang SH, Kwon YH, Lee MY, Lee DY, Hong JH. Difference of neural connectivity for motor function in chronic hemiparetic stroke patients with intracerebral hemorrhage. Neuroscience Letters. 2012 Dec 7;531(2):80–5.

197. Liang H, Yin Y, Lin T, Guan D, Ma B, Li C, et al. Transplantation of bone marrow stromal cells enhances nerve regeneration of the corticospinal tract and improves recovery of neurological functions in a collagenase-induced rat model of intracerebral hemorrhage. Mol Cells. 2013 Jul;36(1):17–24.

198. Mitz AR, Humphrey DR. Intracortical stimulation in pyramidotomized monkeys. Neuroscience Letters. 1986 Feb 14;64(1):59–64.

199. Hilton BJ, Anenberg E, Harrison TC, Boyd JD, Murphy TH, Tetzlaff W. Re-Establishment of Cortical Motor Output Maps and Spontaneous Functional Recovery via Spared Dorsolaterally Projecting Corticospinal Neurons after Dorsal Column Spinal Cord Injury in Adult Mice. J Neurosci. 2016 Apr 6;36(14):4080–92.

200. Piecharka DM, Kleim JA, Whishaw IQ. Limits on recovery in the corticospinal tract of the rat: Partial lesions impair skilled reaching and the topographic representation of the forelimb in motor cortex. Brain Research Bulletin. 2005 Aug 15;66(3):203–11.

201. Kambi N, Tandon S, Mohammed H, Lazar L, Jain N. Reorganization of the Primary Motor Cortex of Adult Macaque Monkeys after Sensory Loss Resulting from Partial Spinal Cord Injuries. J Neurosci. 2011 Mar 9;31(10):3696–707.

202. Tazoe T, Perez MA. Abnormal Changes in Motor Cortical Maps in Humans with Spinal Cord Injury. J Physiol. 2021 Nov;599(22):5031–45.

203. Yamazaki R, Ohno N, Huang JK. Acute motor deficit and subsequent remyelination-associated recovery following internal capsule demyelination in mice. J Neurochem. 2021 Mar;156(6):917–28.

204. Ebrahimi A, Pochet R, Roger M. Topographical organization of the projections from physiologically identified areas of the motor cortex to the striatum in the rat. Neuroscience Research. 1992 Jun;14(1):39–60.

205. Donchin O, Gribova A, Steinberg O, Mitz AR, Bergman H, Vaadia E. Single-Unit Activity Related to Bimanual Arm Movements in the Primary and Supplementary Motor Cortices. Journal of Neurophysiology. 2002 Dec;88(6):3498–517.

206. Nirkko AC, Ozdoba C, Redmond SM, Bürki M, Schroth G, Hess CW, et al. Different Ipsilateral Representations for Distal and Proximal Movements in the Sensorimotor Cortex: Activation and Deactivation Patterns. NeuroImage. 2001 May 1;13(5):825–35.

207. Cramer SC, Finklestein SP, Schaechter JD, Bush G, Rosen BR. Activation of Distinct Motor Cortex Regions During Ipsilateral and Contralateral Finger Movements. Journal of Neurophysiology. 1999 Jan;81(1):383–7.

208. Liang F, Rouiller EM, Wiesendanger M. Modulation of Sustained Electromyographic Activity by Single Intracortical Microstimuli: Comparison of Two Forelimb Motor Cortical Areas of the Rat. Somatosensory & Motor Research. 1993 Jan;10(1):51–61.

209. Domin M, Lotze M. Parcellation of motor cortex-associated regions in the human corpus callosum on the basis of Human Connectome Project data. Brain Struct Funct. 2019 May 1;224(4):1447–55.

210. Wahl M, Ziemann U. The Human Motor Corpus Callosum. Reviews in the Neurosciences [Internet]. 2008 Jan [cited 2024 Sep 25];19(6). Available from: https://www.degruyter.com/document/doi/10.1515/REVNEURO.2008.19.6.451/html

211. Doron KW, Bassett DS, Gazzaniga MS. Dynamic network structure of interhemispheric coordination. Proceedings of the National Academy of Sciences. 2012 Nov 13;109(46):18661–8.

212. Handa T, Zhang Q, Aizawa H. Cholinergic modulation of interhemispheric inhibition in the mouse motor cortex. Cerebral Cortex. 2024 Jul 1;34(7):bhae290.

213. Gazzaniga MS. Forty-five years of split-brain research and still going strong. Nat Rev Neurosci. 2005 Aug;6(8):653–9.

214. Ferbert A, Priori A, Rothwell JC, Day BL, Colebatch JG, Marsden CD. Interhemispheric inhibition of the human motor cortex. The Journal of Physiology. 1992 Jul;453(1):525–46.

215. Meyer BU, Röricht S, von Einsiedel HG, Kruggel F, Weindl A. Inhibitory and excitatory interhemispheric transfers between motor cortical areas in normal humans and patients with abnormalities of the corpus callosum. Brain. 1995 Apr 1;118(2):429–40.

216. Krupnik R, Yovel Y, Assaf Y. Inner Hemispheric and Interhemispheric Connectivity Balance in the Human Brain. J Neurosci. 2021 Oct 6;41(40):8351–61.

217. Assaf Y, Bouznach A, Zomet O, Marom A, Yovel Y. Conservation of brain connectivity and wiring across the mammalian class. Nat Neurosci. 2020 Jul;23(7):805–8.

218. Fries W, Danek A, Scheidtmann K, Hamburger C. Motor recovery following capsular stroke: Role of descending pathways from multiple motor areas. Brain. 1993;116(2):369–82.

219. Nishio T, Inoue T, Takamatsu Y, Mishima T, Takamura H, Soma K, et al. Epigenetic modification of histone acetylation in the sensorimotor cortex after intracerebral hemorrhage. Biomedical Research. 2024;45(1):1–11.

220. Zhang Y, Li KS, Ning YZ, Fu CH, Liu HW, Han X, et al. Altered structural and functional connectivity between the bilateral primary motor cortex in unilateral subcortical stroke. Medicine (Baltimore). 2016 Aug 7;95(31):e4534.

221. Lee J, Park E, Lee A, Chang WH, Kim DS, Kim YH. Alteration and Role of Interhemispheric and Intrahemispheric Connectivity in Motor Network After Stroke. Brain Topogr. 2018 Jul 1;31(4):708–19.

222. Johansen-Berg H, Rushworth MFS, Bogdanovic MD, Kischka U, Wimalaratna S, Matthews PM. The role of ipsilateral premotor cortex in hand movement after stroke. Proc Natl Acad Sci U S A. 2002 Oct 29;99(22):14518–23.

223. Strens LHA, Fogelson N, Shanahan P, Rothwell JC, Brown P. The Ipsilateral Human Motor Cortex Can Functionally Compensate for Acute Contralateral Motor Cortex Dysfunction. Current Biology. 2003 Jul 15;13(14):1201–5.

224. Buetefisch CM. Role of the Contralesional Hemisphere in Post-Stroke Recovery of Upper Extremity Motor Function. Front Neurol [Internet]. 2015 Oct 16 [cited 2024 Apr 19];6. Available from: https://www.frontiersin.org/journals/neurology/articles/10.3389/fneur.2015.00214/full

225. Riecker A, Gröschel K, Ackermann H, Schnaudigel S, Kassubek J, Kastrup A. The role of the unaffected hemisphere in motor recovery after stroke. Hum Brain Mapp. 2010 Jul;31(7):1017–29.

226. Grefkes C, Nowak DA, Eickhoff SB, Dafotakis M, Küst J, Karbe H, et al. Cortical connectivity after subcortical stroke assessed with functional magnetic resonance imaging. Annals of Neurology. 2008 Feb;63(2):236–46.

227. Murase N, Duque J, Mazzocchio R, Cohen LG. Influence of interhemispheric interactions on motor function in chronic stroke. Ann Neurol. 2004 Mar;55(3):400–9.

228. Bloom JS, Hynd GW. The Role of the Corpus Callosum in Interhemispheric Transfer of Information: Excitation or Inhibition? Neuropsychol Rev. 2005 Jun;15(2):59–71.

229. Mordillo-Mateos L, Turpin-Fenoll L, Millán-Pascual J, Núñez-Pérez N, Panyavin I, Gómez-Argüelles JM, et al. Effects of simultaneous bilateral tDCS of the human motor cortex. Brain Stimul. 2012 Jul;5(3):214–22.

230. Waters S, Wiestler T, Diedrichsen J. Cooperation Not Competition: Bihemispheric tDCS and fMRI Show Role for Ipsilateral Hemisphere in Motor Learning. J Neurosci. 2017 Aug 2;37(31):7500–12.

231. Sun M, Deng B, Zhao X, Gao C, Yang L, Zhao H, et al. Isoflurane preconditioning provides neuroprotection against stroke by regulating the expression of the TLR4 signalling pathway to alleviate microglial activation. Sci Rep. 2015 Jun 18;5(1):11445.

232. Raub D, Platzbecker K, Grabitz SD, Xu X, Wongtangman K, Pham SB, et al. Effects of Volatile Anesthetics on Postoperative Ischemic Stroke Incidence. J Am Heart Assoc. 2021 Feb 26;10(5):e018952.

233. Lee JJ, Li L, Jung HH, Zuo Z. Postconditioning with isoflurane reduced ischemia-induced brain injury in rats. Anesthesiology. 2008 Jun;108(6):1055–62.

234. Khatibi NH, Ma Q, Rolland W, Ostrowski R, Fathali N, Martin R, et al. Isoflurane Posttreatment Reduces Brain Injury After an Intracerebral Hemorrhagic Stroke in Mice. Anesth Analg. 2011 Aug;113(2):343–8.

235. Hohlbaum K, Bert B, Dietze S, Palme R, Fink H, Thöne-Reineke C. Impact of repeated anesthesia with ketamine and xylazine on the well-being of C57BL/6JRj mice. PLoS One. 2018 Sep 19;13(9):e0203559.

236. Razoux F, Garcia R, Léna I. Ketamine, at a Dose that Disrupts Motor Behavior and Latent Inhibition, Enhances Prefrontal Cortex Synaptic Efficacy and Glutamate Release in the Nucleus Accumbens. Neuropsychopharmacol. 2007 Mar;32(3):719–27.

237. Hohlbaum K, Bert B, Dietze S, Palme R, Fink H, Thöne-Reineke C. Severity classification of repeated isoflurane anesthesia in C57BL/6JRj mice—Assessing the degree of distress. PLoS One. 2017 Jun 15;12(6):e0179588.

238. Lemke SM, Celotto M, Maffulli R, Ganguly K, Panzeri S. Information flow between motor cortex and striatum reverses during skill learning. Current Biology. 2024 May 6;34(9):1831-1843.e7.

239. Girouard H, Iadecola C. Neurovascular coupling in the normal brain and in hypertension, stroke, and Alzheimer disease. Journal of Applied Physiology. 2006 Jan;100(1):328–35.

240. Sunil S, Jiang J, Shah S, Kura S, Kilic K, Erdener SE, et al. Neurovascular coupling is preserved in chronic stroke recovery after targeted photothrombosis. NeuroImage : Clinical [Internet]. 2023 [cited 2024 Sep 23];38. Available from: https://www.ncbi.nlm.nih.gov/pmc/articles/PMC10034641/

241. Gareev I, Beylerli O, Zhao B. MiRNAs as potential therapeutic targets and biomarkers for non-traumatic intracerebral hemorrhage. Biomark Res. 2024 Feb 2;12:17.

242. Blinkouskaya Y, Caçoilo A, Gollamudi T, Jalalian S, Weickenmeier J. Brain aging mechanisms with mechanical manifestations. Mech Ageing Dev. 2021 Dec;200:111575.